Order Number 9000714

Facies analysis and petrophysical characteristics of the Jurassic Smackover Formation, Conecuh Embayment, Alabama-Florida

Melas, Faye F., Ph.D.

City University of New York, 1989

U·M·I
300 N. Zeeb Rd.
Ann Arbor, MI 48106

FACIES ANALYSIS AND PETROPHYSICAL CHARACTERISTICS OF THE JURASSIC SMACKOVER FORMATION, CONECUH EMBAYMENT, ALABAMA-FLORIDA

by

FAYE F. MELAS

A dissertation submited to the Graduate Faculty in Earth and Environmental Sciences in partial fulfilment of the requirements for the degree of Doctor of Philosophy, The City University of New York.

1989

This manuscript has been accepted for the Graduate Faculty in Earth and Environmental Sciences in satisfaction of the dissertation requirement for the degree of Doctor of Philosophy.

4/17/89
Date

Gerald G. Wiedman
Chair of Examining Committee

4/25/89
Date

Daniel Habib
Executive Officer

Dr. S. Ghosh

Dr. D. Habib

Dr. S. Bhattacharji

The City University of New York

ABSTRACT

Facies Analysis and Petrophysical Characteristics of the Jurassic Smackover Formation, Conecuh Embayment, Alabama-Florida

by

Faye F. Melas

Adviser: Professor Gerald M. Friedman

Carbonate reservoir rocks are heterogeneous and no one model may embrace all the different kinds of carbonate reservoirs. However, studies which include sedimentologic and petrophysical information and effect of wettability in carbonate rocks represent a first step when Enhanced Oil Recovery (EOR) methods are considered.

Detailed sedimentologic studies of the Smackover Formation in the Conecuh Embayment indicate that the upper Smackover grainstones are part of a shoaling-upward carbonate sequence, capped by an evaporite interval. They were deposited in a moderate- to high-energy intertidal shoal, located on a paleobathymetric high most probably produced by salt movements. Pervasive dolomitization of these grainstones created a porous and permeable, high- yield reservoir, the Jay field reservoir.

Jay field is a combination stratigraphic, diagenetic, and structural trap, which produces from a layered upper Smackover grainstone section with high porosity and permeability contrasts among the layers. Thin, horizontally continuous layers which act as barriers to vertical flow and contribute to reservoir inhomogeneity, are interlayered within porous and permeable, high yield zones.

Pore geometry has a great influence on the ability of a rock to contain and produce hydrocarbons, as do porosity and permeability. Knowledge of the pore geometry through mercury-capillary-pressure curves, in conjunction with geophysical logs and visual analyses of the various facies are essential to better understand and predict the hydrocarbon-producing potential of a reservoir, and plan a successful pressure maintenance program for secondary and tertiary recovery methods.

Detailed sedimentologic and petrophysical studies of the Smackover carbonates in the Conecuh Embayment indicate that petrophysical parameters such as porosity, effective porosity, irreducible water saturation, pore-throat sorting, and displacement pressure (i.e., critical pore throat size), reflect the shape of the mercury-capillary-pressure curves to which they correspond. As such, mercury-capillary-pressure

curves are adequate for a comprehensive description of pore geometry.

The Smackover carbonates are classified in terms of their capillary-pressure curves into reservoir and nonreservoir facies. Steeply-sloping curves with flat plateaus correspond to reservoir samples with medium- to high-porosity and effective porosity values, well-sorted pore-size distribution, low-displacement pressures, and relatively low irreducible water saturations. Gently-sloping curves with steep plateaus or no plateau correspond to nonreservoir facies with low-porosity and effective porosity values, poorly-sorted pore-size distribution, high-displacement pressures, and high irreducible water saturations. Because late anhydrite cement has in places altered the petrophysical characteristics of the carbonates, the key criterion used to distinguish reservoir and nonreservoir facies was the pore-size distribution, which was not effected by the anhydrite cement.

Extensive reservoir description during field development (1970-1974) resulted in a wealth of reservoir data which were utilized effectively to optimize recovery in Jay field. Ultimate hydrocarbon recovery from the Jay field carbonates, through secondary and tertiary methods, is now expected to reach 57% of original oil in place.

(OOIP), 10% higher than originally predicted. Further understanding of the petrophysical properties and complexities of this deeply buried reservoir will aid in the selection of additional future EOR schemes, which could substantially increase the expected hydrocarbon recovery. In addition, data developed for this reservoir will aid toward more effective exploitation of other similar reservoirs which are at early stages of development.

ACKNOWLEDGMENTS

I wish to express my grateful thanks to Dr. Gerald M. Friedman, my mentor, who inspired and guided this research. The research was supported by a grant from the United States Department of Energy under Grant No. DE-FG02-84-ER-13322. The study material was made available through the courtesy of Cities Service Oil and Gas Corporation, Exxon Oil Company, and Sun Oil Company. The help of Mr. Billy Moore was most gratefully appreciated. Special thanks to Dr. Daniel Habib for all help provided, my advisory committee members, Dr. D. Habib, Dr. S. Ghosh, and Dr. S. Bhattacharji, for their helpful criticism, Dr. Kopaska-Merkel for repeatedly reviewing this manuscript, Ms. Lina McLain and Mrs. Sue Friedman for handling the paper work, and my fellow students, especially Ali kaya and Golam Sarwar, for their moral support, which was most often accompanied by long discussions and arguments. Most of all I would like to thank my family for their patience, support, and understanding during these long years.

TABLE OF CONTENTS

LIST OF TABLES

LIST OF FIGURES

FIGURE 23. Photomicrographs (plane polarized light) of the cement types of the cores studied. a. Isopachous rim cements in dolomitized peloidal/oolitic grainstone (Humble C. H. Bray #10-4 well; 15,410' or 5,137m). Spalled rim cements (arrow) and sutured grain contacts are indicative of brittle compaction and pressure solution respectively, both the result of overburden pressure. The interparticle pores are wholly or partially filled with hydrocarbons (black) and some display geopetal texture. b. Cement generations in vadose pisolite (Cities Service Lizenby #5-3 well; 16,346' or 5,449m). Pisoids occupy area on left and right of photograph. Central area bordered by micritic rim is an interpisoid void. Three generations of cements are present: fibrous calcite, equant dolomite, and drusy or megaspar calcite, listed in relative chronological order. c. Massive anhydrite cement in peloidal/oolitic grainstone (Humble C. H. Bray #10-4 well; 15,410' or 5,137m). Anhydrite fills the interparticle and moldic pores and postdates all other diagenetic events. d. Replacement anhydrite in pelletal/peloidal wackestone (Humble McDavid Lands #7-1 well; 15,546' or 5,182m). The blocky anhydrite cement cuts indiscriminately across particles and

FIGURE 24. Photomicrographs (plane polarized light) of the porosity types of the study area. a. moldic (m) and interparticle (i) porosity in dolomitized peloidal/oolitic grainstone (Humble Sam Watson #23-4 well; 15,604' or 5,201m). The ooids and peloids are wholly or partially dissolved, indicating incomplete leaching. Although individual oomolds are not interconnected, good interparticle and dolomitic microcrystalline porosities resulted in good permeability and thus an excellent reservoir facies. b. Dolomitic intercrystalline porosity in dolomitized peloidal/oolitic grainstone (Humble C. H. Bray #10-4 well; 15418' or 5,139m). Dolomitization is coarse-crystalline and the intercrystalline pores are large and well interconnected, resulting in very high porosity and permeability values. c. Stylolitic porosity in pelletal wackestone (Humble Mcdavid Lands #7-1 well; 15534' or 5,178m). Stylolitic porosity is found in the lower Smackover peritidal facies. Individual pores characteristically tend to follow weak stylolitic zones. Such pores are, however, very rare and constitute a very small fraction of the available porosity. d. Microfracture porosity (f) in pelletal wackestone (Humble McDavid Lands #7-1 well;

LIST OF APPENDICES

1. INTRODUCTION AND RESEARCH OVERVIEW

1.1 Scope of Research

A comprehensive study of a deeply buried dolostone reservoir (the Smackover Formation in the Conecuh Embayment) for Enhanced Oil Recovery potential is the subject matter of this research. The purpose of this study is to describe and classify the pore geometry using mercury-capillary-pressure curves and relate that information to the depositional environment and diagenetic overprint of the reservoir rocks. The ultimate purpose of this study is to understand the complexities of heterogeneity in dolostone reservoir rocks and aid in the development of proper technology for more efficient hydrocarbon recovery from deeply buried carbonate reservoirs.

Although carbonate reservoirs have been important contributors to United States' oil and gas production for several decades, their importance has increased dramatically as a result of sharp changes in world demand in conjunction with restricted geopolitical locations of many giant carbonate fields. However, as reserves of oil and gas decline, a greater incentive for more efficient recovery from existing oil fields exists.

The volume of oil and gas in a reservoir is equal to its pore volume minus the residual water. On the average, however, less than one third of the Original oil In Place (OOIP) is recovered by conventional primary and secondary recovery methods. Enhanced oil and gas recovery generally may lead to a further 20% or more of additional reserves. Large carbonate reservoirs discovered in the last 50 years will yield more oil through enhanced oil recovery than will be discovered through new exploration. However, only through an understanding of the complexity of such carbonate reservoirs will enhanced oil recovery be successful, especially at depths of burial of 5,000 meters (15,000 feet) and more.

1.2 Rationale for Undertaking Research Study

Carbonate rocks do not exhibit any simple relationship between porosity and permeability development. During the course of diagenesis, the kind and degree of porosity and permeability may be altered so that they are no longer predictable.

The quantification of the degree of heterogeneity within a reservoir, on scales from small clusters of pores to those of the reservoir itself, is the most important issue in reservoir description. As

scale is increased from the microscopic to the macroscopic, new types of heterogeneities appear and there may be no scale at which the carbonate reservoir can be considered homogeneous. Its characteristics, however, may follow definite trends when considering the reservoir as a whole. For this reason, an appreciation of the heterogeneous nature of carbonate reservoirs requires refined predictions based on sedimentological models and the understanding of stratigraphic and structural relationships in combination with the interpretation of petrophysical data and capillary-pressure gradients.

Because our present knowledge of petrophysics and wettability is only peripheral, this proposed study is very important and unique for various reasons:
(1) considers a wide range of carbonate lithofacies representing different depositional environments and diagenetic overprints;
(2) relates detailed petrographic information to petrophysical properties of rocks; and
(3) provides a large petrophysical data set for real-world carbonate reservoir rocks of diverse origins.

The relationship of the petrophysical properties to the sedimentologic lithofacies and diagenetic overprints of the Smackover Formation indicate that three-

dimensional subsurface reservoir modeling is possible in the studied area. Preliminary work indicates that porosity and permeability development is related to diagenetic processes as well as depositional environments.

My studies of petrophysics combined with facies analysis and diagenetic overprint of these rocks should result in improved understanding of the complexities of carbonate reservoirs, which in turn is fundamental when choosing a suitable EOR method.

1.3 Enhanced Oil Recovery (EOR)

Enhanced Oil Recovery is generally considered the last phase of useful oil production. It includes various forms of secondary waterflooding and tertiary caustic flooding, hydrocarbon injection, carbon dioxide flooding, micellar-polymer flooding, and several thermal methods (Morrow and Heller, 1985).

The primary phase of oil production begins with the discovery of an oil field and the extraction of the hydrocarbons using the naturally stored energy. Oil is moved to the wells by the expansion of volatile components and/or pumping of individual wells to assist the natural drive. When this natural energy is depleted, production declines and a secondary phase of oil

production begins when supplemental energy is added to the reservoir by injecting water (Morrow and Heller, 1985). The main driving force for secondary hydrocarbon migration under hydrostatic conditions is buoyancy, while the main resistant force to secondary hydrocarbon migration is capillary pressure (Schowalter, 1979).

The amount of oil which can be recovered economically, by primary production and secondary waterflooding, varies enormously from less than 10% to more than 80% (30% average) of the initial oil in place. Therefore, approximately two-thirds of the oil remains in the reservoir as a potential target for various tertiary EOR schemes (Wardlaw and Cassan, 1978, 1979; Dullien, 1979).

Answers to questions such as: (a) what factors cause the variation in oil-recovery efficiency in reservoirs and, (b) how can recovery be maximized for particular reservoirs, can be derived from information about the nature of the rock pore system, knowledge of rock-liquid interaction, properties of fluids under reservoir conditions and an understanding of the forces which cause fluids to migrate (gravity, viscous and capillary forces). Of these, the rock pore system is the most poorly understood and only with more extensive petrophysical and geological data will the situation

improve, and a better system for EOR be possible.

1.4 Wettability

Wettability is "the tendency of a fluid to spread on or adhere to a solid surface in the presence of other immiscible fluids" (Craig, 1971). In a rock/oil/brine system, wettability is a measure of the preference the rock has for either oil or water, and can range from strongly water-wet to strongly oil-wet, as suggested from angle measurements of the interface the liquids make with the solid surface (i.e., contact-angle measurements). In general, a solid is said to be water-wet when the contact angle is less than 90^{o} and oil-wet when the contact angle is greater than 90^{o} (Fig. 1). In terms of interfacial tensions, the liquid that has the lower interfacial tension (higher adhesion) with the solid is the wetting liquid (Levorsen, 1967; Craig, 1971; Anderson, 1986a).

In water-wet systems the rock is preferentially in contact with the water and would imbibe water preferentially to oil. In oil-wet systems the rock is preferentially in contact with oil and would imbibe oil preferentially to water. When the rock has no strong preference for either oil or water (contact angle of exactly 90^{o}), the system is of neutral wettability

FIGURE 1. Wettability of oil/water/solid system (From Raza et al., 1968). The surface energies in such a system are by the Young-Dupre equation as follows: $\sigma_{os} - \sigma_{ws} = \sigma_{ow}\cos\theta_c$ (Adams , 1941), where σ_{os} = interfacial tension between the oil and the solid (dynes/cm); σ_{ws} = interfacial tension between the water and solid (dynes/cm); σ_{ow} = interfacial tension between the oil and water (dynes/cm); and θ_c angle at the oil/water/solid interface, measured through the water (i.e. contact angle). σ_{ow} and θ_c can be measured directly in the laboratory, while σ_{os} and σ_{ws} cannot be determined independently.

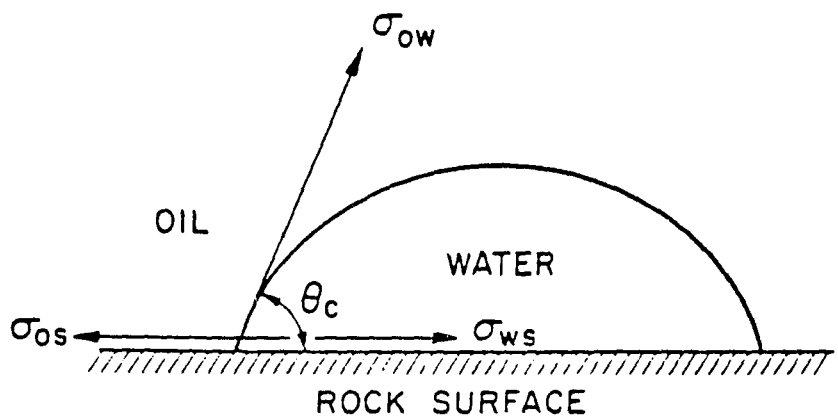
σ_{ow}
OIL
WATER
θ_c
σ_{os}
σ_{ws}
ROCK SURFACE

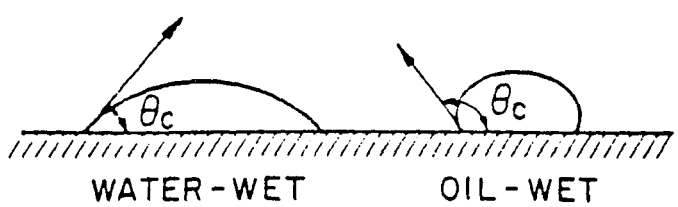
θ_c
θ_c
WATER-WET
OIL-WET

(Levorsen, 1967; Craig, 1971; Schowalter, 1979). Morrow et al (1973), however, stated that 90° may not be the breakover point for an oil-wet surface, and that contact angle of greater than 140° in dolomite laboratory packs was necessary for oil to be imbibed.

If, instead of oil or water, mercury, with a surface tension of about seven times that of water, is used, the mercury will contract into spherical droplets making an angle of about 130 with the solid. Mercury is thus a nonwetting fluid (Anderson, 1986a).

It should be noted, however, that wettability refers to the wetting preference of the rock and does not necessarily refer to the fluid that is in contact with the rock at any given time. Furthermore, mineralogical complexities of reservoir rocks could cause wettability to vary on a scale ranging from submicroscopic to macroscopic (Anderson, 1986a; Morrow and Heller, 1985).

At first, it was generally considered that all reservoir rocks are preferentially water-wet, because water was thought to be the perfect wetting fluid. In addition, most sedimentary rock minerals are water-wet in their natural state (i.e. during sedimentation and early diagenesis) and oil migrates later into their pores. It was later recognized (Nutting, 1934), however, that some reservoirs are partially oil-wet. Treiber et al (1972)

suggested that in most of the Amoco reservoirs studied, oil wets the rock more strongly than water. When a rock is fractionally oil-wet (>25% oil-wet) there is a reduction in the oil-water displacement pressure for that particular oil-water-rock system (Fatt and Klikoff, 1959).

Wettability of originally water-wet reservoirs can be altered by the adsorption of crude oil components (i.e. polar compounds and organic matter; Benner and Bartell, 1941). In the case of cores, wettability may be altered by drilling fluids, packaging preservation, cleaning, test fluids, and test temperature and pressure (Anderson, 1986a).

Wettability is a major factor controlling the location, flow, and distribution of fluids in a reservoir. The wettability of a reservoir affects its capillary pressure, relative permeability, waterflood behavior, dispersion of tracers, irreducible water saturation (IWS), residual oil saturation (ROS), and electrical properties, as well as tertiary recovery (Anderson, 1986a,b,c).

The kinds of mineral surfaces in a reservoir are very important in determining wettability. Chilingar and Yen (1983) found through contact-angle measurements that carbonate reservoirs are typically more oil-wet than

sandstone reservoirs. In addition, rocks rich in organics (such as source rocks) and rocks rich in iron can preferentially adsorb surface-active material from crude oils and may develop grain surfaces that are partially oil-wet (Schowalter, 1979). The salinity and pH of the interstitial brines, however, may influence the above generalizations because brine chemistry strongly affects the surface charge on the rock surface and fluid interfaces, which in turn can affect the adsorption of surfactants (Leja, 1982).

1.5 Capillary Pressure

Capillary pressure (or interface pressure) is the pressure difference across the interface created by two immiscible fluids and is measured in dynes/cm^2.

$$P_c = P_1 - P_2 \qquad 1\text{-}1$$

$$P_c = 2\gamma R \quad \text{for spherical drops} \qquad 1\text{-}2$$

$$P_c = (1/R_1 + 1/R_2) \quad \text{for nonspherical (oval) drops} \qquad 1\text{-}3$$

where: P_c = capillary pressure

P_1 and P_2 = pressures on concave and convex sides of fluids respectively

γ = interfacial tension

R = radius of curvature of spherical liquid drop determined by the pore

size of the rock

R_1 and R_2 = radii of curvature of an oval-shaped liquid drop (Berg, 1975).

Equations 1-2 and 1-3 assume that the rock is water-wet (as is usually the case) and that the fluid boundary is approximately a spherical surface, which may not always hold. Wardlaw (1976), assuming sheet-like pore space, modified the equations as follows:

$$P_c = 2\gamma\cos\theta/d \qquad 1\text{-}4$$

where: d = pore-throat diameter

θ = wettability expressed by the contact angle between the liquid boundary and the solid surface.

For water-wet rocks, θ is zero and the cos is one. Thus equation 1-4 becomes

$$P_c = 2\gamma/d \qquad 1\text{-}5$$

Equation 1-4 and 1-5 approximate realistic conditions because pore throats in dolostone reservoirs are mainly sheet-like.

The term capillary pressure (or displacement pressure), as used in reservoir analyses literature and this work, refers to the injection pressure necessary to invade nonwetting fluids (such as mercury) into the pore spaces of a specific rock, and is plotted as a function of the volume of fluid injected (Berg, 1975).

In this case: $P_c = 2\gamma\cos\theta/r$ 1-6

where: r = the radius of the pore throats.

The magnitude of capillary pressure thus depends on such factors as pore-throat size, density and buoyancy of fluids, oil-water interfacial tension, and the forces associated with the fluid-rock interface, such as surface-free energy, surface tension, interfacial tension, absorption property of rock, and wettability of rock fluids (Schowalter, 1979).

If the magnitude of the capillary (or displacement) pressure for a hydrocarbon-water-rock system can be determined, the minimum vertical hydrocarbon column necessary to migrate hydrocarbons through the rock can be calculated, and the sealing capacity for a caprock or the trapping capacity for a lateral facies change or fault would be estimated (Schowalter, 1979).

From equation 1-6 we note that capillary pressure is proportional to the oil-water interfacial tension and inversely proportional to the contact angle and pore-throat size. Higher capillary pressures are required for fluid migration in a reservoir containing small pore throats, while relatively smaller capillary pressures are required for fluid migration in a reservoir containing large pore throats. Thus specific measurements of pore-throat size via direct view (i.e. electron microscope,

SEM, and resin pore casts) and capillary-pressure tests are necessary to quantify oil recovery.

1.6 Oil Column Definition and Significance

An oil column (Fig. 2) is the vertical dimension of a continuous oil accumulation, with its bottom located at the free-water level (Jennings, 1987).

An oil column can be subdivided into three zones as follows: (1) 100% oil-production zone; (2) oil-water transition zone (producing both oil and water); and (3) 100% water production zone (Fig. 2). All three zones, however, may not be present within a reservoir because their existence is a function of the presence of a free-water table, the magnitude of the oil column, and the relative permeability characteristics of the reservoir (Jennings, 1987).

The oil-water transition zone which must exist in any reservoir with a free-water table, is a depth interval within which water saturation changes gradually from 100% to approximately 30-10%. The thickness of the transition zone depends on fluid properties as well as petrophysical properties of the reservoir (Calhoun, 1953). In a reservoir, if all pore throats were of the same size, the reservoir would have a sharp, well-defined boundary between oil and water (Jordy, 1972).

FIGURE 2. Example of an oil column. Oil saturations are approximate; O/W = oil/water (from Jennings, 1987).

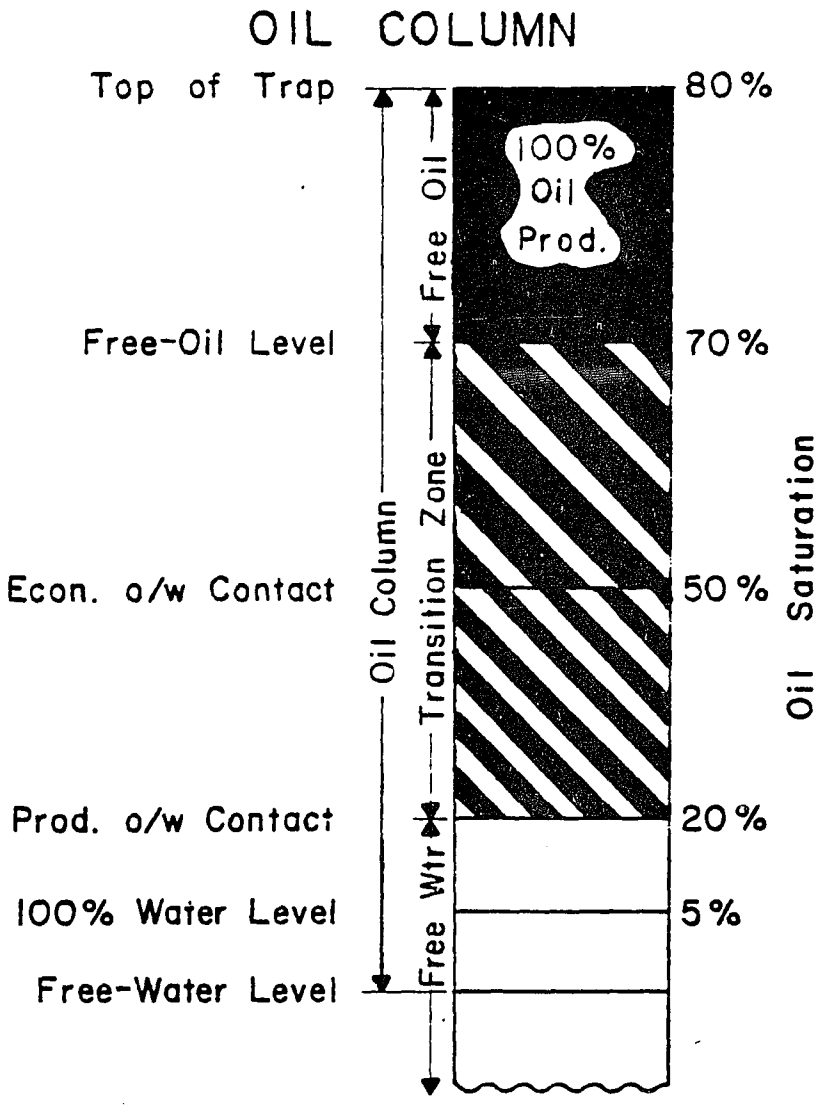
OIL COLUMN
Top of Trap
Free-Oil Level
Econ. o/w Contact
Prod. o/w Contact
100% Water Level
Free-Water Level
Oil Column
Free Oil
Transition Zone
Free Wtr
100%
Oil
Prod.
80%
70%
50%
20%
5%
Oil Saturation

In the section above the oil-water transition zone, the amount of water saturation cannot be reduced farther without excessive pressure gradient. This section is called the region of irreducible water saturation and represents the connate water of the reservoir. Capillarity holds this water in place and flow differentials do not remove it, resulting in 100% oil production in this zone (Calhoun, 1953).

Capillary-pressure curves have been used to calculate the height of an oil column for any given oil saturation above the free-water level (Hobson, 1954; Arps, 1964; Stout, 1964; Jodry, 1972; Schmidt et al., 1977), and to determine the thickness of the transitional and oil-bearing zones, the potential for secondary migration, and the effectiveness of reservoir seals. Jodry (1972) showed that the height of the oil column above the oil-water interface is related to structural and stratigraphic closures, as well as the fluid and petrophysical properties of the reservoir.

2. PREVIOUS WORK

2.1 Capillary-Pressure Curves

The relationship between fluid saturation at a point in a porous body and the capillary pressure at that point, is known as the capillary-pressure curve (Fig. 3).

The role of capillary pressure in the migration and accumulation of hydrocarbons in reservoir rocks was recognized early (Munn, 1909). Experimentally derived capillary pressures for carbonate reservoirs in conjunction with physical properties of the reservoir were used in the classification of pore size and geometry by Purcell (1949), Brown (1951), Archie (1952), and Stout (1964). Thomeer (1960) developed a mathematical description of capillary-pressure curves which reflects differences in pore geometry of samples. This technique is based on the observation that graphical location and shape of a capillary-pressure curve reflect pore-structure characteristics of the rock sample.

Using pore size and capillary pressure, the conditions for oil migration in carbonate rocks were considered by Aschenbrenner and Achauer (1960). Hubert (1953) in a comparable study of clastic rocks suggested that high capillary pressures caused the removal of oil from small pores and its accumulation in larger pores.

FIGURE 3. Relationship of a typical capillary pressure curve to the distribution and production of fluids in a reservoir.

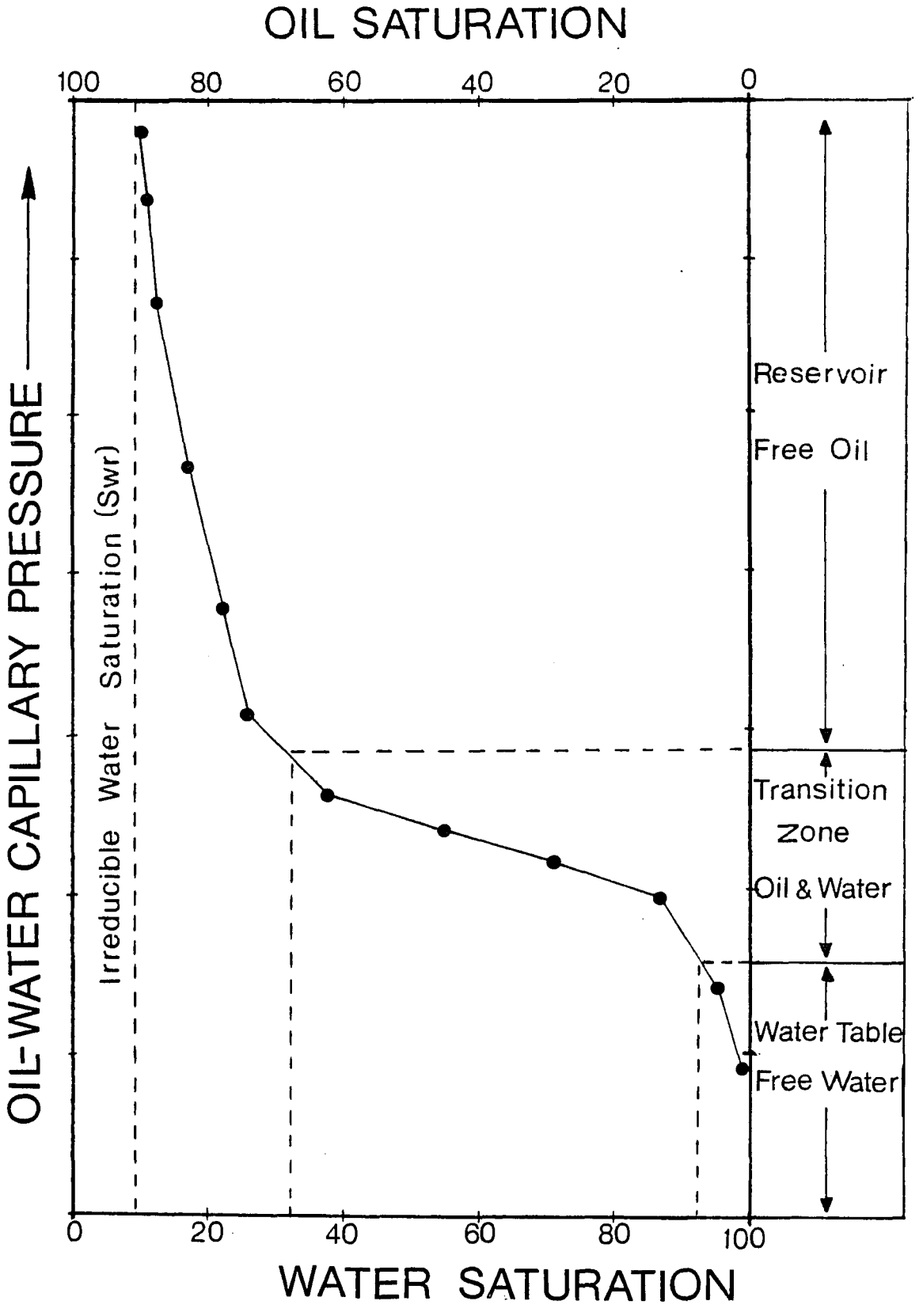
OIL SATURATION
100
80
60
40
20
0
OIL-WATER CAPILLARY PRESSURE
Irreducible Water Saturation (Swr)
Reservoir
Free Oil
Transition
Zone
Oil & Water
Water Table
Free Water
0
20
40
60
80
100
WATER SATURATION

In addition, capillary-pressure curves are used to determine the height of the oil column necessary for secondary migration (Arps, 1964; Stout, 1964; Jordy, 1972). Because capillary pressure must vary with height above the free water table, the capillary-pressure curve shows the relationship of fluid saturation to the height above the free water table (Fig. 3; Calhoun, 1953).

Hobson (1954) and Smith (1966) derived equations (based on the rock and fluid properties) for the height of oil necessary for secondary migration. Jennings (1987) simplified the Smith (1966) equation, for calculating the oil column above the free-water level, using mercury capillary-pressure data.

A new line of investigation on the use of capillarity was initiated by Dullien and Dhawan (1974) and Wardlaw (1976). In their studies, pores and pore throats were identified separately by scanning electron microscopy, stereology, and porosimetry, and the results were used together to predict reservoir conditions.

2.1.1 Capillary-Pressure Curves using Mercury Porosimetry

Mercury porosimetry is the method by which mercury is forced under pressure into the evacuated pores of solids in order to produce capillary-pressure curves for porous media. Mercury acts as a nonwetting agent and may

be considered as equivalent to oil entering a water-wet reservoir, while mercury vapor may be considered as the wetting phase. Mercury-porosimetry was first used and discussed by Purcell (1949).

The mercury injection-withdrawal method does not provide a close analogue for an oil-water system (Wardlaw, 1976), however, it best produces reservoir conditions (Stout, 1964); it is reliable, has good reproducibility (Burdine et al, 1950), and may give a relative indication of the efficiency with which various rock types can expel a nonwetting phase when pressure is reduced (Wardlaw, 1976). In addition, it is a simple and rapid method compared with other direct methods in which typical reservoir fluids are used (Wardlaw and Taylor, 1976).

Oil cannot migrate under hydrostatic or hydrodynamic conditions, unless the displacement pressure exceeds the entry pressure of the pore throats (Aschenbrenner and Achauer, 1960). When displacement occurs, the surface forces (or capillary forces) are responsible for trapping a large portion of the oil phase within the pores of the rock, limiting recovery efficiency (Melrose and Brandner, 1974).

Mercury-capillary-pressure experiments are designed to obtain values for the petrophysical properties of

rocks by injecting a nonwetting liquid (in these experiments mercury) into the pores, and displacing the fluids which saturate the pore interstices. Air or mercury vapor was assumed to be the wetting agent in our experiments.

Mercury forms a 140° contact angle against the solid. The action of the surface forces involved thus opposes the entrance of the liquid into the solid and pressure must be applied to the liquid to cause penetration of the pores (Purcell, 1949).

When capillary-pressure values are plotted against the volume of mercury injected, the resulting curve is known as the mercury capillary-pressure curve (or simply capillary-pressure curve Fig. 4). Mercury capillary-pressure curves are used to estimate hydrocarbon-displacement pressures, irreducible water saturations, permeability, and the thickness of the oil-water transition zone.

Most capillary-pressure curves are divided into three segments: (1) An initial steep part, where little mercury is injected for a relatively large pressure increase; (2) a flattened segment (or plateau) defined by a narrow range of capillary-pressure values (or pore-throat sizes) at which maximum injection of mercury takes place. The change in gradient from 1 to 2 is called the

FIGURE 4. Typical mercury capillary-pressure curve, plotted on a semilog paper; Swi = irreducible water saturation.

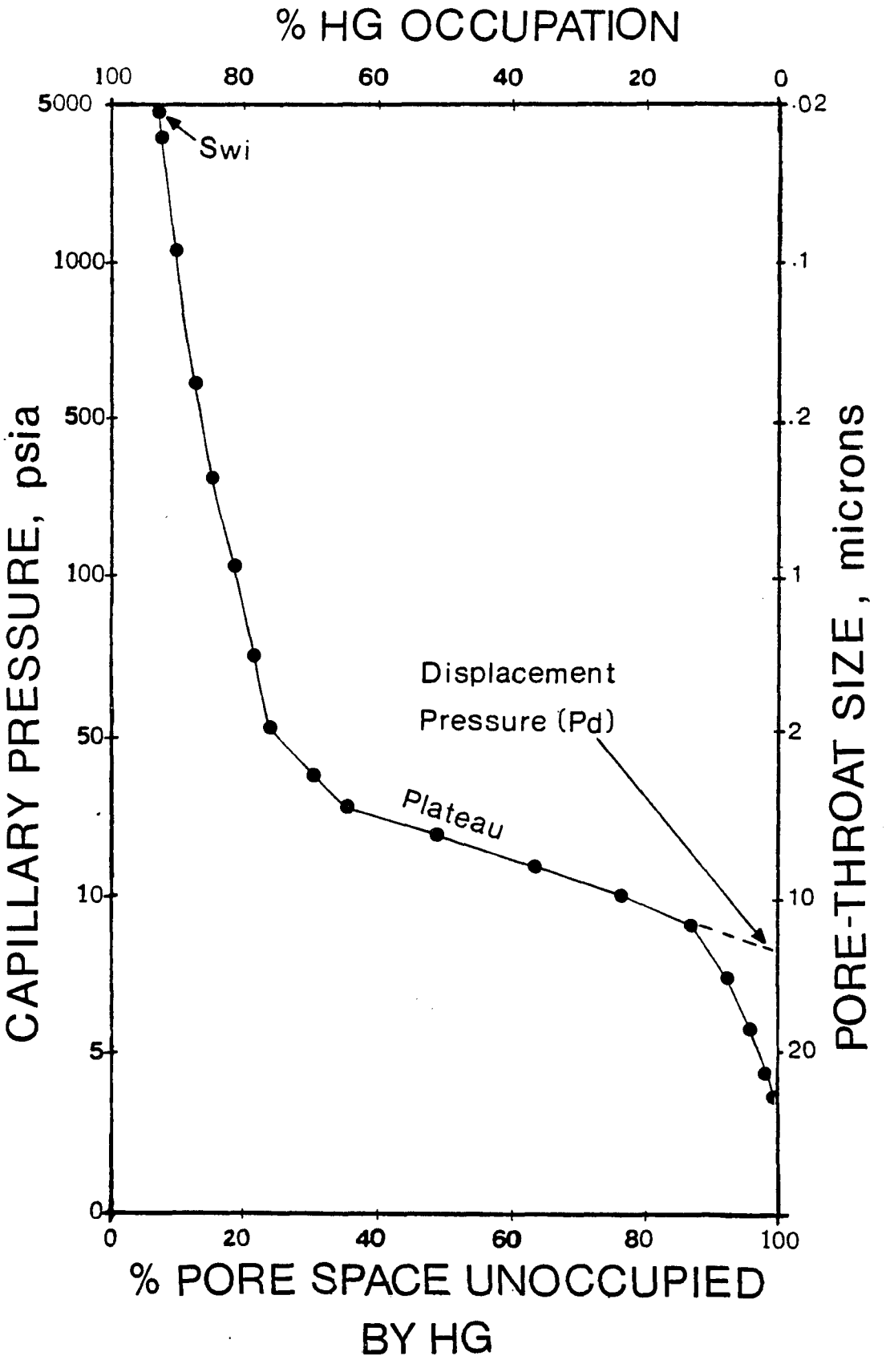
% HG OCCUPATION
100
80
60
40
20
0
5000
1000
500
100
50
10
5
0
.02
.1
.2
1
2
10
20
Swi
Displacement
Pressure (Pd)
Plateau
CAPILLARY PRESSURE, psia
PORE-THROAT SIZE, microns
0
20
40
60
80
100
% PORE SPACE UNOCCUPIED
BY HG

critical pore-throat size or "threshold" injection pressure (Wardlaw, 1976) or displacement pressure (Schowalter, 1979) and is important in estimating reservoir seal capacity. Displacement pressure is a measure of the degree of rock wettability, the oil-water interfacial tension, and the diameter of the largest pore on the exterior of the rock sample (Craig, 1971): As such, it is the pressure which will determine the minimum buoyant pressure needed for secondary migration (Schowalter, 1979); (3) an asymptotic segment, defined by the irreducible minimum of the rock-pore system at the maximum capillary pressure attained. In our experiments, this maximum capillary pressure was 5000 PSI air-mercury. Above this maximum, no farther displacement of air or mercury vapor occurs, and the remaining pores were not invaded by mercury.

2.2 The Fluid-Rock System

The understanding of occurrence, migration, and recovery of hydrocarbons in a reservoir depends upon the knowledge of the reservoir properties (such as porosity, permeability, pore-size distribution, and surface area) and the combined reservoir rock- fluid properties (such as capillary pressure and relative permeability; Craig, 1971).

Hydrocarbon production involves the flow of water, oil, and gas through porous rocks. The rock properties most indicative of fluid flow are porosity (i.e., storage capacity of fluids), permeability (i.e., the ability to transmit fluids), and pore-size distribution (i.e., the capacity to retain fluids selectively; Robinson, 1966). Decisions concerning how economic recovery from a reservoir can be maximized must, therefore, be based on the understanding of the entire reservoir as a conducting system for multiphase fluids. This requires a knowledge of the chemical and physical interactions of fluids within the containing rock-pore system as well as quantitative information about the nature of the flow pathways.

In addition, a knowledge of fluid properties combined with interpretations of depositional environments and diagenetic overprints is a significant tool in hydrocarbon exploration, especially when dealing with simple stratigraphic traps, where there is no structural evidence of their existence (Berg, 1975).

Studies of the petrophysical properties of reservoir rocks include size, shape, sorting, and skewness of pores and throats, and arrangement of pores and throats. From capillary-pressure curves and other petrophysical data, it is possible to derive secondary petrophysical

properties such as aspect ratio (pore- to throat-size ratio), coordination number or connectivity of pores and throats, surface area to volume relationships, and available porosity (Wardlaw, 1976; Dullien and Dhawan, 1974).

Having observed, classified and quantified the essential geometric and topologic properties of pores in rocks, the next step is to understand the interaction of water, oil, and gas with the rocks and to determine wettability characteristics which govern the relative importance of various pore-fluid variables to oil and gas recovery. Hydrocarbons in a reservoir may initially be a continuous and flowing phase, but as waterflooding progresses and water saturation increases, the oil becomes disconnected and trapped. Recovery efficiency is controlled by the degree and type of these "disconnecting" events.

2.2.1 Study of the Pore System

The objective of carbonate-reservoir description is to recognize and quantify the properties of the rock-pore system which affect fluid flow under specified conditions. This requires characterization of individual pores to scales approaching those of reservoirs.

As scale is increased from the microscopic to the macroscopic, new types of heterogeneities appear and there may be no scale at which the carbonate reservoir can be considered homogeneous (Morrow and Heller, 1985). For this reason, an appreciation of the heterogeneous nature of carbonate reservoirs requires refined predictions based on sedimentologic models and the understanding of stratigraphic and structural relationships in combination with the interpretation of petrophysical data and capillary-pressure gradients.

2.2.2 Pore-System Characterization

The pore system in a rock is a conceptualized ideal arrangement of (1) void spaces (i.e., pores) which may be interconnected by (2) micron-sized channels called pore throats or necks (Fig. 5a,b).

The size and shape of the pores, roughness of the pore surface, length of the pore throats, number of throats per pore, and whether pore throats are interconnected or isolated need to be established experimentally. Some of these properties (i.e., pore size and shape, number of throats per pore, and roughness of pore surface and throat surface) are directly observable through SEM and light microscopy. Others must be experimentally determined from theories designed

FIGURE 5. Schematic diagram of a pore-system network (diagram a), consisting of pores (A, B, C) and pore throats (T_1, T_2, T_3) having diameters d_1, d_2, and d_3 respectively. With progressive pressure increase (diagram b), mercury invades first the larger-diameter pore throats (T_1 at P_1), secondly the intermediate-diameter pore throats (T_2 at P_2), and finally the smaller-diameter pore throats (T_3 at P_3). The mercury-capillary pressure curve (diagram c) relates the percent volume of mercury (V_1, V_2, V_3) occupying the pore system to pressure (P_1, P_2, P_3) and pore-throat diameters (d_1, d_2, d_3) respectively (Ghosh and Friedman, 1989)

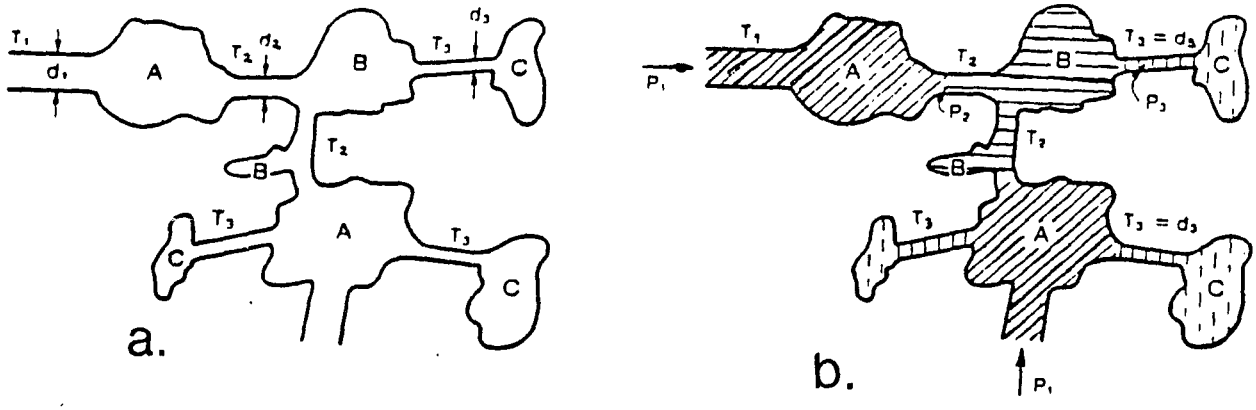

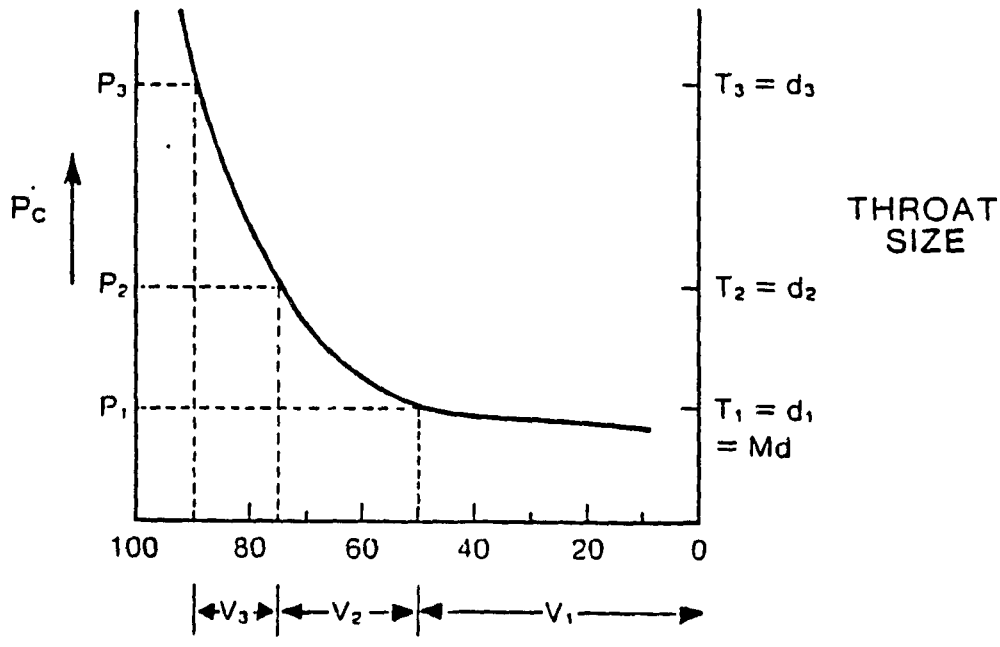

C. % VOLUME OF Hg OCCUPATION

specifically for the identification of petrophysical properties (Wardlaw, 1980; Dullien, 1979).

Properties such as available porosity, pore-throat geometry, permeability, and pore-throat size ratios may be derived experimentally using mercury porosimetry-derived capillary pressure gradients. The relationship between capillary pressure, pore-throat size, and volume of mercury occupying the pore spaces is shown in figure 5. At capillary pressure P_1 the largest diameter (d_1) pore throats are invated by mercury, filling pores A. At higher capillary pressure P_2, smaller pore-throat diameters (d_2) are invated by the mercury, filling pores B. At still higher capillary pressure P_3 even smaller pore-throat diameters (d_3) are invated by mercury, filling pore spaces C. In this hypothetical case, 90% of the pore space is occupied by mercury (i.e., V_1, V_2, V_3), indicating 10% irreducible water saturation.

Capillary-pressure studies give information on the geometrical properties of the throats, not on the volume of pores. Values for porosity and pore volume obtained from mercury porosimetry analyses yield the total volume of pores, but no information concerning their size range. Direct view of the pore system, through SEM and and resin pore casts, is necessary to properly define the pore-system characteristics, otherwise data obtained

exclusively from mercury porosimetry-derived capillary pressure curves may give erroneous values for the volume of pore throats.

2.3 Petrophysical Properties of Carbonate Reservoirs: Heterogeneities and Complexities

The carbonate rocks in this study are characterized by porosity developed diagenetically through dolomitization and solution processes. Carbonate rocks, however, are heterogeneous and do not exhibit any simple relationship between porosity and permeability development. The distribution and size of pores within carbonate rocks has no direct or predictable relationship and may vary greatly over short distances both laterally and vertically (this work; Jardine et al, 1977; Reitzel and Callow, 1977). Carbonate rocks are subject to leaching by diagenetic fluids. In such examples, pore size and distribution may conceivably have little or no direct relationship to the particle size or density of the original sediment, as generally holds for clastics.

Carbonate rocks are particularly susceptible to replacement. If calcium is replaced by mineralogically more stable magnesium, to form dolomite, a 13% increase in porosity and permeability may result, because magnesium ions are smaller in size than calcium ions.

This increase in porosity and permeability is mostly true in metamorphic rocks. In sedimentary rocks this relationship is unpredictable. A carbonate may be composed entirely of dolomite and have less than 1% porosity.

In general, however, rocks with low dolomite concentration have low porosity, low permeability, and poor pore-space sorting. Better reservoir properties appear to be associated with higher dolomite content (Robinson, 1966).

Porosity and pore size increase as dolomitization approaches completion. Dolomitization, however, does not begin to produce appreciable porosity until more than 70% of the rock becomes dolomitized (Murry, 1960). When the replacement process is complete, the original porosity and permeability may be vastly altered.

Wayhan and McCaleb (1969), in their study of the Madison carbonate reservoir of Elk Basin Field, Montana and Wyoming, Concluded that porosity zonation resulted from (1) differential depositional environments, (2) variations in the degree of dolomitization, (3) later erosion and solution of the reservoir rocks, and (4) various amounts of ground-water leaching and remineralization.

Recognition of rapid lateral and vertical variations

of porosity and permeability in carbonate reservoirs is necessary in order to understand reservoir performance.

2.3.1. Petrophysical Properties of Dolostone Reservoirs

Pore spaces in dolomitized carbonates are defined mainly by dolomite crystal faces and intercrystal boundaries. Consideration of the mode of dolomite growth is thus important before describing the pore system. The complexity of pore geometry and amount of pore space are inversely proportional to the ability of dolomite crystals to grow (Fig. 6). Inhibition of crystal growth is thus of fundamental importance in porosity preservation (Wardlaw, 1976).

Dolostones consisting of a mosaic of rhombohedral crystals (i.e., sucrosic texture) have optimum reservoir properties, which include high porosity and permeability values. Individual pore spaces (i.e., dolomite intercrystalline pores) are well sorted, and defined by polyhedral, randomly oriented, planar crystal faces, which are welded at points of contact. The sizes of the intercrystalline pores are related to the sizes of the containing rhombohedra, and pore throats are large and numerous in relation to the pores (Fig. 6; Robinson, 1966; Wardlaw, 1976).

Where dolomite growth continued, a more interlocking

FIGURE 6. Changes from polyhedral to tetrahedral to interboundary-sheet pores that accompany progressive growth of dolomite crystals. Porosity and pore-throat size are inversely proportional to the ability of dolomite crystals to grow. The mercury-injection curves associated with each type of pores indicate higher capillary pressures are required for sufficient mercury to be injected.

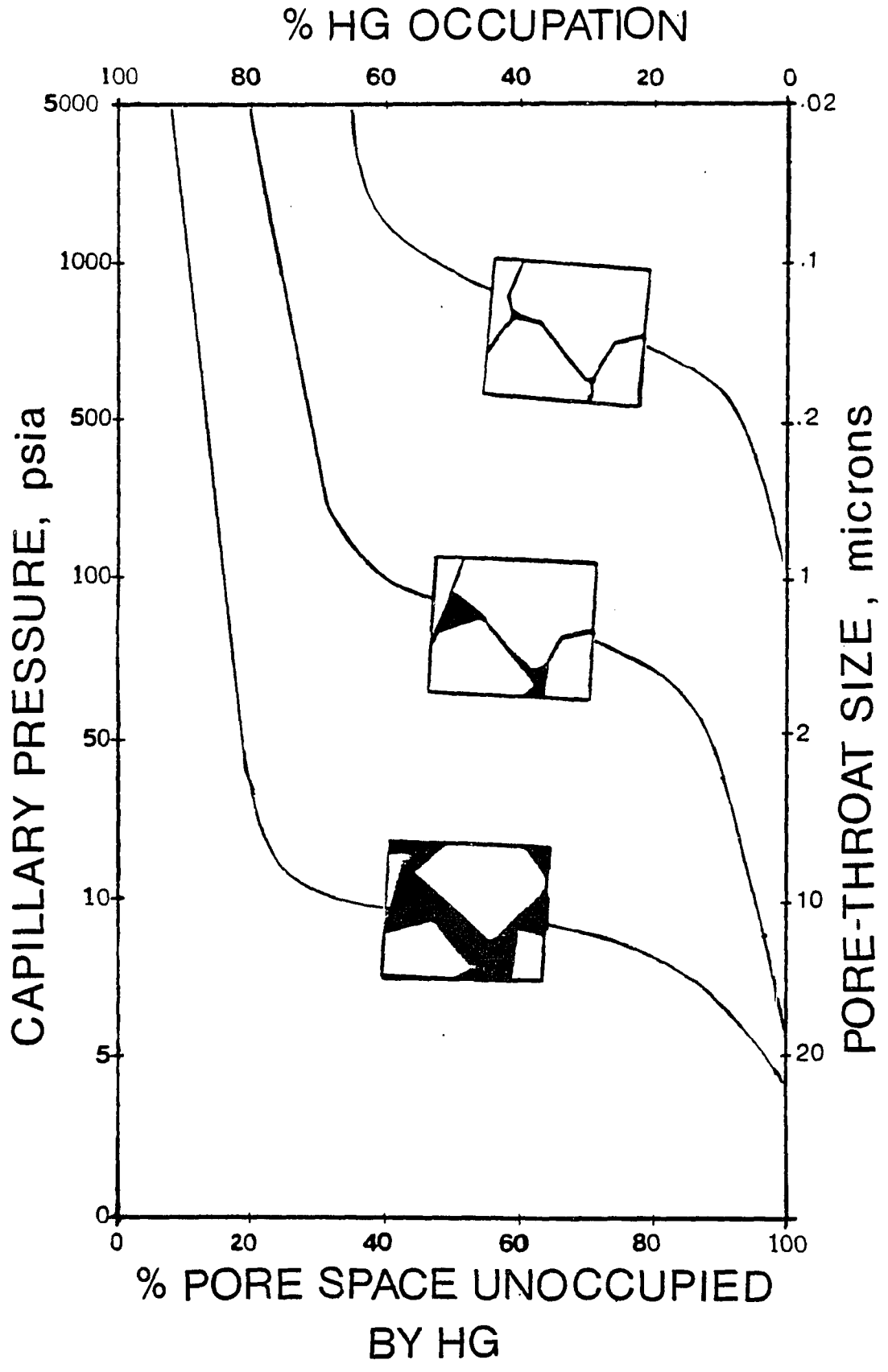
% HG OCCUPATION
100
80
60
40
20
0
5000
1000
500
100
50
10
5
0
.02
.1
.2
1
2
10
20
CAPILLARY PRESSURE, psia
PORE-THROAT SIZE, microns
0
20
40
60
80
100
% PORE SPACE UNOCCUPIED BY HG

texture develops, planar compromise boundaries form, rhombohedral form is lost, and the intercrystalline pores are reduced in size and geometric complexity. Simplified, more poorly sorted tetrahedral pores, connected by interboundary-sheet pores are common in lower porosity dolostones (Fig. 6; Bathurst, 1975; Wardlaw, 1976).

With further progressive growth, dolomite crystal boundaries meet at triple junctions, and the tetrahedral pore spaces are eliminated. The only pore spaces remaining at this stage are thin (only a few microns thick), sheet-like spaces at crystal boundaries (Fig. 6). The formation of sheet-like pores or compromise boundaries increases the pore-to-throat-size ratio for the rock, which in turn reduces efficiency for a nonwetting phase (i.e., decrease in mercury-injection efficiency; Bathurst, 1975; Wardlaw, 1976).

3. GEOLOGIC HISTORY OF THE SMACKOVER FORMATION

3.1 Area of Study and Production History of the Smackover Jay Field Reservoir

The Smackover Formation of the Gulf Coast Basin (Fig. 7) was chosen for this study because it contains deeply buried hydrocarbon reservoirs producing predominantly from dolostones.

The examined areas and well-depths include Escambia county, Alabama (15,571- 15,629 ft.), Escambia County, Florida (16,329-16,448 ft.), Santa Rosa County, Florida (15,586-15,779 ft.), Santa Rosa County, Florida (15,389-15,747 ft.), and Santa Rosa County, Florida (15,295-15,702 ft.; Table 1, Figs. 7 and 8) as well as numerous well logs within Jay field.

In Mississippi, Alabama, and Florida, 121 Smackover fields and pools have been discovered (through December 1984) and have resulted in the production of more than 569,800,000 barrels of oil, 63,700,000 barrels of condensate, and 1,500,000,000 thousand cubic feet (MCF) of gas. Two recent (1986) Smackover discoveries in northern Florida, east and west of the study area, have boosted interest in the Smackover Formation of the Florida Panhandle (McCaslin, 1987).

FIGURE 7. Generalized map of the Smackover and Buckner lithofacies along the United States Gulf Coast (from Crevello and Harris, 1984). The enlarged section (from Mancini and Benson, 1980) shows the regional paleogeographic features surrounding the Conecuh Embayment during the time of deposition, and the location of Jay field.

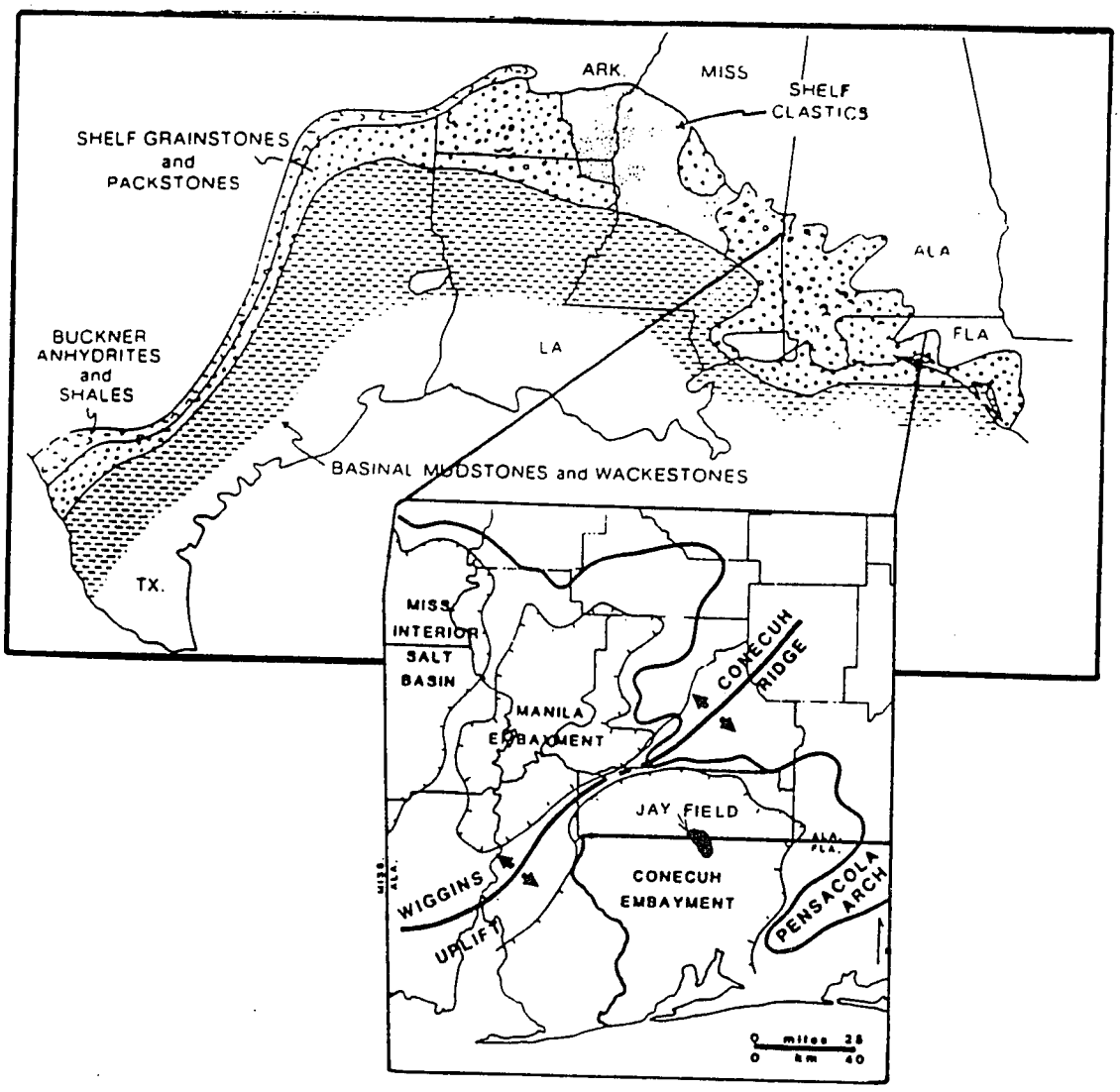
ARK.
MISS
SHELF CLASTICS
SHELF GRAINSTONES and PACKSTONES
ALA
FLA
LA
BUCKNER ANHYDRITES and SHALES
BASINAL MUDSTONES and WACKESTONES
TX.
MISS. INTERIOR SALT BASIN
MANILA EMBAYMENT
CONECUH RIDGE
JAY FIELD
ALA.
FLA.
MISS.
ALA.
WIGGINS UPLIFT
CONECUH EMBAYMENT
PENSACOLA ARCH
miles 25
0 km 40

TABLE 1. Well cores studied.

Core No.	Company	Well Name	Location (Sec. T. R.)	Interval (ft)
1	Cities Service	Brown 32-8	32 2N 6E Escambia Co	15,571-15,629
2	Cities Service	Lizenby 5-3	5 5N 32W Escambia Co	16,329-16,448
3	Humble	McDavid Lands 7-1 (Jay field)	7 5N 29W Santa Rosa Co	15,295-15,640
4	Humble	C.H. Bray 10-4 (Jay field)	10 5N 29W Santa Rosa Co	15,389-15,747
5	Humble	Sam Watson 23-4 (Jay field)	23 5N 6E Santa Rosa Co	15,586-15,779

FIGURE 8. Well location map, major oil and gas fields and structural features of the Jay Trend (from Sigsby, 1976). Table 1 gives the names, depth and location coordinates of wells 1 through 5 shown in this map.

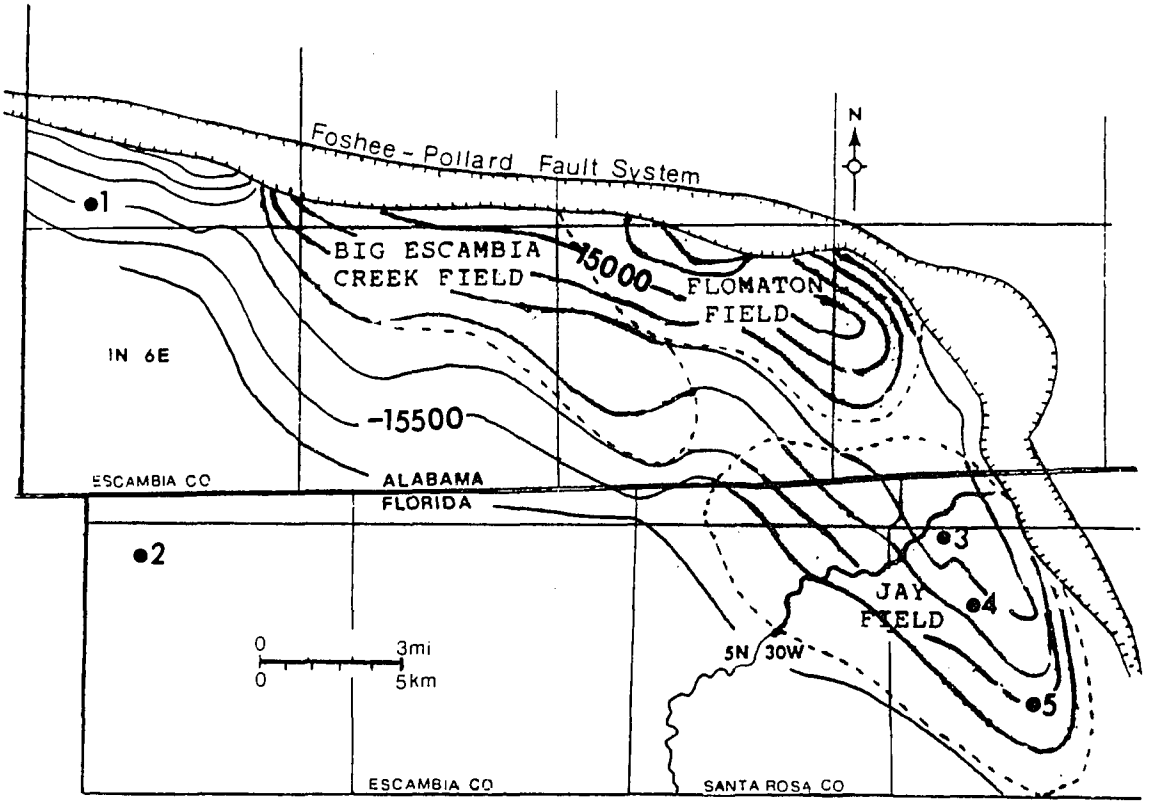
Foshee - Pollard Fault System
N
●1
BIG ESCAMBIA
CREEK FIELD
-15000
FLOMATON
FIELD
IN 6E
-15500
ESCAMBIA CO
ALABAMA
FLORIDA
●2
●3
JAY
FIELD
●4
0 3mi
0 5km
5N 30W
●5
ESCAMBIA CO
SANTA ROSA CO

The largest field in the tri-state area is Jay field located in northwest Florida, 35 miles north of Pensacola (Figs. 8 and 9). The field was discovered in June 1970 by Exxon Co., U.S.A., and contained 730 million STB of Original Oil In Place (OOIP). Ultimate recovery was predicted at 47.5% of OOIP or 346 million STB. Since then it has produced over 359 million STB of oil and 426,300,000 MCF of gas (Shirer et al., 1978; Mink, Bearden, and Mancini,1985). Jay field alone accounts for 71% of Florida's total oil production. Special emphasis is given in this study to the petrophysical properties of the reservoir facies of Jay field.

The Jay field reservoir produces from dolomitized carbonates found approximately 1,500 ft (or 5 km) below surface. The field (Figs. 8,9), located on the downthrown side of the extensional post-Smackover (Kimmeridgian) Foshee fault system, is a combination stratigraphic, diagenetic, and structural trap, intergrading favorable stratigraphy and diagenesis as well as extensional faulting and salt movement.

Hydrocarbon production occurs on the southern plunge of a large subsurface anticline with the updip (northern) trap formed by a facies change (from dolomitized porous grainstones to dense micritic limestones; i.e., "updip facies pinchout") perpendicular

FIGURE 9. Jay field structure-contour map contoured on top of the Smackover formation, compiled from Jay-LEC Unit Geological Committee (1974). Note the location of studied wells 3, 4, and 5 listed in Table 1.

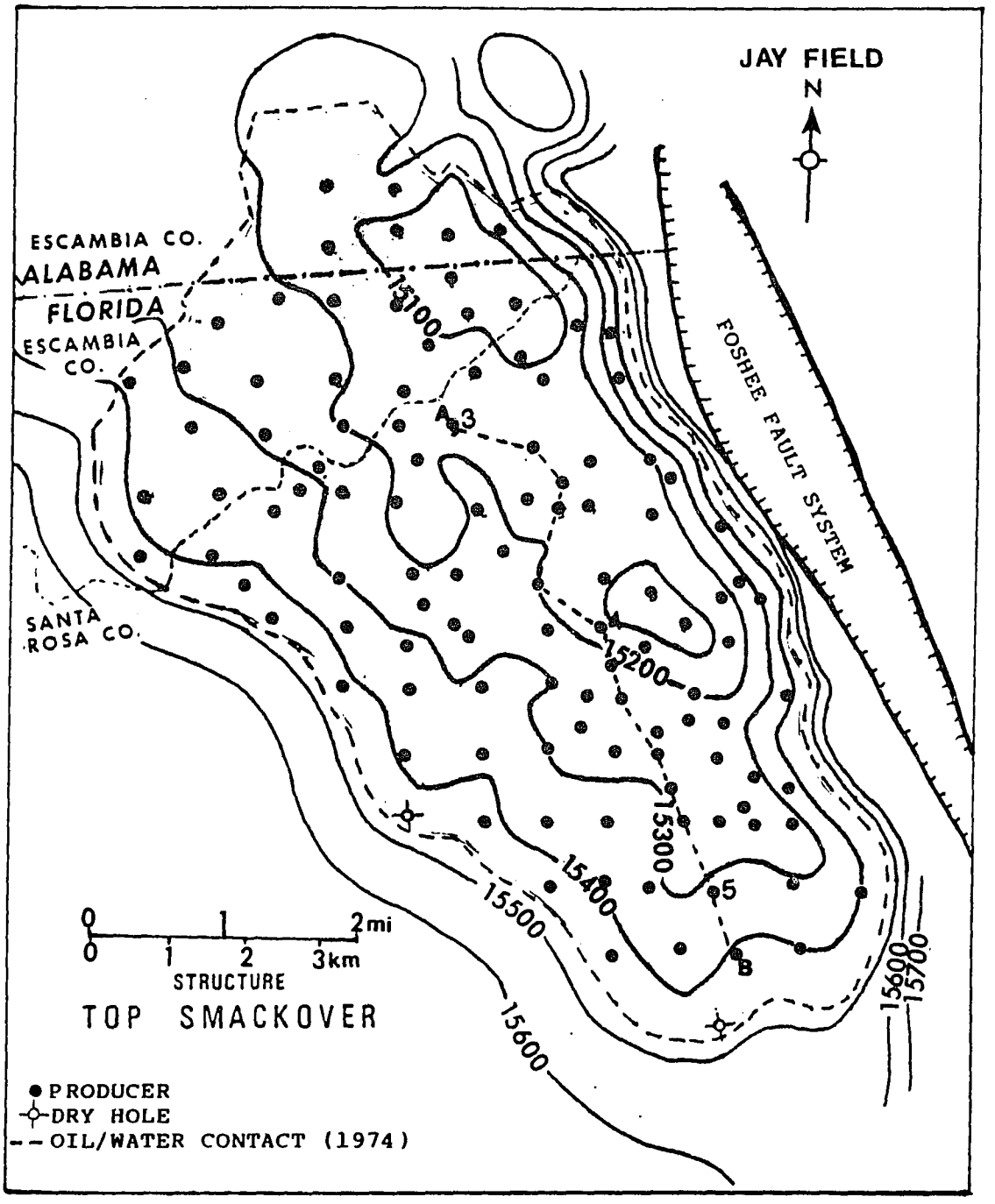
JAY FIELD
N
ESCAMBIA CO.
ALABAMA
FLORIDA
ESCAMBIA CO.
SANTA ROSA CO.
FOSHEE FAULT SYSTEM
15100
15200
15300
15400
15500
15600
15700
A3
5
B
0 1 2mi
0 1 2 3km
STRUCTURE
TOP SMACKOVER
PRODUCER
DRY HOLE
OIL/WATER CONTACT (1974)

to strike.

Movement on the downthrown fault block caused "roll-over" closure in the eastern part of the field, which resulted in an abrupt increase of dip. Paleoenvironmental analysis indicates, however, that some structure-induced paleogeographic high was present prior to faulting. This high might have been caused by salt movement prior to deposition of the upper Smackover (Sigsby, 1976).

The average pay thickness is 98 feet (32 meters), and extends over an area seven miles (4.35 km) long and three miles (1.85 km) wide. Porosities within the reservoir range from less than 8% to 31%, with an average of 15%, whereas permeability .pn44 averages 35 millidarcies (Ottmann et al, 1974).

Early drilling indicated that oil was contained in a pressure-depletion reservoir, requiring the development of early pressure-maintenance programs. The rapid reservoir-pressure decline was arrested by water injection which began in March 1974, soon after completion of the field. Most injection wells as well as production wells were acid fractured to create connecting vertical fracture systems between productive layers and increase the amount of recoverable oil (Shirer et al., 1978).

Oil from primary and secondary recovery is expected to exceed 51% of OOIP (original oil in place) or 373 million STB (stock-tank barrels). In January 1981 a miscible gas displacement project began, using available field methane gas. High-pressure nitrogen gas injection began in December 1981 (Langston et al., 1981).

The reservoir is currently under mature water flood and early tertiary operations, where energy is furnished by a combination of water flooding and injection of nitrogen gas. Miscible gas and water will be injected for about 12 years, until 20% of hydrocarbon pore volume (HCPV) of gas has been injected. Water will then be injected for an additional 8 years. Ultimate recovery is expected to reach 57% of OOIP or 420 billion STB (Langston and Shirer, 1985).

3.2 Structural Framework

The Gulf Coast Basin is a large bathymetric depression, roughly outlined by the updip limits of the Jurassic sediments, which originated in the early and middle Mesozoic accompanying the breakup of Pangea. Specifically, the Gulf originated as a result of the opening of a sphenochasm and left lateral displacement of the central part of the eastern mobile belt along two or three megashears, all of which were related to crustal

rifting and separation of the North American plate from the South American-African plate (Walper and Rowett, 1972).

As the continents separated, several marginal basins developed in the Early and Middle Jurassic along the northern edge of the growing Gulf of Mexico. Continuing tectonic activity led to basin restriction and deposition of an extensive evaporite sequence (the Louann Belt), while continuing subsidence led to shallow marine deposition in the Late Jurassic on a southeasterly tilting basement (Beall, 1973; Rogers, 1984).

Evidence for gulfward basement tilting throughout the Mesozoic Era, from elevations of a few hundred feet at the outcrops to estimated depths below -40,000 feet (-13.3 km) under the Gulf of Mexico, is shown by the gradual thickening of most sedimentary units in that direction (Beall, 1973).

The study area is located in the Conecuh Embayment. Marine deposition was influenced by major pre-Jurassic structural features, which include the Wiggins-Conecuh Ridge and the Pensacola Arc (see Figure 7). These tectonic highs influenced deposition of the Louann Salt and probably served as sources for the Norphlet Jurassic sands, underlying the Smackover Formation (Fig. 10; Sigsby, 1976).

While the origin of the Pensacola Arc is uncertain, the Wiggins-Conecuh Ridge, of Mississippian age, probably represents a continental block that formed during rifting or a southwestward extension of the Appalachian structural front (Mancini et al., 1985). This ridge formed the northern margin of the basin during the early stages of subsidence, and was probably located within a zone of crustal weakness, along which a hinge line developed, and early basin subsidence and deposition took place (Wilson, 1975).

3.3 Stratigraphic Framework

Shown in figure 10 is the Triassic and Jurassic stratigraphic column of the United States Gulf Coast. In the Florida Panhandle the Louann Salt is overlain by intertidal, lacustrine, and eolian sands of the Norphlet Formation. Above the Norphlet is the Upper Oxfordian Smackover carbonate sequence, which is conformably overlain by the Buckner sabkha evaporites. On top of the Buckner Formation is the Haynesville Formation of the Cotton Valley Group, which consists mostly of terrigenous clastics interbedded with evaporites. The sequence is capped by the fine- and coarse grained-clastics of the Cotton Valley Group (i.e., Bossier and Schuler Formations).

FIGURE 10. Stratigraphic column for the Triassic and Jurassic Epochs of the United States Gulf Coast (Crevello et al., 1985).

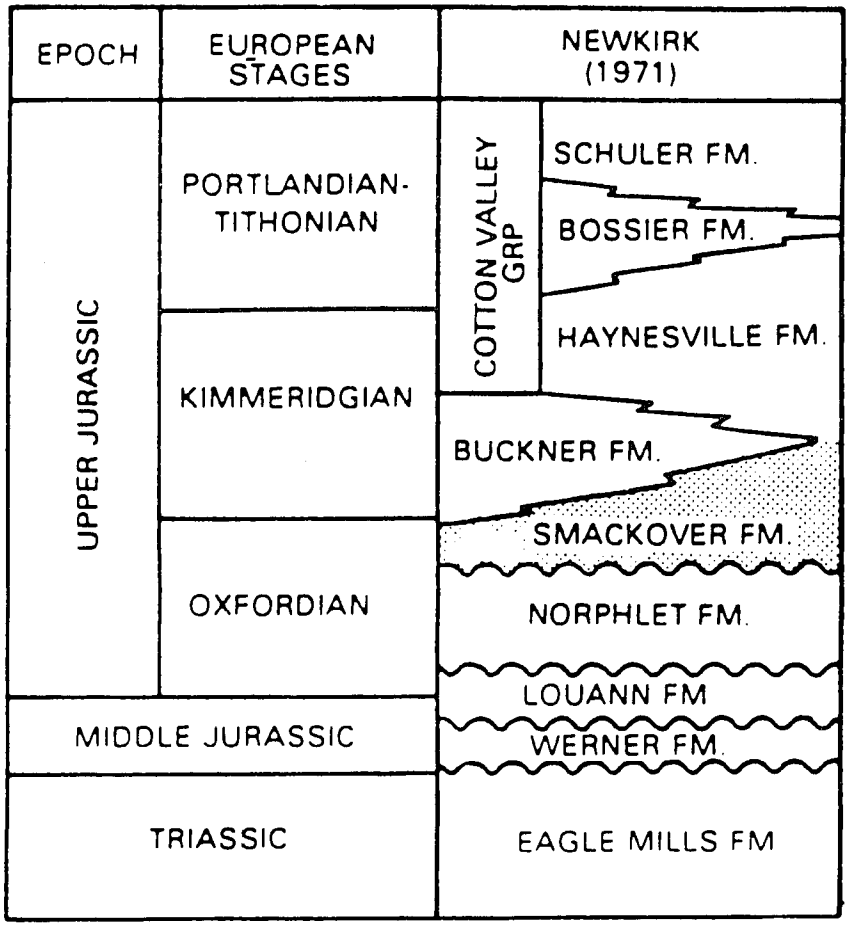
EPOCH
EUROPEAN STAGES
NEWKIRK (1971)
UPPER JURASSIC
PORTLANDIAN-TITHONIAN
KIMMERIDGIAN
OXFORDIAN
COTTON VALLEY GRP
SCHULER FM.
BOSSIER FM.
HAYNESVILLE FM.
BUCKNER FM.
SMACKOVER FM.
NORPHLET FM.
LOUANN FM
WERNER FM.
MIDDLE JURASSIC
TRIASSIC
EAGLE MILLS FM

The Smackover Formation of the study area can be subdivided into a lower member of low-energy laminated mudstones and pelletal wackestones, and an upper member of moderate- to high-energy ooid and peloidal carbonate sands. The carbonate sands change gradationally updip into moderate-energy backshoal wackestones and supratidal evaporites and red beds of the Buckner Formation (Fig. 11).

The lower Smackover lithofacies represent a marine transgression over the Norphlet intertidal, lacustrine, and eolian sands. Upward change from laminated mudstones and pelletal wackestones to well-sorted grainstones records part of a regressive sequence. Deposition of the overlying Buckner evaporites in a supratidal sabkha setting, followed by subaerial detrital sedimentation of the Haynesville Formation, completes the regressive sedimentation phase.

Log information for nine wells was used to construct a stratigraphic crossection of Jay field (Fig. 12). The wells are located on a north to south trend within Jay field (Fig. 9, A-B crossectional line). Neutron and gamma-ray logs were selected for this facies correlation because they most clearly illustrate distinct responses for reservoir, nonreservoir, and caprock facies.

Figure 12 is a northwest-southeast crossection

FIGURE 11. Idealized vertical sequence of the Smackover depositional system, Conecuh Embayment.

ROCK UNIT	SEDIMENTARY ENVIRONMENT	GENERAL SEQUENCE	LITHOLOGY
BUCKNER FORMATION	Supratidal Sabkha		Red beds and evaporites
SMACKOVER FORMATION	Backshoal		Wackestone with oncoids, ooids, and pellets
	Barrier Shoal	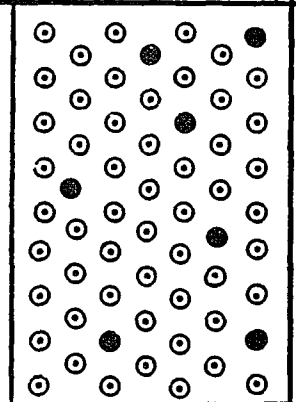	Grainstone with ooids and peloids
	Upper Intertidal to Shallow Subtidal	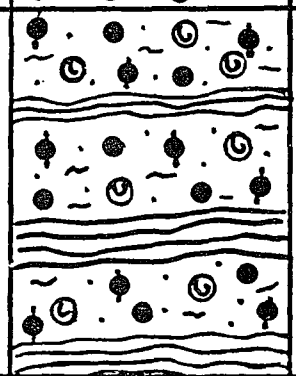	Laminated mudstone alternating with wispy laminated wackestone with pellets, peloids, oncoids, and rare skeletal debris
NORPHLET FORMATION	Intertidal and Terrestrial	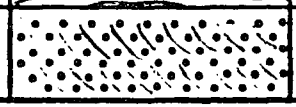	Crossbedded quartz sand grainstone

FIGURE 12. North to south (A to B) stratigraphic correlation of the Smackover Jay field, based on neutron and gamma-ray logs. The site of the section is shown in figure 9.

A – B

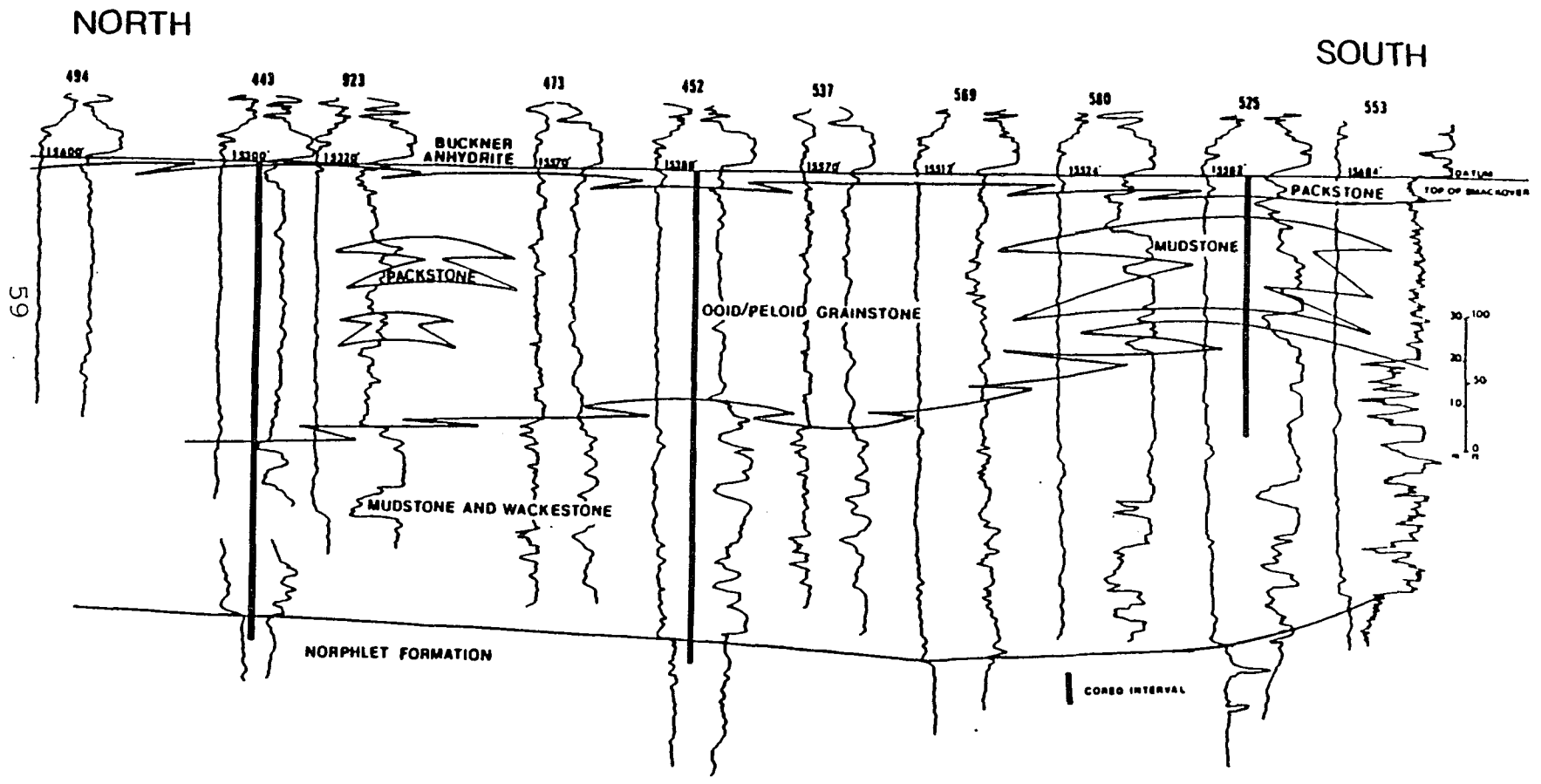
NORTH
SOUTH
494
443
923
473
452
537
589
580
525
553
BUCKNER ANHYDRITE
PACKSTONE
MUDSTONE
OOID/PELOID GRAINSTONE
MUDSTONE AND WACKESTONE
NORPHLET FORMATION
CORED INTERVAL
PACKSTONE
TOP OF BRACKOVER

through Jay field. The lower boundary of the Buckner anhydrite was used as a subsea datum, because its physical properties are distinctive. The anhydrite has negative neutron porosity values, and as such, it has distinctive log signature. This ahnydritic peritidal facies caps the Smackover Formation throughout the field, and acts as a barrier to fluid migration.

The reservoir grainstone directly underlying the caprock facies thickens to the north, whereas the lower Smackover nonreservoir facies thicken to the south. The reservoir facies generally has characteristically smooth gamma-ray and neutron log signatures, indicating uniform lithology and constant petrophysical characteristics. This uniformity is disrupted where layers of lower porosity and permeability are incorporated within the reservoir (Fig. 12, wells 923, 969).

3.4 Sedimentologic Framework

During the Late Jurassic (Oxfordian) a carbonate ramp controlled deposition in the Gulf Coast region. The Smackover Formation on which this study is focused is a major sedimentary sequence deposited on this gently sloping carbonate ramp (Ahr, 1973). It surrounds the Gulf of Mexico and lies in the deep subsurface along the northern Gulf Coast Basin from Texas to Florida (Fig. 7).

On a regional scale the Smackover Formation forms a 300 feet (100 m) thick belt of shelf oolitic grainstone, about 50-130 miles (30-80 km) wide with a narrow slope facies of peloidal bioclastic wackestone. This belt grades gulfward into a much thicker basinal facies 900-1,800 feet (300-600 m thick) of dark colored lime mudstone or wackestone (missing from the studied cores) which contains pelagic and crinoid fossil fragments and fecal pellets (Bishop, 1968; Budd and Loucks, 1981; Mitchell-Tapping 1984).

As the shoreline migrated seaward possibly due to lateral accretion by storms and/or sea-level lowering, shallow-water facies came to overlie deeper-water facies producing a shallowing-upward sequence. The end of Jurassic carbonate deposition was marked by the progradation of the Buckner coastal sabkha evaporites over the top of the Smackover lithofacies (Fig. 11). A modern analogue for such carbonate deposition in an arid climatic setting is the Trucial Coast of the Persian Gulf.

Local deposition of the Smackover Formation was significantly influenced by a number of topographic highs, present throughout Smackover time. Such features essentially divided the Smackover depositional basin into smaller sub-basins, one of which is the Conecuh Embayment

(Fig. 7). These sub-basins and the paleotopographic highs that separated them were responsible for a very irregular pattern of lithofacies distribution.

The Conecuh Embayment (Fig. 7) is a large shallow basin which was flooded by transgression of the sea over the eolian and intertidal sands of the Norphlet Formation. It is bounded on the northwest by the Wiggins-Conecuh Ridge and on the southeast by Pensacola Arc. Early differential subsidence of the basement and local structural features had a marked influence on the thickness and distribution of accumulating sedimentary deposits (Wilson, 1975).

Depositional conditions in the Conecuh Embayment show significant evidence of restriction. The lower Smackover interval consists of oncolitic and peloidal wackestone/packstone interbedded with laminated mudstone (Fig. 11). This sequence grades upward into dark-gray, laminated mudstones (missing from the studied cores), which are overlain by peloidal wackestones and packstones of the upper part of the Smackover interval. Oolitic grainstones occur locally, commonly on paleobathymetric highs (Benson and Mancini, 1984).

Reservoir-grade porosity is restricted to the upper Smackover peloidal or oolitic grainstone/packstone deposits (Fig. 11) and is greatest where these deposits

are dolomitized. The importance of dolomitization to overall reservoir development is well- illustrated in the Big Escambia Creek-Flomoton Field areas (Fig. 8) where upper Smackover carbonates are dolomitized and gas is productive on top of the structure and nondolomitized and nonproductive off the structure (Bradford, 1984).

The Smackover Formation has a very complex diagenetic history, the sequence and timing of which are very important. Reservoir-grade porosity is restricted to the high-energy shoal environment (i.e., oolitic grainstones and packstones), and consists of solution-enlarged, primary interparticle, moldic, and intercrystalline (dolomite) porosity. The core sections with the highest porosity are almost all dolomitized.

Moore and Druckman (1981) recognized a distinct north-to-south diagenetic gradient in the upper Smackover grainstone, which is apparently related to regional differences in burial and mineral-stabilization history. This gradient, present in Arkansas and Louisiana, is expressed as regional changes in secondary carbonate-rock textures and fabrics and is divided into three zones, northern, transitional, and southern, each of which has a unique suite of diagenetic characteristics.

4. RESEARCH EQUIPMENT AND METHODS

4.1 Research Equipment

4.1.1 Petrographic Microscope

A Leitz Wetzlar Ortholux microscope, equipped with a Leitz Orthomat automatic 35mm camera system for high resolution photomicrography in both plane and polarized light, was used for this study. This microscope was the basic research instrument for petrographic thin-section study. Several binocular microscopes were employed for sample analysis and preparation.

4.1.2 Mercury Porosimeter

A Micromeritics 9305 Pore Sizer was used in studies of pore-throat geometry for the purpose of reservoir rock characterization (Fig. 13). Mercury is injected into samples at pressures ranging from 0.5 to 5,000 psia. The equipment also has the capability of accurately measuring extrusion (mercury recovery) data from 5,000 down to 14 psia. This equipment has been used primarily for the characterization of reservoir rocks.

In addition to the porosimeter, a high-speed centrifuge, convection warming oven, and precision balance were used in sample preparation.

FIGURE 13. Schematic diagram of the Micromeritics mercury Porosimeter (Pore Sizer Model 9305) used in this research. A are the low-pressure ports for penetrometer B containing the rock sample to be analyzed. C is the high-pressure chamber, E and D are controls for high pressure manipulations. G is the on/off switch, F is the control panel, and H are the pressure and mercury intrusion/withdrawal displays (from Ghosh and Friedman, 1989).

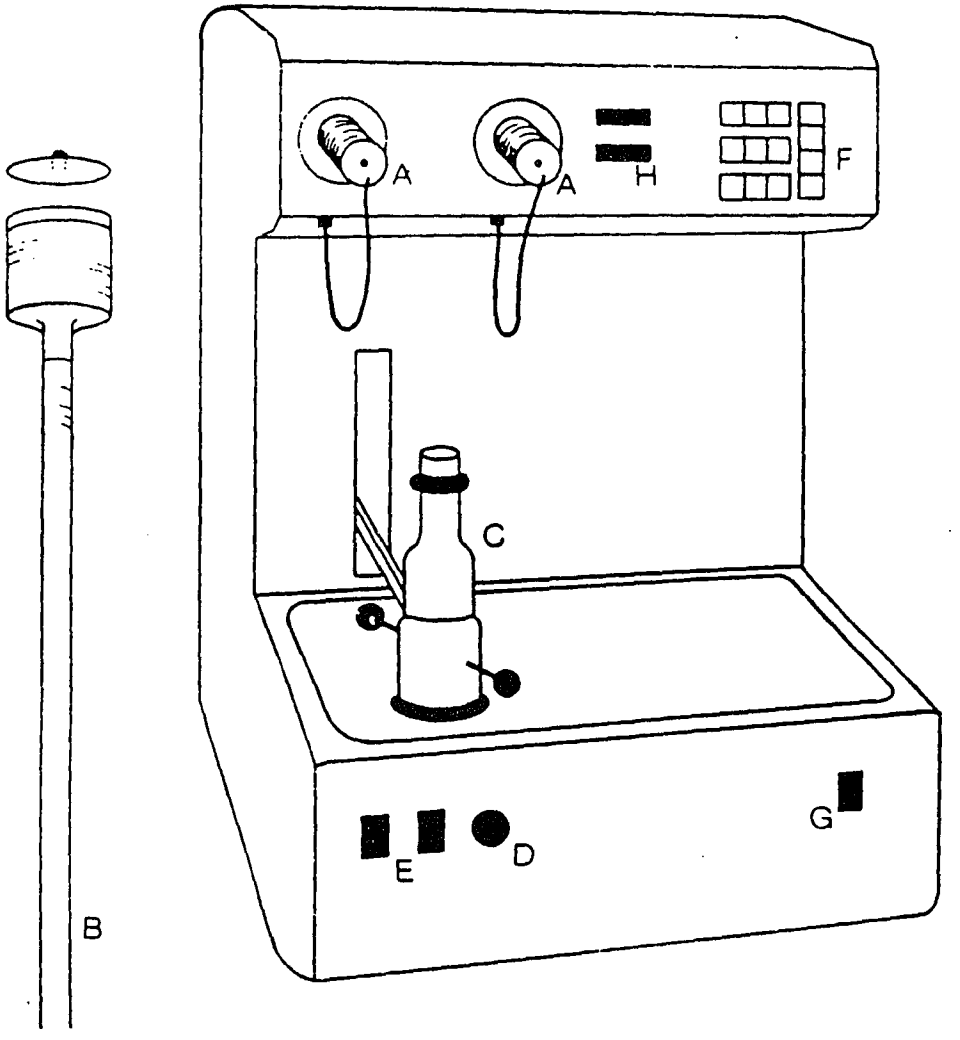
A
A
H
F
C
G
E
D
B

4.1.3 Computer Facilities

Two personal computers were used for this research, a Leading Edge Model M and an IBM PC-XT. The Leading Edge is equipped with 360K RAM memory, two disc drives, an auxiliary RAM drive and an RS-232 interface. The IBM has 640K memory and a color card. There are two printers, an Epson FX-85 dot matrix printer and a Comrex daisywheel printer. The software used included several programs written in BASIC and some specialized statistical packages to facilitate data analyses.

4.2 Research Methods

To model fluid flow and to predict oil recovery from reservoirs, one must study three broad controlling factors. They are: (1) the properties of rock; (2) flow behavior and fluid distribution in the pore system; and (3) details of the petrophysics of the rock-pore system. Both pore geometry and pore topology dictate the motion and distribution of fluids within reservoir rocks. This work interprets and relates data both qualitatively and quantitatively with reference to the pore geometry and topology.

The reservoir properties examined in this project are: (a) porosity, (b) pore topology, (c) size and shape of pores and pore throats, (d) roughness of pore

surfaces, and (e) the degree of connectivity of pores by pore throats. Porosimetric studies, along with geophysical logs and light microscopy were used to describe the pore system.

4.2.1 Sampling of Cores and Sample Preparation

Core samples from five deep wells, 12,000-17,000 feet (4,000-5,700 meters), three within Jay field, together with complete well-log coverage of these and ten additional wells, were used in the study of the Jay Field dolostone reservoir. Approximately 200 small, 5-7 grams cylindrical plugs were taken from the studied cores at regular intervals, 5-10 feet (1.5-3 meters) apart. Each sample was carefully selected to represent a particular facies and was accompanied by a thin section, taken from the exact same place, so that microscopic analysis of the texture and composition of each cylindrical plug could be made.

The plugs were treated with a solution of 50% toluene and 50% acetone for 48 hours to remove organic impurities from the pore spaces. They were then placed in 100% acetone for 24 hours and later dried in a Fisher Isotherm oven (model 215F), at 60°C for 24 hours, to remove any fluids that were trapped within the pore spaces.

This method of cleaning was devised by S. Ghosh, S. Urshel, and G. M. Friedman, and was proven as effective as the more rigorous methods used by others.

4.2.2 Mesoscopic Study of the Core Sequence

Facies were defined and correlated between the five deep wells. Mesoscopic study of the core sequence is very important, because it is the best way to understand both the vertical and lateral relationships between the various facies and their contacts.

4.2.3 Light Microscopy

Approximately 200 standard thin sections were taken from the cores, at regular intervals, from the exact same place from which the plugs were taken. The thin sections were impregnated with blue-epoxy resin under vacuum to highlight porosity, and were partially stained with Alizarin Red S to distinguish calcite from dolomite (Friedman, 1959). These thin sections were studied for three purposes: (a) to determine the texture and composition of each cylindrical plug, (b) to establish the kinds of pores present within each facies, and (c) to determine the depositional environment and diagenesis of the various facies present in the studied area.

4.2.4 Mercury Porosimetry

Experiments were carried out in a Micromeritics mercury porosimeter (Pore Sizer, Model 9305; Fig. 13) in order to generate data for capillary-pressure curves.

Mercury injection/withdrawal curves offer a simple and rapid way to predict the behavior of fluids in pore systems of reservoir rocks under variable pressures. These curves permit examination and interpretation of the shape and size of pores and throats, and the relationships between them (Wardlaw and Taylor, 1976). The validity of these curves, however, is a function of the scale of heterogeneity of the rock.

Each cylindrical plug was cleaned, sealed in a penetrometer (Fig. 13B) and was placed in a calibrated low-pressure chamber (Fig. 13A), where it was evacuated until a stabilized pressure of about 20 microns was obtained. Mercury (a nonwetting phase) was then allowed to fill the penetrometer and completely surround the sample.

The low-pressure tests, ranging from 1.5-14 psia (air-mercury), were performed in the low-pressure ports, and the pressure was incrementally increased with an external source of nitrogen gas. The penetrometer containing both sample and mercury was then installed in the high-pressure chamber (Fig. 13C) where the high-

pressure tests ranging from 14-5,000 psia (air-mercury) were carried out. The pressure was slowly increased, allowing time for equilibration, to 5,000 psia to produce data for mercury injection curves. The cumulative volume of mercury injected at each pressure is a measure of the nonwetting phase saturation. When 5,000 psia was reached, the pressure was slowly reduced to 14 psia to produce data for mercury-withdrawal curves.

An average of 25-30 data points was recorded for each sample plug. Graphs were generated using a BASIC program in an IBM compatible computer. The mercury saturation at each pressure increment increase was plotted on a chart, with the vertical scale as capillary pressure (psia) and the horizontal scale as mercury saturation. Appendix 1 contains the computer-generated sample analyses for all samples, in a digital form.

4.2.5 Geophysical Well-Log Analysis

Wireline logs such as neutron, sonic, density, resistivity, and gamma-ray, were studied in accordance with procedures set forth in the literature (Asquith and Gibson, 1982; Asquith, 1985; Schlumberger, 1987), to determine log-derived petrophysical values. Gamma-ray and resistivity curves were used to correlate strata and estimate clay-mineral concentration in the carbonate rock

units. Neutron logs were used to determine porosity in the reservoir units. Density logs were used to establish lithology of the various facies. The difference in porosity values obtained from neutron logs (which signify total porosity) and sonic logs (which give values for matrix porosity) indicates the presence of secondary pores, which may relate to pore interconnections or pore throats.

To predict pore topology, one must establish a relationship between pore geometry obtained in the laboratory and the petrophysical parameters obtained by the study of wire-line logs. Since cores are usually drilled only in a few selected areas of any given field, the wire-line logs, once correlated to petrophysics, can be used for subsurface mapping. Geological trends, such as lithofacies, depositional environments and diagenetic regimes, must be established to permit interpolation of data between existing well control.

5. DEPOSITIONAL AND DIAGENETIC SEQUENCE OF EVENTS

5.1 Lithofacies Description and Depositional Environment Intepretation

Based on texture, fabric, composition, and association the studied cores are divided into six distinct facies groups: (1) Pelletal-oncoidal wackestones and associated laminated mudstones; (2) pelletal-oncoidal mudstone; (3) vadose pisolite; (4) oolitic packstone; (5) oolitic-peloidal grainstone and associated oncolitic wackestone and pelletal-peloidal packstone; and (6) supratidal anhydrite (Buckner Formation). Variations within each facies may be considerable, but common characteristics help in facies identification.

5.1.1 Pelletal-Oncoidal Wackestone and Associated Laminated Mudstone Facies

Description

This facies is found in the lower Smackover, and consists of repetitive shoaling-upward sequences, 3-90 feet (1-30 m) thick, separated by surfaces of truncation. Each sequence consists of partially dolomitized, wispy laminated and/or bioturbated pelletal-oncoidal wackestones, which grade upward, with interbedding, into horizontally laminated mudstones (Figs. 14-17).

FIGURE 14. Legend of symbols used in core description of figures 15, 16, 17, 19, 20.

ALLOCHEMS

 Pellets

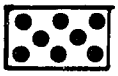 Peloids

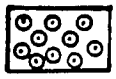 Ooids

 Ghost Allochems

 Oncoids

 Pisoids

 Anhydrite Nodules

 Carbonate Mud

 Soil

STRUCTURES

 Fenestral Fabric

 Geopetal Structures

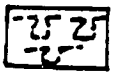 Bioturbation

 Stylolites

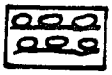 Inverse-Graded Beds

 Cross Bedding

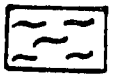 Wispy Laminae

 Horizontal Laminae

 Truncation Surface

Rare

Common

Abundant

FIGURE 15. Humble McDavid Lands #7-1 well. Core description, summary of important lithologic features, environments of deposition of the various facies, and sea-level fluctuations during the time of deposition of these facies. For location and symbol legend refer to table 1 and figures 8, 9, and 14.

McDavid Lands 7-1

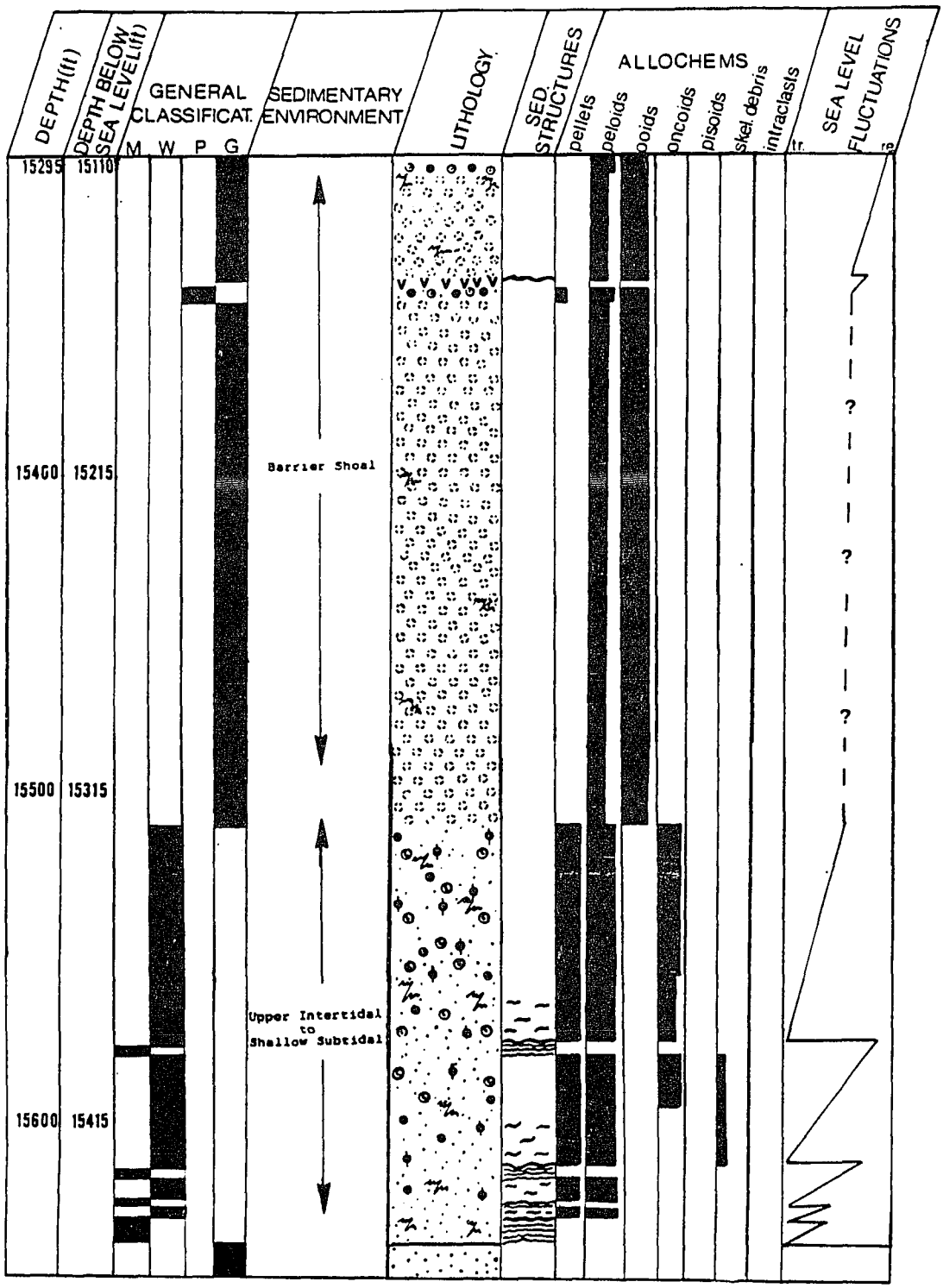

FIGURE 16. Humble C.H. Bray #10-4 well. Core description, summary of important lithologic features, environments of deposition of the various facies, and sea-level fluctuations during the time of deposition of these facies. For location and symbol legend refer to table 1 and figures 8, 9, and 14.

C.H. Bray 10-4

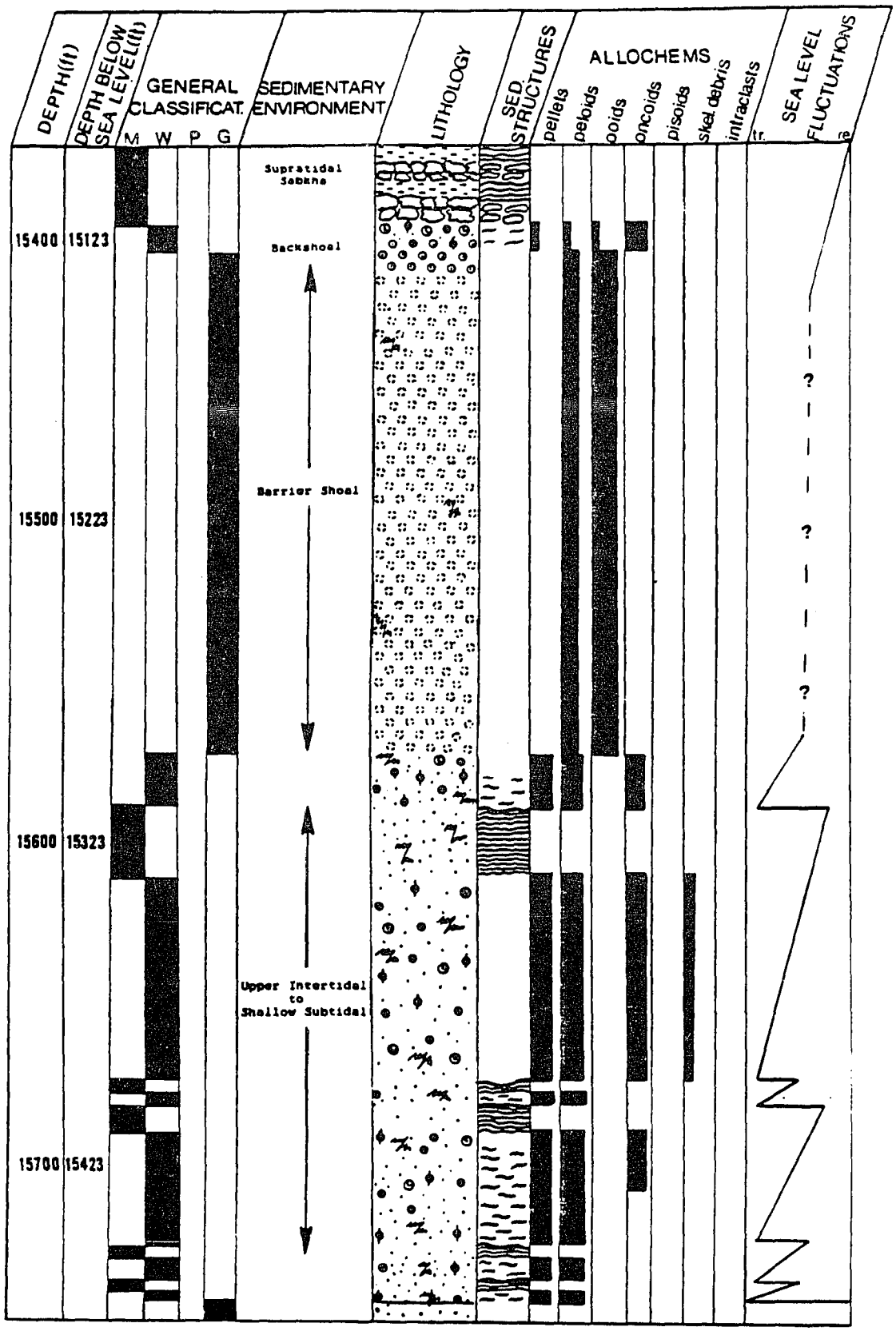
DEPTH(ft)
DEPTH BELOW SEA LEVEL(ft)
GENERAL CLASSIFICAT.
M W P G
SEDIMENTARY ENVIRONMENT
LITHOLOGY
SED. STRUCTURES
ALLOCHEMS
pellets
peloids
ooids
oncoids
pisoids
skel debris
intraclasts
SEA LEVEL FLUCTUATIONS
15400
15123
15500
15223
15600
15323
15700
15423
Supratidal Sabkha
Backshoal
Barrier Shoal
Upper Intertidal to Shallow Subtidal
?
?
?

FIGURE 17. Humble Sam Watson #23-4 well. Core description, summary of important lithologic features, environments of deposition of the various facies, and sea-level fluctuations during the time of deposition of these facies. For location and symbol legend refer to table 1 and figures 8, 9, and 14.

Sam Watson 23-4

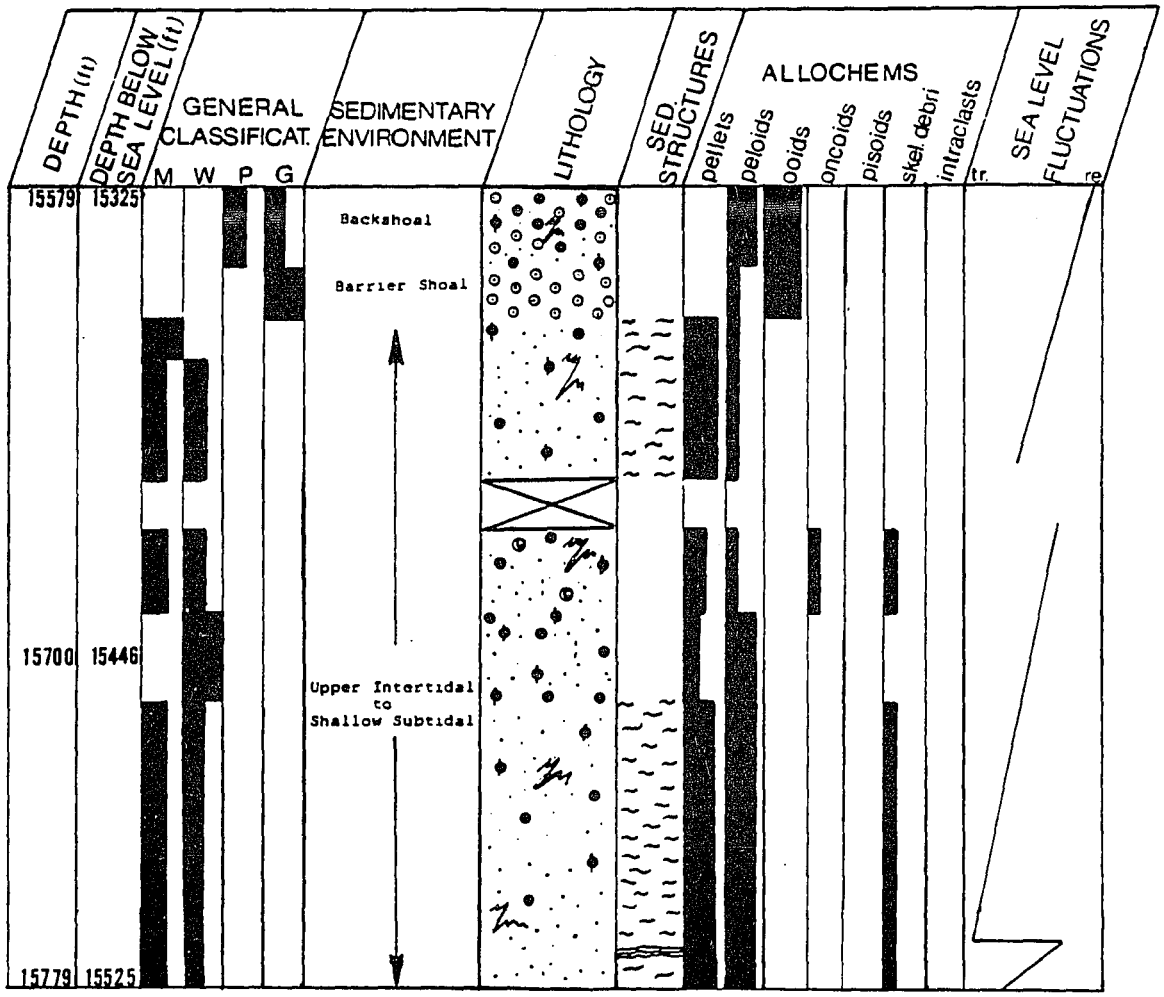

The dominant allochems in the wackestones are Favreina (crustacean fecal pellets), algal oncoids, and fragments of the calcareous algae Tubiphytes, with lesser amounts (<10%) of peloids and algal intraclasts, and even lesser amounts (1-2%) of skeletal debris (ostracod, pelecypod, and pelmatozoan fragments).

The Favreina pellets, although fractured or broken in places, are exceptionally well preserved (fig. 18a). They are ovoid or round in shape, and range in size from 0.05-0.75 mm (with some as much as 1.00 mm). They are almost always dolomitized, and have complex internal tubule patterns indicative of their origin (i.e., pellets of crustacean Callianassa sp.).

The oncoids (Fig. 18b) are subspherical in shape; they resemble miniature "cabbage heads", and are very similar to Jones and Wilkinson's (1978) lacustrine pisoliths and Riding's (1983) cyanoliths, which are formed by calcified cyanophytes. They range in size from 2 mm to 5 cm, averaging 1-2 cm. They consist of simple or compound nuclei, enveloped by irregular sets of continuous or discontinuous, wavy to crenulated laminae of micrite and fine-grained pellets and some skeletal debris. The laminae are in places difficult to observe owing to obliteration by micritization and dolomitization.

FIGURE 18. Photomicrographs of the lower Smackover wackestone and mudstone facies (plane polarized light). a. Favreina pellets in pelletal-oncoidal wackestone (Humble Sam Watson #23-4 well; 15,773'or 5,257m). The pellets are exceptionally well preserved indicating early mineralogical stabilization, prior to any significant compaction. Note the internal texture of the pellets, consisting of complex tubular patterns, characteristic of fecal pellets of the crustacean Callianassa. b. Algal oncoid in pelletal-oncoidal wackestone (Humble McDavid Lands #7-1 well; 15,590' or 5,196m). Typical oncoids of this facies have relatively small nuclei (not shown in photomicrograph) and abundant irregular algal coatings. Individual oncoids resemble miniature cabbage heads. c. Algal laminae in laminated mudstone (Humble Bray #10-4 well; 15,728' or 5,260m). The laminae consist of irregularly alternating layers of lime mud, finely-crystalline dolomite, and quartz silt separated by organic-rich algal films whose presence is accentuated through later stylolitization. d. Algal laminae in wispy laminated mudstone (Humble Bray #10-4 well; 15,593'or 5,197m). The laminae are not horizontally continuous; instead they are short, interrupted by burrows. The light-colored grains are quartz silt.

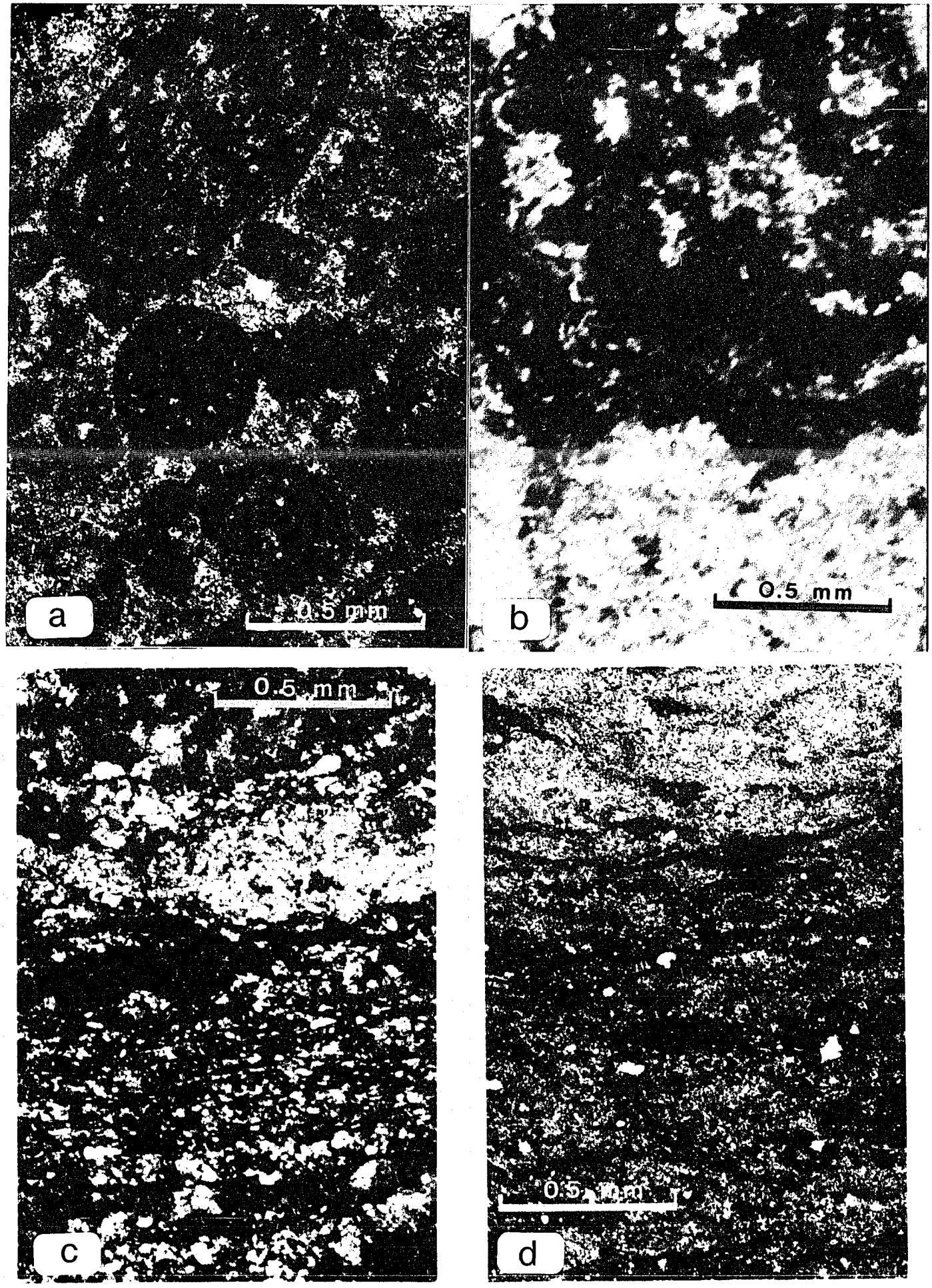
a
0.5 mm
b
0.5 mm
0.5 mm
c
0.5 mm
d

Oncoids vary locally from very abundant to rare. In some areas (e.g., the McDavid Lands core) the oncoidal units are reversely graded, with truncated lower contacts indicating that the oncoids were brought from elsewhere.

The laminated mudstones (Fig. 18c,d) consist of fine (approximately 0.5 mm thick), fairly continuous, organic-rich, horizontal (Fig. 18c) to wavy (Fig. 18d) laminae recognized by color banding. The laminae separate alternating finely-crystalline (20-70 microns) dolomite, lime mudstone, and quartz silt layers, one to three millimeters in thickness. When broken, rocks of this facies separate into "poker chips" which show pressure solution stylolitic surfaces.

The lime mudstone laminae contain local dolomitized peloids and Favreina, as well as abundant quartz silt, anhydrite laths, and black, opaque, organic material. The quartz silt laminae contain local anhydrite laths, and represent mostly insoluble residues of pressure solution as indicated by the abundant stylolites.

Depositional Environment

This facies (i.e., pelletal-oncoidal wackestones and associated laminated mudstones) marks the initial transgression of the Smackover sea over the Norphlet Formation.

The pelletal-oncoidal wackestones were deposited in

a low-energy lower intertidal to shallow subtidal environment. In this environment, the sediment-ingesting bottom fauna was prolific, as indicated by the abundance of fecal pellets in the wackestone facies. Algal mats could not flourish in this environment either because of competition, or predation, or both; however, algal-oncoid formation was favored as indicated by the abundance of oncoids present.

Esposito and King (1987) believe that the characteristics of the wackestones, especially the grading of the oncoids, parallel characteristics of other interpreted carbonate debri flows, and thus, interpret the wackestones to have formed as the result of channelized debri flows. The interbedding of the wackestones with the laminate mudstones, however, suggests these wackestones are not debri flows: Instead, the grading of the oncoids might have been caused by storms which selectively removed the fine material, sorting the larger oncoids.

The kind of algal oncoids present in this facies may not require turbulence for their formation. According to Jones and Wilkinson (1978) modern cyanoliths forming in the Michigan Marl Lakes grow <u>in situ</u> and are only rarely overturned.

The laminated mudstone facies is interpreted to have

been deposited in a protected lower supratidal to upper intertidal carbonate environment, where algae were prolific. Algal mats trapped and bound carbonate and siliciclastic grains and occasional small anhydrite laths. The lack of skeletal allochems and the presence of small amounts of anhydrite demonstrates a relatively harsh, from the biological point of view, occasionally hypersaline environment.

Similar algal-laminated mudstones are currently being deposited in the upper intertidal zones of the Persian Gulf (Schneider, 1975) and Shark Bay, Western Australia (Davies 1970), the sea-marginal hypersaline pools in the Gulf of Aqaba, Red Sea (Friedman et al., 1973; Friedman et al., 1975), and the supratidal zone of Andros Island, Bahamas (Monty, 1983). In upper intertidal environments, the algal mats are frequently flooded by semi-diurnal and spring tides, while in humid supratidal environments, the algal mats are periodically flooded by exceptionally high tides and storms.

Algal-laminated sediments are composed of mechanically deposited particles trapped and bound by a film of algae (Logan et al., 1964; Davies, 1970). Environmental and ecological control probably limited the distribution of algal mats. Davies (1970) believed that predation is the factor limiting the distribution of

algal mats, and he described, in detail the grazing and destruction of algae by various organisms. Monty (1983), however, believed that competition for habitat and not predation is the factor limiting the environmental distribution of algal mats.

The quartz grains are silt-sized and subangular to subrounded. Their size, shape, and distribution suggest that they may have been brought into the environment of deposition by wind and then been trapped on the sticky surface of the algal mat.

The pelletal-oncoidal wackestones and associated laminated mudstones represent deposition during marine regressions. During each regression, shallow water-facies came to overly deep-water facies, resulting in shoaling-upward cycles. Transgressions are marked by truncation surfaces which separate the cycles from one another.

5.1.2 Pelletal-Oncoidal Mudstone Facies

Description

This facies is only present in the Cities Service Lizenby #5-3 well (Fig. 19, 20a). It is devoid of sedimentary structures, and largely consists of dark greenish-brown elongated to oval silt-sized pellets and pellet aggregates incorporating oncoids (5-30%), peloids (2-15%), Favreina pellets (2-3%), ooids (1-2%), algal filaments (1-2%), skeletal debris (1-2%; thin-shelled

FIGURE 19. Cities Service Lizenby #5-3 well. Core description, summary of important lithologic features, environment of deposition of the various facies, and sea-level fluctuations during the time of deposition of these facies. For location and symbol legend refer to table 1 and figures 8 and 14.

Lizenby 5-3

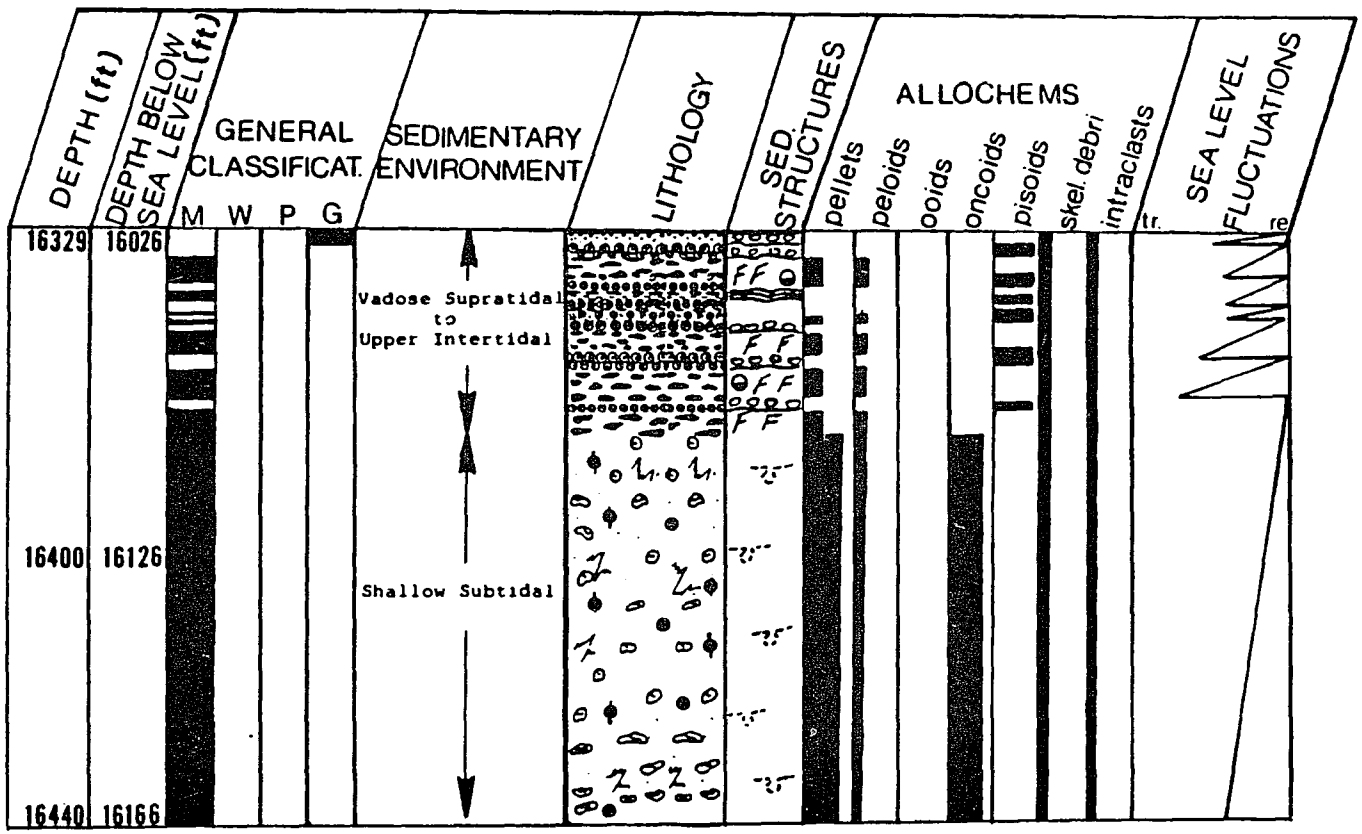
DEPTH (ft)
DEPTH BELOW SEA LEVEL (ft)
GENERAL CLASSIFICAT.
M W P G
SEDIMENTARY ENVIRONMENT
LITHOLOGY
SED. STRUCTURES
ALLOCHEMS
pellets
peloids
ooids
oncoids
pisoids
skel. debri
intraclasts
tr.
SEA LEVEL FLUCTUATIONS
re
16329
16026
16400
16126
16440
16166
Vadose Supratidal to Upper Intertidal
Shallow Subtidal

FIGURE 20. Photomicrographs (plane polarized light) of various facies (pelletal mudstone, vadose pisolite, oolitic packstone and oncolitic wackestone) of the studied cores. a. Algal oncoids in pelletal mudstone (Cities Service Lizenby #5-3 well; 15,622'or 5,207m). The pellets are silt-sized and lack internal texture. The oncoids have relatively large nuclei and thin, irregularly-shaped algal coatings. b. Pisoid textures in vadose pisolite (Cities Service Lizenby #5-3 well; 1,6346'or 5,449m). Lopsided sediment inclusions are perched in the upper part of radially fractured pisoid (arrow). Note the compound pisoid at the upper left corner. c. Oolitic packstone (Cities Service Brown #32-8 well; 15,588'or 5,196m). Ooid cortices are composed of medium-crystalline dolomite, whereas ooid nuclei are composed of lime mudstone. Silt-sized pelletal mud matrix fills the inter-ooid space. More commonly, this pelletal mud is recrystallized to calcite spar. d. Algal oncoids in oncolitic wackestone (Humble C. H. Bray #10-4 well; 15,392' or 5,130m). The oncoids are relatively small, and very irregular in shape. They are stacked on top of one another in a way which indicates in-place growth in a low energy depositional environment. Late anhydrite cement (a) has occluded all available porosity.

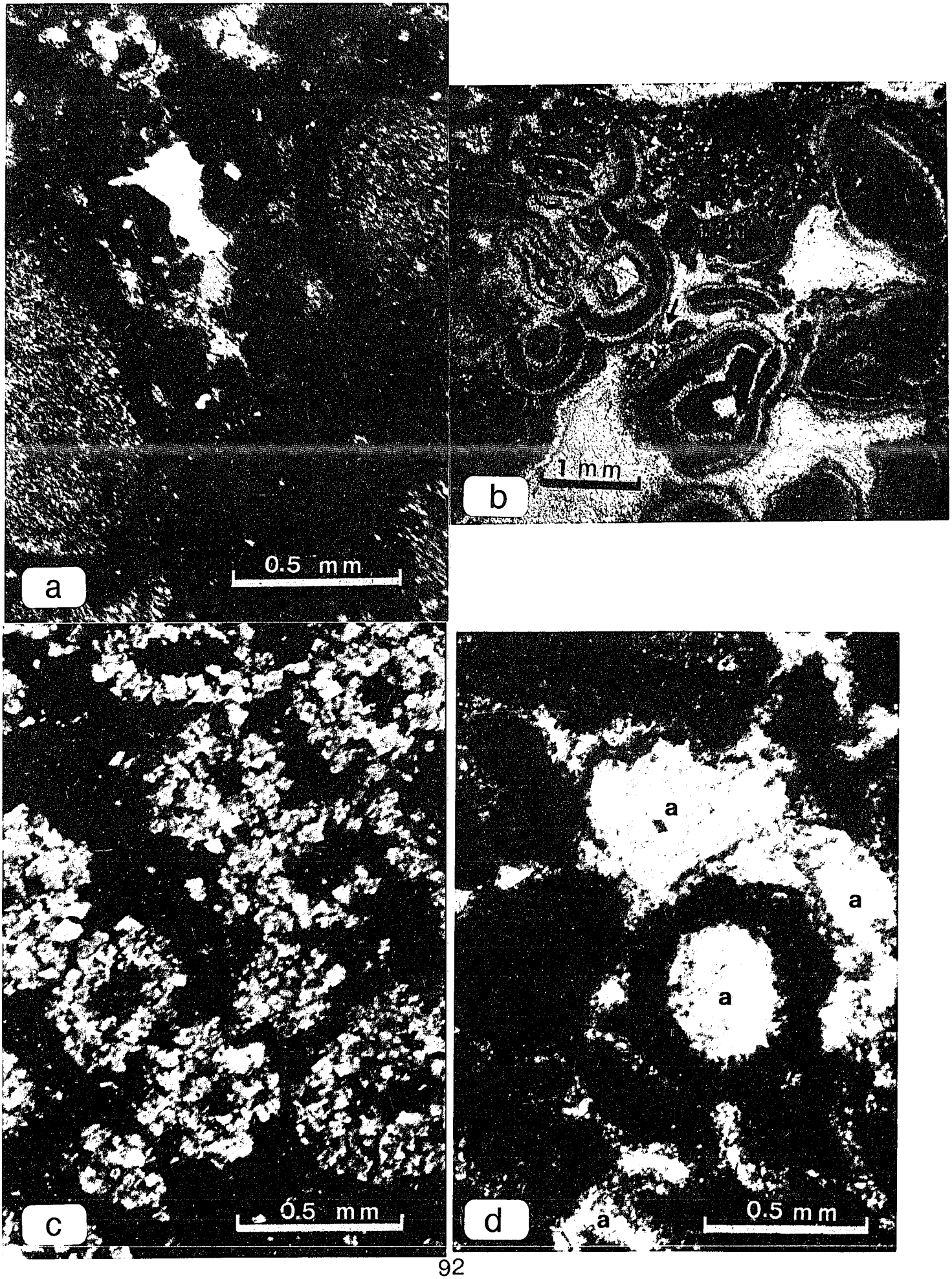
a
0.5 mm
b
1 mm
c
0.5 mm
d
a
a
a
a
0.5 mm

pelecypods and ostracods, echinoid fragments and miliolid forams), quartz grains (1-5%), and occasional (<1%) anhydrite laths (Fig. 20a).

The pellets range in diameter from 0.05-0.20 mm and lack the characteristic complex internal structure of the larger (0.05-0.75 mm) Favreina pellets (Fig. 20a). They are very abundant (70-95% of all constituent grains), and form the framework of the rock. Irregularly shaped clusters of silt-sized pellets are separated by calcite megaspar cement. This megaspar cement forms irregular patches which contain mudstone inclusions and form irregular contacts with the mudstone, showing evidence of alteration and replacement of the pelletal mudstone by the growing calcite spar.

The oncoids are the most distinctive allochems in this facies (Fig. 20a). They range in size from 0.4 mm to 20 mm, and their abundance decreases upward through the facies. The oncoids of the lower section are flat, elongated coated grains, consisting of a large flat nucleus (commonly a pelletal mud intraclast) surrounded by thin, irregular, and incomplete algal coatings, into which pellets, peloids, quartz silt, and anhydrite laths are incorporated. In places the nuclei of the oncoids are composed of rounded crinoid fragments, thin pelecypod shells, or coated- grain grainstone intraclasts.

The flat, elongated oncoids show a preferred orientation, long axes horizontal. The abundance as well as the size and shape of the oncoids changes upward through the facies. The oncoids become less abundant, smaller in size, and more round in shape, whereas the ratio of the nucleus size to the coating thickness decreases (i.e., the nuclei are smaller, whereas the algal coatings are thicker).

Except for local thin zones, the mineralogy of the silt-sized pellets is calcitic, whereas that of the remaining constituent grains is almost always dolomitic. Dolomite concentration ranges from 10-75% (average 30-40%). Where the dolomite content exceeds 50% of the carbonate present the primary rock texture is destroyed and it may only be inferred from the presence of some ghost grains and from stratigraphic relationships with less altered units above and below.

The dolomite replacing the constituent grains is finely- crystalline (dolomicrite), whereas the dolomite scattered within the pellets consists of medium-sized (40-150 micron) euhedral crystals. Some of the ooid cortices as well as most of the peloids have been selectively converted to dolomicrite.

Dolomitization of the oncoids varies. Most commonly the nuclei are converted to dolomicrite, whereas in

others the nuclei are preserved and the algal coatings are dolomitized. In the latter example, the nuclei are composed of pelletal mud intraclasts with local crinoid fragments.

With few exceptions, dolomitization has not destroyed the shape and internal structure of the constituent grains. Preservation of shape and internal structure of grains such as pellets, indicates that the sediment was well-indurated during dolomitization, and that dolomitization was piecemeal and penecontemporaneous to deposition. The selective nature of dolomitization (i.e., oncoids, ooids, Favreina pellets, and peloids are dolomitized, whereas the silt-sized pellets and algal filaments are not) also indicates that there must have been differences in the texture and/or composition of these grains.

Depositional Environment

The lack of primary sedimentary structures as well as the abundance of pellets suggests deposition in a low-energy subtidal environment with prolific bottom fauna. The abundance of flat, irregularly-shaped oncoids in these pelletal mudstones reflects long periods of tranquillity, during which algae flourished, alternating with short periods of mild agitation, during which currents were strong enough to overturn particles and

allow coating on all sides. Similar marine oncoids are currently forming, by disruption of algal mats, in tropical shallow subtidal settings in Bermuda (Gebelein, 1969) and the Bahamas (Newmann et al., 1970).

This mudstone was most probably deposited in a shallow lagoon, which was sheltered by barrier shoals. The absence of abundant and diverse fossils suggests restricted, highly stressful conditions must have prevailed in this shallow lagoon. Sediment-ingesting organisms adapted to live in such conditions homogenized the carbonate mud and converted it to pellets.

5.1.3 Pisolite Facies

Description

The term pisoid is used here to describe coated carbonate particles of non-algal origin and variable size and shape. Pisolite is a rock facies composed predominantly of pisoids.

The pisolite facies, present in the Cities Service Lizenby #5-3 well (Figs. 19, 20b) consists of thin (0.5-5 feet [0.17-1.7 m]; average 2 feet [0.7 m]) repetitive, shoaling-upward sequences separated from one another by surfaces of truncation. Each cycle consists of fenestral algal-pelletal mudstone, containing abundant calcified algal remains, and/or laminated or bioturbated mudstone which generally grades upward into a pisolite. At least

eight such cycles have been identified.

The pisoids commonly display reverse grading, but in general lack sorting or packing order. Pisoids of all sizes and shapes are incorporated together without preferred orientation. Grading, where present, is abrupt. The basal pisoids are fine (0.3-1.0 mm), whereas size increases sharply upward to 0.5-15.0 mm. Pisoid packing varies. Within small areas (few mm apart), pisoids range from loose to densely packed.

Pisoid diameter ranges from 0.3 mm to (rarely) 2.0 cm with an average size of 1-4 mm. Pisoids are round to irregular to amoeboid. Inclusions of carbonate silt, into which quartz silt is incorporated, are commonly perched on the upper sides of pisoid coatings (Fig. 20b). In places, these perched inclusions are later recoated by pisoid growth layers, indicating that deposition of this diagenetic sediment was penecontemporaneous with pisoid formation (see Melas and Friedman, 1987b).

The pisoid nuclei vary considerably in size and shape, and consist mostly of individual and compound fragments of other pisoids. Locally, the nuclei may be composed of fenestral pelletal mud, isolated or compound pellets typical of the host rock, or unidentified particles. As a general rule, the larger the nuclei the fewer the coatings and vice versa. All nuclei are

dolomitic except those of pelletal mudstone.

The pisoid cortices (rims) are of variable thickness; they are generally isopachous and continuous and are composed of dolomicrite in alternate light and dark layers (Fig. 20b). Discontinuous horizontal to subhorizontal laminated crusts are abundant. Laterally, these crusts may grade into pisoid coatings.

Asymmetrical coatings with downward, upward, or lateral thickenings are present, indicating a non-preferred, in-place growth into the available pore space. Dunham (1969) pointed out that downward directional growth is not a characteristic of algal oncoids because algae require solar radiation for photosynthesis, and thus would not preferentially grow downward.

Individual pisoids may show evidence of nontectonic penecontemporaneous fragmentation (i.e., they are broken or fractured, and are very angular). Radial and dendritic fracturing is relatively common (Fig. 20b).

Polygonal fitting described by Dunham (1969), Wardlaw and Reinson (1971), and Esteban and Pray (1983) is not well developed. Concavo-convex and sutured contacts (the result of pressure solution) between the pisoids are, however, relatively common, indicating late diagenetic altering of the facies.

Depositional Environment

Pisoids have been reported and described from many modern and ancient carbonate environments. The origin of ancient pisolites, however, is controversial. Most early workers considered the pisoids to have formed as products of algal activity in subtidal marine environments (Ruedemann, 1929; Jonson, 1942). Lang (1942) and Newell et al. (1953) questioned the algal origin. However, the subaqueous, syndepositional formation hypothesis of ancient pisoids prevailed until the mid-1960's when Dunham (1965, 1969) and Thomas (1965) proposed, in their study of the Guadalupe Reef complex, that pisoids are products of ancient soil caliche formed in-situ in the vadose diagenetic environment from a precursor carbonate sediment. Esteban (1976), Esteban and Pray (1977, 1983) and Pray (1986), who have also done extensive work in the same area, believe the pisoids were predominantly deposited in a peritidal environment as free sedimentary particles, and that only sporadic pisoids (botryoidal macroids) formed as soil concretions.

Scholle and Kinsman (1974), in their study of the modern pisoids of the Persian Gulf, concluded that the pisoids are formed in a marine vadose diagenetic environment. In strongly evaporitic settings, supratidal vadose areas are characterized by marine brines and not by fresh water. Handford et al. (1984), in their study

of the pisoids and tepee structures of Lake McLeon in Western Australia (a modern carbonate-evaporite salina), infer that the tepee-pisoid facies actively forms by "speleanlike diagenesis operating in a marine groundwater discharge zone". Sneh and Friedman (1985) described pisoids as pseudo-oncolites in their study of supratidal flats and hypersaline sea-marginal pools of the Red Sea.

The pisoid facies of the studied area is interpreted as the product of marine vadose diagenesis in an arid climatic setting analogous to the modern Persian Gulf or Red Sea. The cyclic nature of the pisolite beds (i.e. thin shallowing-upward cycles separated by truncation surfaces) demonstrates recurring sea-level changes, probably of short duration, during the time of deposition and diagenesis. Pisoids formed during low sea-level stands as underlying intertidal fenestral mud was subaerially exposed (Melas and Friedman, 1987a,b). Such sea-level oscilations are recorded by Barret (1989) for the Chunchula Field area in southwest Alabama. Vadose diagenetic products, such as the ones described here are also recorded by the author.

Evidence of multigeneration coating, fracturing, and leaching of the pisoids indicates a complexly variable environment, in which conditions favorable to carbonate

precipitation (hypersalinity) alternated with conditions favorable to carbonate dissolution (freshwater influx due to occasional rains) and/or fracturing (desiccation and soil formation). According to Dunham (1969) such variability is the outstanding characteristic of the vadose zone.

5.1.4 Oolitic Packstone Facies

Description

The oolitic packstone facies is present only in the Cities Service Brown #32-8 well (Fig. 20c, 21). Lithologically, it is composed of 60-75% dolomite and 25-40% calcite, with minor amounts (<5%) of quartz and anhydrite.

The constituent grains in this facies are mostly ooids (approximately 75-95%), with sporadic pellets, peloids, composite grains, flattened and laminated mud intraclasts, and rare skeletal fragments, supported by carbonate mud matrix, now recrystallized to coarse calcite cement. In areas where the matrix is not recrystallized (Fig. 20c), it consists of pelletal mudstone composed entirely of small (0.1-0.2 mm) pellets with some quartz silt and anhydrite laths. Dolomitization is selective; only the ooids are dolomitized, whereas the matrix and some of the grains

FIGURE 21. Cities Service Brown #32-8 well. Core description, summary of important lithologic features, environment of deposition and sea-level fluctuations of the various facies. For location and symbol legend refer to Table 1 and figures 8 and 14.

Brown 32-8

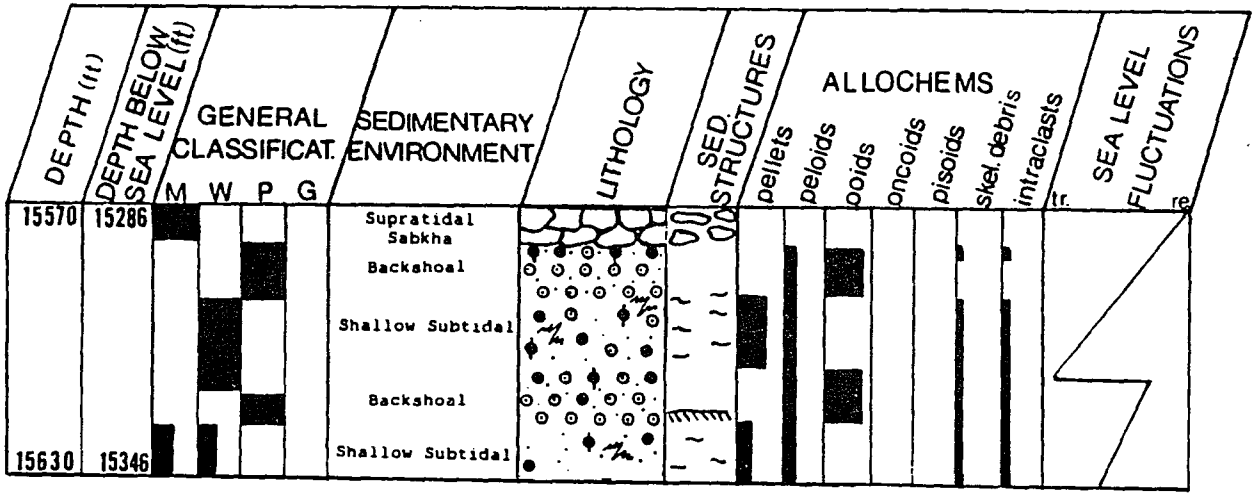
DEPTH (ft)
DEPTH BELOW SEA LEVEL (ft)
GENERAL CLASSIFICAT.
M W P G
SEDIMENTARY ENVIRONMENT
LITHOLOGY
SED. STRUCTURES
ALLOCHEMS
pellets
peloids
ooids
oncoids
pisoids
skel. debris
intraclasts
SEA LEVEL FLUCTUATIONS
15570
15286
15630
15346
Supratidal Sabkha
Backshoal
Shallow Subtidal
Backshoal
Shallow Subtidal

composed of carbonate mud, such as pellets and peloids present are partially or completely non-dolomitized. The internal texture of most constituent grains was destroyed by dolomitization.

The ooids are well sorted, they range in size from 0.3 to 0.7 mm, and are composed of coarse (25-150 microns) dolomite crystals. In many examples, the cortices of the ooids are dolomitized, whereas the nuclei are not. The nondolomitized nuclei are composed of carbonate mud. In the 15607-15620' (5202-5206 m) interval of the Cities Service Brown #32-8 well (Fig.21) dolomitization of the allochems is incomplete. In this segment the constituent grains are composed of 75% ooids and 25% others. The oval-shaped pellets and peloids of this interval show a preferred alignment, with their long axes horizontal.

Quartz occurs as silt-sized detrital grains in the matrix, but mostly as secondary replacement and void filling cement. This secondary quartz is irregularly shaped and cuts across both the calcite matrix and dolomitized grains. Anhydrite replacement by quartz is evident in areas of incomplete replacement of anhydrite cement. In these areas, the replacement quartz is associated with anhydrite cement and contains anhydrite inclusions.

Depositional Environment

The oolitic packstone facies was deposited in a shallow-water backshoal environment. Great quantities of ooids were transported off the adjacent oolitic shoals, into the pelletal mud of the sheltered backshoal area. Sedimentary structures such as cross bedding and horizontal alignment of elongated grains suggest moderate water agitation.

The oolitic packstone facies occurs in two different parts of the core indicating a shift in depositional environments between quiet water lagoon and moderately agitated backshoal, most probably related to sea-level fluctuations. The sedimentary cycle in the Cities Service Brown #32-8 well is completed with deposition of the Buckner anhydrite deposited during rapid progradation of the sabkha over the Smackover shallow-water carbonates.

5.1.5 Peloidal/Oolitic Grainstone Facies

Description

The peloidal/oolitic grainstone facies of the study area is composed of nearly pure dolostone (90-97%) with minor amounts (3-10%) of anhydrite cement, quartz silt and replacement quartz, and relic calcite. This facies composes the upper part of three of the five studied cores, located within Jay field (i.e., McDavid Lands,

C.H. Bray, and Sam Watson; Figures 15, 16, 17), and its thickness diminishes from north to south from approximately 175 feet (58.3 m; McDavid Lands and C. H. Bray) to 20 feet (6.7 m; Sam Watson).

A thin layer of mixed-allochem packstone is present above the grainstone in the Sam Watson and McDavid Lands wells, whereas in the Bray well, the grainstone grades up into a thin layer of oncolitic wackestone. The Buckner anhydrite caps the facies in all three wells.

Whereas the original depositional texture of the grainstone is well preserved in some areas (Fig. 22a,b), the depositional features are generally much altered or completely destroyed, and the facies consists of pervasively dolomitized carbonate containing local ooid and peloid ghosts (Fig. 22c,d). The dolomite crystals are large (20-300 microns; average 150-200 microns) subhedral rhombs, of mostly equigranular hypidiotopic fabric. Within the facies, however, lenses of carbonate composed of fine subhedral dolomite crystals are common. Ooid and peloid ghosts are more common and better defined in these lenses than in the coarsely dolomitized areas (Fig. 22d).

In areas where the original depositional texture is well preserved (Fig. 22a,b), dolomite crystals are small, and the facies is composed predominantly of well sorted

FIGURE 22. Photomicrographs of the various textures of the Smackover grainstone facies of the study area (plane polarized light). a. Well preserved ooids in peloidal/ oolitic grainstone (Humble C. H. Bray #10-4 well; 15,410' or 5,137m). Dolomite is finely-crystalline, allowing pre-servation of previously micritized allochems. Isopachous marine phreatic cement, indicative of high-energy environ- ment of deposition, coats the allochems. Most of the interparticle pore space is still preserved.b. Anhydrite-filled allochems in dolomitized peloidal/ oolitic grainstone (Humble Sam Watson #23-4 well; 15,596' or 5,199m). The ooids and peloids most probably survived early dolomitization and were leached during subaerial exposure by meteoric water. Anhydrite cement later occluded the moldic pores. c. Coarsely-crystalline hypidiotopic dolomite in peloidal/oolitic grainstone (Humble C. H. Bray #10-4 well; 15,418' or 5,139m). All original depositional and early diagenetic texture was destroyed through dolomitization. Core segments composed of such dolomitic textures have high porosity and permeability values. d. Ghost allochems in peloidal/ oolitic grainstone (Humble McDavid Lands #7-1 well; 15,422' or 5,141m). The outlines of the allochems have been accentuated by stylolitization. Dolomite is medium crystalline, allowing preservation of some of the original depositional texture.

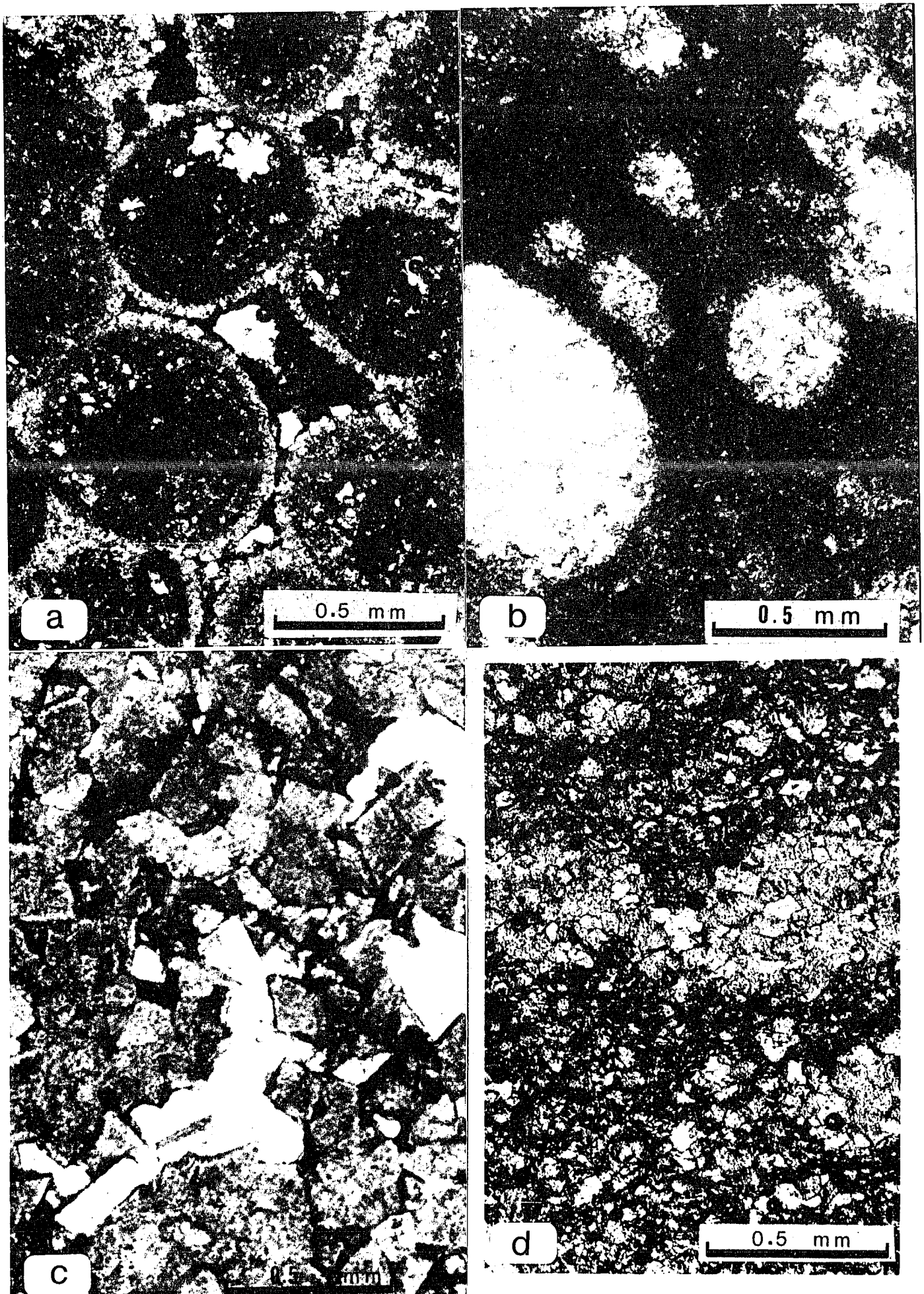
a
0.5 mm
b
0.5 mm
c
d
0.5 mm

(0.3-0.8 mm; average diameter 0.4-0.5 mm; maximum size 1.1 mm) ooids with some peloids, composite grains, and sporadic skeletal debris.

With the exception of some horizontally aligned oval grains and a thin (approximately 3 ft; 1 m) layer of unconsolidated carbonate soil in the McDavid core, sedimentary structures are not apparent. The texture of the carbonate above and below the soil horizon is typical of the facies.

The grainstone facies is porous and permeable wherever present, however, porosity types vary according to texture. In areas where the facies is pervasively dolomitized and dolomite is coarse, pores are intercrystalline or vuggy, whereas in areas where the original depositional texture is preserved, pores are moldic, vuggy pores, and primary interparticle.

Depositional Environment

Ooids form in areas where sea water supersaturated with calcium carbonate is subjected to current agitation (Newell et al, 1960, Purdy, 1963). The peloid/ooid sandbars of the study area were deposited in an intertidal "shoal" setting, located on local paleobathymetric highs most probably produced by salt movement. The positive topography provided a focus for mild to moderate agitation by waves and currents.

This facies was described by other workers (Sigsby, 1976; Ottmann et al., 1973) as pelletal grainstone deposited in a low- energy environment as a result of reworking, ingestion, and recycling of the organic mud by filter-feeding organisms. Extensive dolomitization of this facies in my study area destroyed the original depositional texture, preventing determination of the origin of most allochems.

Where particles could be identified, ooids are the dominant allochems, whereas pellets are minor constituents. The peloids in this facies might be micritized fecal pellets which have lost their internal structure. Their association, however, with ooids indicates at least mild agitation during deposition. Agitated environmental conditions are further supported by bladed isopachous cement crusts observed coating particles where preservation is good. Such cements are characteristic of high- energy intertidal areas (Bathurst, 1975; Longman, 1981). The peloids (former pellets?) may have been deposited in a low-energy environment, and periodically swept by currents or tides on to the sandbars.

A thin layer of mixed-allochem wackestone-packstone and oncolitic wackestone overlies the sandbar indicating that lower- energy conditions succeeded the agitated

shoal environment. These lower-energy facies most probably represent deposition leeward of the shoal, in a more sheltered environment. The upward succession of mild- to moderate-energy shoal sands to low- energy backshoal deposits to supratidal evaporites represents a shoaling-upward sequence deposited during regression.

According to Moore and Druckman (1981) such thick oolitic grainstone units confute the hypothesis that the upper Smackover and Buckner represent a single shoaling upward progradational cycle. In such a setting the vertical topography between shoreface and shelf would have been approximately 300 feet (100 m), a highly unlikely situation. The sequence is alternatively interpreted by these authors, for the Arkansas Smackover shelf, as a widespread submarine oolitic shoal complex similar to the modern Bahamian Platform interior sand blanket (Ball, 1967), where sedimentation kept pace with subsidence across the shelf, and has resulted in the exceptionally thick oolitic grainstone unit of the upper Smackover.

Moore and Druckman (1981), however, do not consider the effects of sea-level fluctuation on deposition of the oolitic sands. The grainstone may not have been deposited as a single, uniform depositional unit, but instead it may represent many small depositional cycles

stacked on top of each other. The preservation of at least one soil horizon in the Humble McDavid lands #7-1 well indicates at least one period of exposure caused by low sea-level stands during deposition. Additional evidence of sea-level fluctuations during the Smackover time is preserved in the intertidal shoaling-upward cycles of the lower Smackover.

5.1.6 Supratidal Anhydrite Facies (Buckner Formation)

Description

The Buckner anhydrites overlie the Smackover Formation in the study area (Figs. 16, 21). They are characterized by interlayered white to gray anhydrite and vaguely laminated dolomicrite devoid of fossils, argilaceous dolomicrite, and green and brown terrestrial shale. The anhydrite is the dominant rock type and is massive, nodular, and laminated (for more detailed textural analysis, refer to Lowenstein, 1987). Repetitive depositional sequences, 2-7 feet (0.67-2.33 m) thick, were observed in the Humble C. H. Bray #10-4 well. From the bottom upward, a complete sequence consists of bedded anhydrite, bedded nodular anhydrite, vaguely-laminated anhydrite, interlaminated green dolomitic claystones and anhydrite, and terrestrial mudstones (brown).

Individual anhydrite nodules and laminae are separated by varying amounts of dolomicrite and

siliciclastic mudstone. The nodules are of varying sizes and shapes and are flattened parallel to bedding. When viewed with the aid of a petrographic microscope, individual nodules are composed of bundles of radiating fibrous anhydrite crystals.

Depositional Environment

In general, the Buckner Formation represents an arid shoreline progradation of evaporites and continental deposits over the Smackover shallow water carbonates, very much analogous to the modern Persian Gulf.

In the Persian Gulf sabkhas, evaporite minerals form by diagenetic displacement in the intertidal and supratidal sediments after deposition, in a zone up to 3 feet (1 m) thick, immediately above the groundwater table. The predominant evaporite texture is nodular to enterolithic (Kendall and Skipwith, 1969; Kinsman, 1969; Warren and Kendall, 1985).

In modern salinas, evaporites occur as thick (up to 30 ft.; 10 m) shoaling-upward lacustrine sequences. Each sequence is characterized by massive, poorly laminated domes of selenite at the bottom, which pass upward into horizontally laminated selenite, laminated gypsarenite, and massive gypsarenite. The succession is capped by eolian gypsum (Warren, 1982; Warren and Kendall, 1985).

When evaporites are buried, much of the original

depositional texture is lost as gypsum dehydrates to anhydrite. Characteristics that distinguish subaerial (sabkha) and subaqueous (salina) evaporites may be preserved in the deeply buried anhydrites. The Buckner anhydrites of the studied area show similarities with modern salina deposits described by Warren and Kendall (1985) in that they occur as thick shoaling-upward sequences which include bedded nodular anhydrite units. In addition, Lowenstein (1987) observed upright elongated nodules of anhydrite (former upright twined gypsum) in the Buckner Formation of Alabama, which he interpreted as the product of subaqueous gypsum deposition.

On a large scale, the Buckner Formation represents progradation of supratidal evaporites and siliciclastics over shallow-water marine carbonates (Budd and Loucks, 1981; Lowenstein, 1987). The Buckner anhydrite of the studied area, however, represents localized salina depression deposits on the sabkha surface.

5.2 Diagenetic Processes and Products

5.2.1 Dolomitization

Three kinds of dolomite are identified in the Smackover Formation of the study area, indicating at least three separate dolomitization events. They include finely crystalline dolomite common in the lower Smackover, coarsely crystalline subhedral dolomite common in the upper Smackover shoal facies, and saddle dolomite present as pore-filling cement throughout the facies. Although dolomitization is not facies selective, it is more extensive in the grainstones (95-98% of the rock) than in the other carbonate facies. The porous grainstones most probably provided a conduit for the diagenetic fluids to be transmitted and dolomitize the facies.

Dolomitization of the lower Smackover laminated mudstones and associated pelletal-oncoidal wackestones is finely-crystalline (1-50 microns) and ranges from 0-95% of the rock, 10-40% being the most common range. Dolomitization of these facies was most probably penecontemporaneous with deposition, as indicated by the presence of exceptionally well preserved fecal pellets and the relative absence of crushing or flattening of these originally delicate allochems (Fig. 20a).

Preservation of the originally soft pellets indicates they were indurated during or soon after deposition, prior to any significant compaction.

This early dolomitization may be the result of hypersaline brines formed by "capillary concentration" and "evaporative pumping" (Friedman and Sanders, 1967; McKenzie et al, 1980) at or near the vadose diagenetic environment in an arid climatic setting, analogous to the modern Persian Gulf, where evaporation exceeds precipitation and run-off. Using stratigraphic and geochemical evidence, and comparing it to the modern carbonate environments, Vinet (1984) showed that the lower Smackover dolomitized carbonates are the result of penecontemporaneous dolomitization by evaporative brines in an arid climatic setting.

The presence of scattered anhydrite crystals within the lower Smackover facies as well as evidence of recurring sea-level fluctuations further attest to shallow-water deposition in an arid climatic setting in which dolomitization was penecontemporaneous.

The shoal facies are characterized by fine- to coarsely-crystalline (50-250 microns) hypidiotopic turbid dolomite. In areas where dolomite is finely-crystalline, the original depositional and early diagenetic textures of the facies are preserved (Figs. 22a,b, 23a, 24a).

FIGURE 23. Photomicrographs (plane polarized light) of the cement types of the cores studied. a. Isopachous rim cements in dolomitized peloidal/oolitic grainstone (Humble C. H. Bray #10-4 well; 15,410' or 5,137m). Spalled rim cements (arrow) and sutured grain contacts are indicative of brittle compaction and pressure solution respectively, both the result of overburden pressure. The interparticle pores are wholly or partially filled with hydrocarbons (black) and some display geopetal texture. b. Cement generations in vadose pisolite (Cities Service Lizenby #5-3 well; 16,346' or 5,449m). Pisoids occupy area on left and right of photograph. Central area bordered by micritic rim is an interpisoid void. Three generations of cements are present: fibrous calcite, equant dolomite, and drusy or megaspar calcite, listed in relative chronological order. c. Massive anhydrite cement in peloidal/oolitic grainstone (Humble C. H. Bray #10-4 well; 15,410' or 5,137m). Anhydrite fills the interparticle and moldic pores and postdates all other diagenetic events. d. Replacement anhydrite in pelletal/peloidal wackestone (Humble McDavid Lands #7-1 well; 15,546' or 5,182m). The blocky anhydrite cement cuts indiscriminately across particles and other cements.

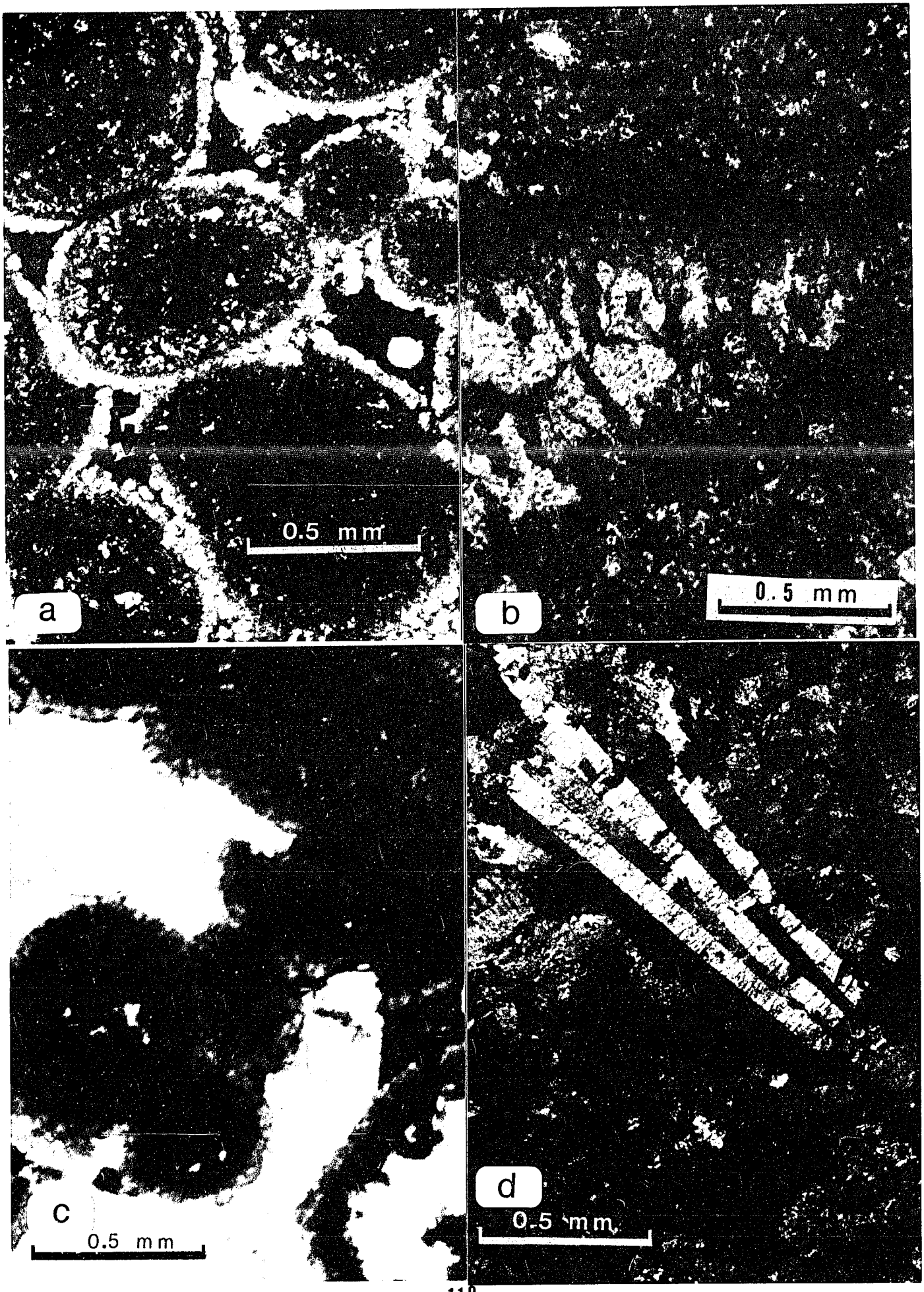
a
0.5 mm
b
0.5 mm
c
0.5 mm
d
0.5 mm

FIGURE 24. Photomicrographs (plane polarized light) of the porosity types of the study area. a. moldic (m) and interparticle (i) porosity in dolomitized peloidal/oolitic grainstone (Humble Sam Watson #23-4 well; 15,604' or 5,201m). The ooids and peloids are wholly or partially dissolved, indicating incomplete leaching. Although individual oomolds are not interconnected, good interparticle and dolomitic microcrystalline porosities resulted in good permeability and thus an excellent reservoir facies. b. Dolomitic intercrystalline porosity in dolomitized peloidal/oolitic grainstone (Humble C. H. Bray #10-4 well; 15418' or 5,139m). Dolomitization is coarse-crystalline and the intercrystalline pores are large and well interconnected, resulting in very high porosity and permeability values. c. Stylolitic porosity in pelletal wackestone (Humble Mcdavid Lands #7-1 well; 15534' or 5,178m). Stylolitic porosity is found in the lower Smackover peritidal facies. Individual pores characteristically tend to follow weak stylolitic zones. Such pores are, however, very rare and constitute a very small fraction of the available porosity. d. Microfracture porosity (f) in pelletal wackestone (Humble McDavid Lands #7-1 well; 15534' or 5,178m). Microfracture porosity is limited to the lower Smackover peritidal facies, where porosity values are the lowest, and the carbonate is very dense.

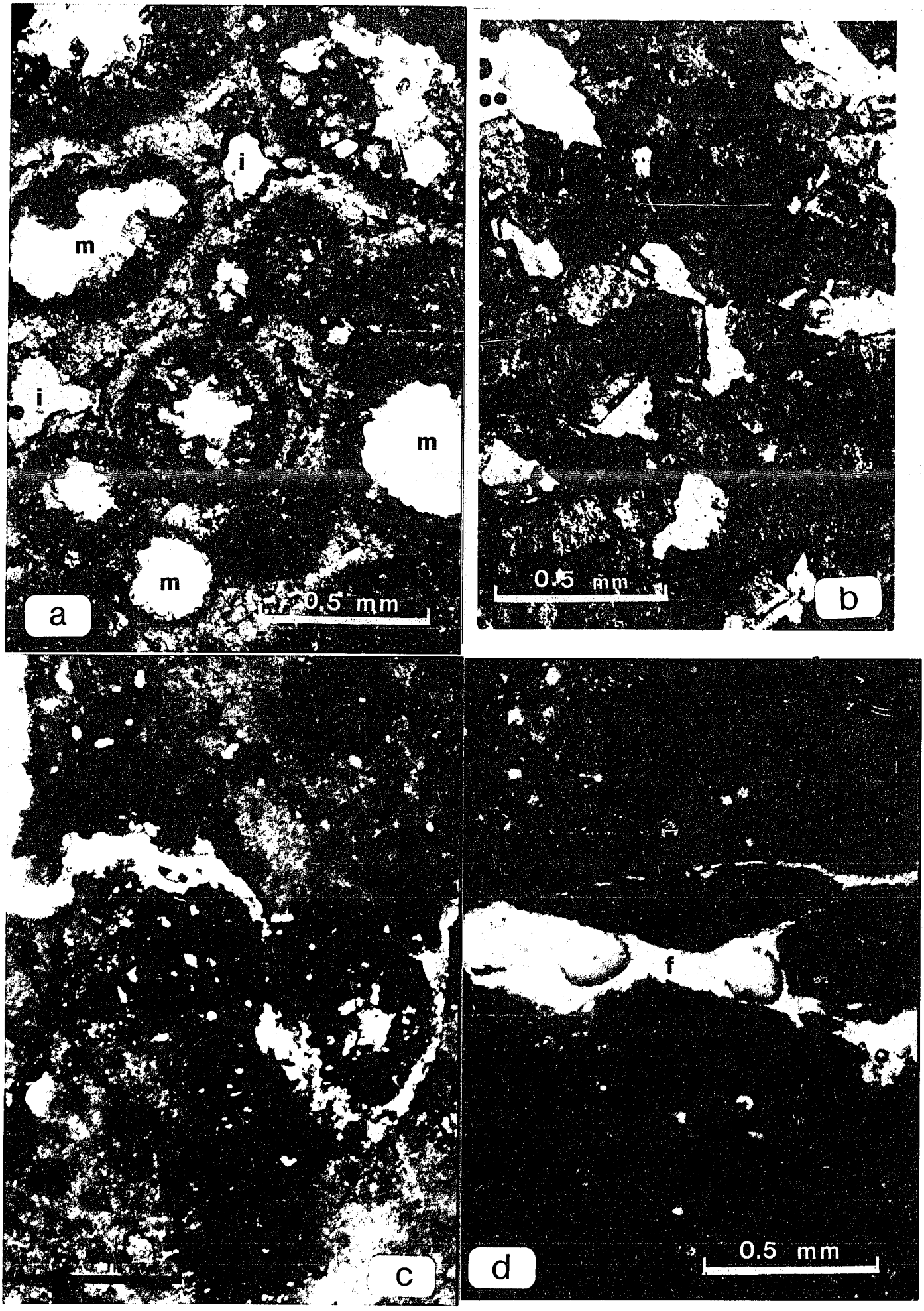
i
m
i
m
m
0.5 mm
a
0.5 mm
b
c
f
d
0.5 mm

Porosity in these zones consists mostly of moldic and interparticle pores, whereas dolomitic micro-intercrystalline pores enhance permeability of the otherwise isolated molds. In areas where dolomite is medium-crystalline the original depositional texture and early cements are destroyed, however, the presence of allochem ghosts makes identification of the facies possible (Fig. 22d). Porosity and permeability in these zones are much lower than in the rest of the shoal facies because dolomite crystals form an interlocking network with little intercrystalline void space. Finally, in areas where crystal size is large (100-250 microns), dolomitization is neomorphic (Figs. 22c, 24b). Good intercrystalline porosity and permeability characterize these coarsely crystalline zones.

This kind of dolomite (coarsely-crystalline, subhedral to euhedral) is interpreted to have formed in a meteoric mixing environment. In such environment, groundwater mixes with sea water, at the base of the fresh water lens, increasing dolomite saturation (Land, 1973; Badiozomani, 1973; Folk and Land, 1975; Sears and Lucia, 1980; Land, 1982). Within the upper Smackover dolomites of the Humble McDavid Lands 7-1 well is a thin (3 feet; 1 meter) soil horizon, indicative of subaerial meteoric water influence.

Questions have been recently raised as to the validity of the mixing environment. Hardie (1987) explains the serious uncertainties the mixing model carries, and emphasizes the importance of time and temperature in the formation of dolomite. No alternative model is, however, offered by the author. Perhaps it is implied that dolomitization as a concept may not be modeled.

Using geochemical evidence and assuming the original chemical composition was preserved, Vinet (1984) compared the upper Smackover dolomite of Jay field to modern (Land, 1973) and ancient (Badiozomani, 1973) mixed marine-meteoric water counterparts and found similarities in isotopic and trace element compositions. He further found a chemical discontinuity between the lower Smackover, upper Smackover, and Buckner dolomites. This discontinuity is marked by a sharp change in crystal size, trace-element composition, and oxygen-isotopic composition, attesting to their different origins.

The presence of this sharp discontinuity at the boundaries of the lower, upper Smackover, and Buckner dolomites indicates that each dolomitization event took place prior to deposition of the overlying units. In addition, dolomitization of the upper Smackover grainstones by reflux of brines from the overlying

Buckner Formation is not possible, since the upper Smackover and Buckner dolomites are genetically unrelated.

Loucks and Budd (1984) also suggested a regional mixing model for the finely- to medium-crystalline dolomitization of the upper Jurassic of south Texas.

A recurring sea-level fluctuation mechanism must also be employed here to explain the periodic exposure of these thick grainstone units to the mixing environment, as well as to explain the thickness of the grainstone unit. As previously explained, this thick shoal unit was not deposited as a single uniform cycle. Instead, it may represent small repetitive cycles deposited during recurring sea-level fluctuations. With deposition of each shoaling upward cycle, the unit was exposed to the meteoric mixing environment. As such, dolomitization of the shoal grainstones did not take place as a single diagenetic event. Rather dolomitization was piecemeal and and took place right after deposition of each cycle. Overlapping between cycles may have erased evidence of cyclicity. However, the presence of finely- to coarsely-crystalline lenses in the shoal grainstones, as well as the soil horizon in the McDavid well, attest to this cyclicity.

The third kind of dolomite is saddle dolomite,

present as pore-filling cement, and consisting of large curved crystals of characteristic undulose extinction. This kind of dolomite was precipitated during deep burial at elevated temperatures, as indicated by geochemical evidence (light δ^{18}; Vinet, 1984), low strontium and sodium content (Moore and Druckman, 1981), and two-phase fluid-inclusion data (Moore and Druckman, 1981). Such cement, however, is uncommon in the cores studied.

5.2.2 Cementation

Cementation in the cores of the study area is minimal, and has played a relatively minor role in reducing porosity. At least six kinds of cement occur in Smackover Formation of the cores studied, listed below in interpreted chronological sequence: 1) bladed isopachous dolomite, formerly aragonite or high-Mg calcite (Fig. 23a); 2) coarse fibrous calcite cement, formerly aragonite or high-Mg calcite (Fig. 23b); 3) equant dolomite spar, formerly calcite (Fig. 23b); 4) drusy calcite, mineralogically unaltered since original precipitation (Fig. 20b); 5) saddle dolomite; and 6) massive bladed anhydrite, formerly partially gypsum (Fig. 23c,d). Compactional features (i.e. stylolites) precede the precipitation of evaporite cements, as indicated by cross-cutting relationships, and are probably responsible

for the minor amounts of saddle dolomite cements in the lower Smackover. Excluding the minor amounts of saddle dolomite, bladed anhydrite, and partial recrystallization of the facies, cements are not common in the lower Smackover mudstone and wackestone facies.

The allochems in the well-preserved areas of the oolitic/peloidal grainstone facies are rimmed with bladed isopachous dolomite cements, 30-50 microns in thickness, that intersect at polygonal junctions (Fig. 21a) and are very similar to the fibrous or bladed aragonite or high-Mg calcite isopachous crusts on grains described by Longman (1981) and Bathurst (1975). These kinds of cements are deposited in high-energy intertidal areas (i.e. Bathurst's "beach rock" and Longman's "active phreatic zone" cements) in which sea water moves readily into the sediment, resulting in marine cementation, and possible formation of hardgrounds.

Cement-filled cavities of the pisoid facies are preferentially located, in a shelter-like manner, on the underside of the pisoids. They are reversely graded where the pisoids are reversely graded. Cement kinds 2, 3, and 4 fill the interpisoid voids (Fig. 21b). The same sequence of cements fills the fenestral pores of the host pelletal mudstone.

All coated particles were first rimmed with coarse fibrous calcite cement, which lines the pore cavities between the individual pisoids (Fig. 23b). This cement occurs as clear fibrous crystals, most probably aragonitic in origin, similar to the one described by Friedman and Sanders (1967) and Friedman et al. (1973). Formerly high-Mg calcite cements are finely crystalline and semiopaque.

Individual needle crystals are oriented perpendicular to the substrate. Lengths vary, some crystals are as long as 100 microns. The longer needles show a slightly splayed orientation. In places the cements may be crudely isopachous and may show thickening near particle boundaries. Gravitational and meniscus fabrics indicative of vadose diagenesis are, however, not well defined. Later cementation in the phreatic zone could have obliterated such fabrics.

Similar fibrous cements have been described by Scholle and Kinsman (1974) from modern coastal caliche in the Persian Gulf. These authors suggested that such cements can develop in strongly evaporitic, low relief, marine-influenced settings, where vadose zones are characterized by hypersaline brines. Ion concentration of such vadose waters in arid climates may be the result of wind-driven marine flooding (Kinsman, 1969), marine

waters drawn into the sediments by capillarity (Hsu and Siegenthaler, 1969), and/or hypersalinity as a result of evaporation of continental groundwaters (Scholle and Kinsman, 1974).

The fibrous calcite cement is always followed by a thin shell of equant spar, now selectively dolomitized (Fig. 23b). Such cement textures have been described by Buchbinder and Friedman (1980), Longman (1980), and James and Choquette (1984) as indicative of active freshwater phreatic environments. Selective dolomitization of this cement is indicative of changes in the pore-fluid chemistry. Badiozomani (1973), Land (1973), Folk and Land (1975), and Sears and Lucia (1980) attribute such dolomitization to diagenetic processes in a schizohaline environment (i.e., a floodable sabkha or a phreatic mixing zone), now controversial (Hardie, 1987).

The remaining interparticle pore space is filled with coarse blocky calcite megaspar, whose crystals show a gradual size increase away from the walls (drusy texture). This kind of cement is likewise indicative of freshwater phreatic diagenetic conditions (Friedman, 1964; Longman, 1980; Buchbinder and Friedman, 1980; James and Choquette, 1984).

Late, massive fibrous to blocky anhydrite cement is present locally throughout all facies (Fig. 23c,d). it

occurs as void-filling or replacement of the pre-existing rock. Calcite inclusions, allochem ghosts, and earlier cements are, in places, incorporated into the anhydrite cement, attesting to its replacive nature. Some of the anhydrite crystals are lenticular and are probably pseudomorphous after gypsum. The anhydrite cuts indiscriminately across particles and cements and postdates all depositional and diagenetic features, indicating a late, deep-burial origin (Fig. 23c,d).

Moore and Druckman (1981) described this kind of anhydrite cement as the product of large quantities of SO_4-rich brines which originated in the underlying Louann Salt and migrated into the Smackover Formation late in its diagenetic history. These Louann brines may have displaced the original connate fluid and caused the precipitation of gypsum and anhydrite cements.

5.2.3 Leaching

Leaching affected only the upper Smackover grainstone and packstone units and was a very important process in porosity enhancement (Fig. 23a). Fabric-selective moldic and vuggy porosity types are abundant in these facies.

Two leaching episodes are evident from petrographic analysis. Early leaching followed penecontemporaneous

dolomitization and marine phreatic cementation and preceded meteoric cementation, later dolomitization, compaction, and late anhydrite cementation as indicated by the presence of whole or crushed rings of isopachous rim cements (Fig. 23a) and dolomitized, leached, crushed ooids filled with blocky anhydrite cement (Fig. 23c). This stage of dissolution most probably occurred during subaerial diagenesis when the grainstone and packstone units became exposed to meteoric solutions undersaturated with respect to carbonate. The original metastable mineralogy of the ooids had not yet been converted to relatively more stable dolomite. Porosity of the shoal grainstones was greatly enhanced during this early stage of leaching.

A second, less extensive, leaching episode is indicated by rare enlarged oomolds (larger in size than average ooids), corroded particles and interparticle voids, and partial dissolution of early and late cements. This stage of dissolution postdates compaction and late anhydrite cementation. Moore and Druckman (1981) and Benson and Mancini (1984) associated this stage of dissolution with the introduction of CO_2- and H_2S-charged fluids generated during hydrocarbon maturation within the pore voids.

5.2.4 Compaction

The dominant evidence of compaction is stylolitization, the result of pressure solution. Stylolites are more abundant in the lower units of the Smackover Formation (mudstone and wackestone facies). In these units pressure solution has dissolved out considerable amounts of lime mudstone leaving a residue of detrital quartz silt, local anhydrite laths, and dolomitized allochems sutured by stylolite seams (Fig. 18c,d).

Compaction features such as crushed grains, sutured grain contacts, and pressure solution stylolitization are present in the upper Smackover grainstone and packstone facies, however, they are not common, and have had little or no effect on porosity preservation (Fig. 23a).

Stylolitization selectivity is most probably related to dolomitization selectivity and extent, as well as early cementation. Stylolitization was extensive where dolomitization was limited and where early cement is absent. Stylolites never cut across allochems that are selectively dolomitized; instead there was preferential dissolution of the lime mudstone around the allochems.

5.2.5 Porosity Types

Porosity in the study area varies from 0, in the lower Smackover facies, to 27%, in the upper Smackover grainstones. Five different kinds of pores are present in the studied cores; they are primary interparticle, dolomitic intercrystalline, fabric selective moldic, dissolution vuggy, and microfracture/stylolitic (Fig. 24a,b,c,d).

The lower Smackover mudstone and wackestone facies contain the lowest porosity values (<10%) in the studied area. Porosity types include mostly stylolitic and microfracture (Fig. 24c,d). Moldic, vuggy and intercrystalline pores are uncommon, and poorly interconnected. Where dolomite exceeds 50% of the total carbonate, porosity is higher. Extensively dolomitized zones of this type are, however, thin (<3ft.; 1 m) and uncommon in the lower Smackover.

Reservoir grade porosity is restricted to the upper Smackover peloidal/oolitic grainstones and packstones. The highest porosity values (up to 27%) were observed in zones where the facies is completely obliterated by neomorphic growth of coarse rhombic dolomite crystals in loose contact (i.e., hypidiotopic to idiotopic fabric; Figs. 22c, 24b). In zones where dolomite is finely-crystalline and the original depositional texture preserved, porosity is lower and includes interparticle,

moldic, and vuggy pores (Figs. 22a, 24a).

Diagenetic leaching and mineral replacement have enhanced original depositional porosity, whereas cementation and compaction were minor and had no profound effect in reducing porosity. Late, clear, fibrous and bladed anhydrite cement occluded some of the early diagenetic and depositional porosity. This cement, however, rarely exceeds 10% of the mineral components of the facies and thus its effect in reducing porosity is not great.

Porosity development is facies selective and is related to the degree of dolomitization and size of dolomite crystals as well as to the extent of leaching.

5.3 Summary of Depositional and Diagenetic Sequence

5.3.1 Depositional Summary

The Conecuh Embayment is a large shallow basin which formed by marine transgression over the eolian and intertidal sandstones of the Norphlet Formation. Paleobathymetric highs encircled the embayment creating restricted conditions and poor circulation, and controlling deposition.

In general, the Smackover Formation and overlying Buckner Formation comprise a prograding coastal complex analogous to the Holocene sedimentation in the Persian

Gulf. This complex consists of shallow-water carbonates deposited in protected lagoons and barriers, and evaporites and siliciclastic sediments deposited in supratidal flats (Fig. 25).

The lower Smackover laminated mudstones and pelletal-oncoidal mudstones and wackestones were deposited during recurring sea-level fluctuations in a low-energy intertidal to shallow subtidal environment, at the time of a regional transgression of the sea over the Norphlet Formation, which controlled deposition during the early Smackover time.

The upper Smackover dolomitized oolitic-peloidal sands reflect moderate- to high-energy intertidal deposition on a local paleotopographic high. Deposition of these sands marked the beginning of a regional regression. The shoal sands were deposited during small, recurring sea-level fluctuations when sedimentation rates were in equilibrium with local subsidence, producing a thick, relatively monotonous shoal sequence.

Toward the end of Smackover deposition, however, regression rate increased rapidly, causing infilling of the backshoal lagoons and rapid progradation of the sabkha over the shoal grainstones.

The relative absence and scarcity of fossil assemblages suggest relatively restricted, stressful

FIGURE 25. Idealized schematic block diagram of the environmental setting during deposition of the upper Smackover lithofacies along the ancestral Alabama-Florida shelf margin. Oolitic shoals, formed on top of paleobathymetric highs, restricted circulation in the shallow lagoons, leeward of the shoals, where pelletal muds and algal oncoids were deposited. Landward of the embayment, evaporitic sabkha flats were rapidly prograding over the upper Smackover shoaling upward sequence.

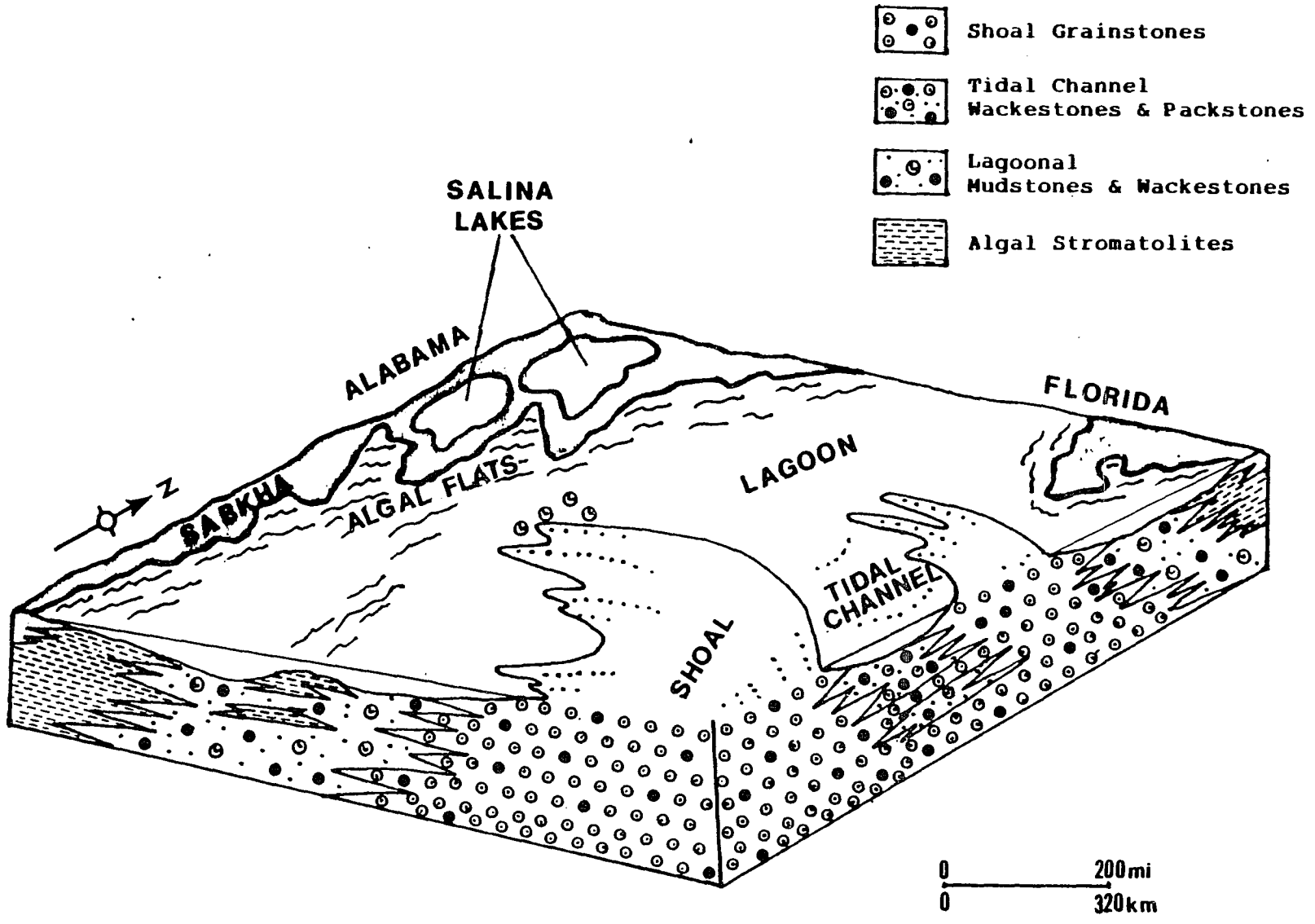
Shoal Grainstones
Tidal Channel
Wackestones & Packstones
Lagoonal
Mudstones & Wackestones
Algal Stromatolites
SALINA
LAKES
ALABAMA
FLORIDA
SABKHA
ALGAL FLATS
LAGOON
TIDAL
CHANNEL
SHOAL
N
0
200mi
0
320km

conditions during the time of deposition. Local paleohighs may have inhibited water circulation in the Conecuh Embayment (labeled lagoon in figure 25). The few normal marine taxa present include algae, ostracods, echinoids, and benthic foraminifers. The abundance of fecal pellets, however, indicates that soft-bodied sediment-ingesting organisms were abundant in this inhospitable environment.

The skeletal limestone found in the upper middle part of the Smackover in the Jay trend area and interpreted to represent maximum transgression of the Jurassic sea (Sigsby, 1976), is not present in the studied cores. Local restriction may be responsible for the absence of this facies from the studied cores.

5.3.2 Diagenetic Summary

The sequence of diagenetic events played a very important role in the development of reservoir facies in Jay field. Four general stages of diagenesis affected the cores of the study area, and are described below in a chronological order:

1-Penecontemporaneous diagenesis-Bladed isopachous carbonate cement with polygonal intersections coats the allochems of the moderate- to high-energy shoal facies. This cement was precipitated (penecontemporaneously) in

the marine phreatic environment. In addition, allochems were extensively micritized by boring microorganisms. Early dolomitization of the low-energy peritidal carbonates began during the time of deposition of these facies, as a result of recurring sea-level fluctuations which at times resulted in subaerial exposure of the peritidal carbonates.

2-Shallow meteoric diagenesis-recurring sea-level fluctuations periodically exposed the shoal carbonates. Meteoric fluids of the subaerial vadose environment selectively leached the metastable carbonate resulting in well-developed moldic porosity. Meteoric fluids rarely penetrated the peritidal low-energy carbonates as indicated by the relative scarcity of molds and vugs in these facies. Early syndepositional conversion of metastable carbonate to stable dolomite and low porosity and permeability values may have inhibited the meteoric fluids from penetrating and leaching these carbonates.

In the Cities Service Lizenby #5-3 well, subaerial exposure resulted in the formation of vadose pisoids and the precipitation of fibrous marine vadose cements in the interpisoid voids. These fibrous cements were followed by fresh-water phreatic cements, filling the remaining interpisoid pore voids and completely occluding porosity.

3-Fluid (meteoric-marine) mixing diagenesis-replacement

of carbonate by finely- to coarsely-crystalline rhombic dolomite in the shoal facies. This later dolomitization did not noticeably affect the lower Smackover mudstones and wackestones. The relative scarcity of pressure solution stylolites suggests that dolomitization started before significant burial, stabilizing the carbonate framework and inhibiting dissolution of the grains.

4-Subsurface diagenesis-Pressure solution stylolitization, the result of overburden pressure, affected mostly the lower Smackover mudstones and wackestones. The upper Smackover shoal grainstones were mineralogically stabilized through extensive dolomitization prior to significant burial, and thus were not significantly affected by pressure solution. Solutions released during stylolitization were probably responsible for the minor amounts of saddle dolomite cement, as indicated by the relative abundance of these cements in the lower Smackover extensively stylolitized facies, and the relative absence of these cements from the upper Smackover grainstones.

Subsurface migration of SO_4-rich brines, possibly from the underlying Louann Salt, resulted in the precipitation of gypsum and anhydrite cements, and partial replacement of the carbonate minerals by evaporite minerals. These evaporitic cements occluded

some of the earlier-generated porosity, however, their effect was minor. CO_2- and H_2S-rich fluids, generated during hydrocarbon maturation (Moore and Druckman, 1981), resulted in some late-stage dissolution the effects of which were, however, insignificant in enhancing porosity.

6. PETROPHYSICAL MODELING OF THE SMACKOVER CARBONATES

The occurrence and migration of fluids in a porous rock body depend on the physical and chemical properties of the fluids as well as the petrophysical properties of the porous body. To evaluate a capillary system properly, one must, therefore, define, characterize and quantify these properties. One must, however, keep in mind that these properties are heterogeneous and complicated, particularly from the microscopic viewpoint.

It is difficult to get direct measurements of factors such as porosity, permeability, hydrocarbon saturation, and thickness of rock unit in place by coring or other physical measurements, because complete recovery of cores cannot be assumed, cores may be contaminated with fluids, and/or fluid conditions may have changed due to pressure and temperature changes on bringing the core to the surface. We must, therefore, resort to indirect measurements, such as geophysical logs as well as experimentally derived petrophysical and fluid properties (Archie, 1950).

Mercury porosimetry is an experimental method which best reproduces reservoir conditions, allowing accurate determinations of pore geometry. However, caution must be used because it does not include the effects of inhomogeneities caused by fractures, stylolites, or

sedimentary structures that may be present in the reservoir, adding to the effective porosity.

Petrophysical data on the Smackover Jay field dolostones were attained primarily from the mercury-capillary-pressure curves generated from Hg-porosimetry, thin section analyses, and wire-line logs. These experiments determined total porosity, available porosity, pore-throat geometry and pore-size sorting, permeability, and height of oil column. A number of petrophysical properties were then utilized in different combinations, in order to evaluate and classify the reservoir.

6.1 Parameters Obtained From Capillary-Pressure Data

6.1.1 Height of Oil Column

One of the many applications of capillary-pressure data is to calculate the vertical length of an oil column necessary for migration and entrapment of hydrocarbons. Vertical height is the height necessary for the buoyant force to equal the internal-pressure gradient. Any increase in this height will cause the oil to move upward.

The vertical oil column height may be calculated in terms of rock and fluid parameters using the following equation from Jennings (1987).

$$H = \frac{Pc}{(Ww - Wo)(CF)} \qquad 6\text{-}1$$

Where H = height of oil column (feet) needed to achieve the oil saturation,

Pc = capillary pressure (psi) at a given saturation,

Ww = density gradient of the formation water (psi/ft),

Wo = density gradient of the oil (psi/ft),

CF = conversion factor, needed to convert from a mercury-air system to an oil-water system.

In order to accumulate in a reservoir rock, oil must first migrate through water-filled pores. Migration is promoted by buoyant forces but is inhibited by the capillary pressures which must be overcome for an oil globule to pass from a rock pore through an adjacent pore throat (Berg, 1975).

Higher capillary pressures, the result of throat-size reduction, may be overcome by an increase in the vertical length of the oil column. Thus, equation 6-1 may be used to calculate the height of oil necessary for migration, as well as the height of oil that can be trapped; i.e., the seal capacity of the reservoir.

The difference in density gradients (Ww - Wo) defines a buoyancy force which is the main driving mechanism for migration and entrapment of hydrocarbons through water-saturated rocks in the subsurface. The

greater this density difference, the greater the buoyant force for a given length of hydrocarbon column (Schowalter, 1979).

The density gradients of the formation water and oil were calculated from two nomographs (Figs. 26, 27), using formation temperature, formation pressure, gas-oil ratio, API gravity, and water salinity for Jay field, listed in table 2.

The conversion factor (CF) converts the injection pressure from a mercury-air system to an oil-water system, and is as follows from Purcell (1949):

$$CF = \frac{T_{Hg}\cos\theta_{Hg}}{T_{o/w}\cos\theta o/w} = 24.76 \qquad 6\text{-}2$$

Where T_{Hg} = interfacial tension of mercury to air (480 dynes/cm),

θ_{Hg} = contact angle of mercury to air (40°),

$T_{o/w}$ = interfacial tension of oil to water (21 dynes/cm),

$\theta_{o/w}$ = contact angle of oil to water (45° for a 25% oil-wet reservoir).

When accurate measurement of interfacial tension ($T_{o/w}$) is not available, an estimate must be made. Published values for interfacial tension range from 13 to 36 dynes/cm (Hocott, 1938; Livingston, 1938; Schowalter, 1979; Hjelmeland and Larrondo, 1986; Jennings, 1987).

FIGURE 26. Nomograph to determine oil density of Jay field, using API gravity and gas-oil ratio (from Schowalter, 1979).

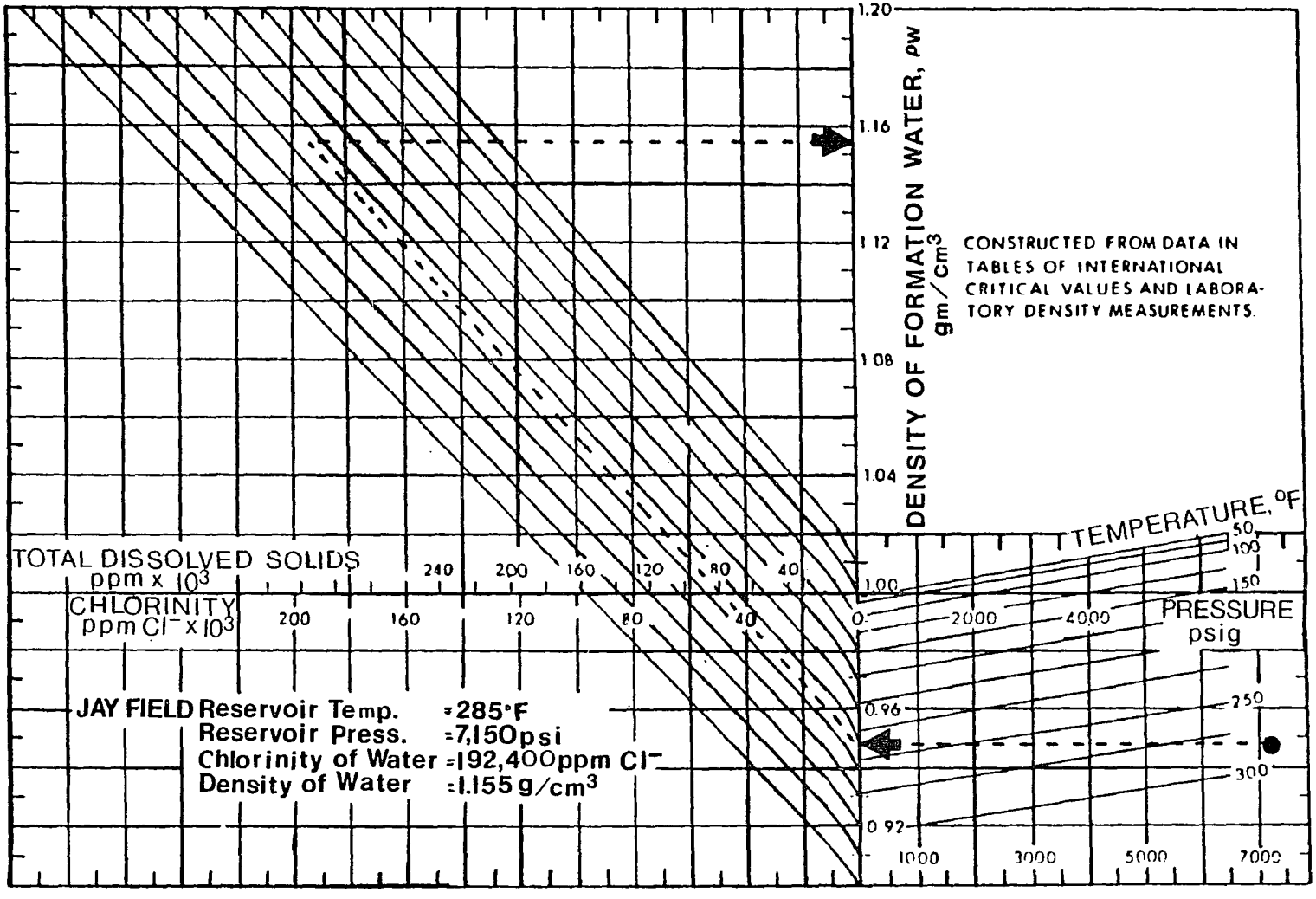
DENSITY OF FORMATION WATER, ρw gm/cm3
1.20
1.16
1.12
1.08
1.04
1.00
0.96
0.92
CONSTRUCTED FROM DATA IN TABLES OF INTERNATIONAL CRITICAL VALUES AND LABORATORY DENSITY MEASUREMENTS.
TEMPERATURE, °F
50
100
150
250
300
0
2000
4000
PRESSURE psig
1000
3000
5000
7000
TOTAL DISSOLVED SOLIDS ppm x 10³
240
200
160
120
80
40
CHLORINITY ppm Cl⁻ x 10³
200
160
120
80
40
JAY FIELD Reservoir Temp. =285°F
Reservoir Press. =7,150psi
Chlorinity of Water =192,400ppm Cl⁻
Density of Water =1.155 g/cm³

FIGURE 27. Nomograph to determine formation water density of Jay field, using reservoir pressure, reservoir temperature, and chlorinity of brine (from Schowalter, 1979).

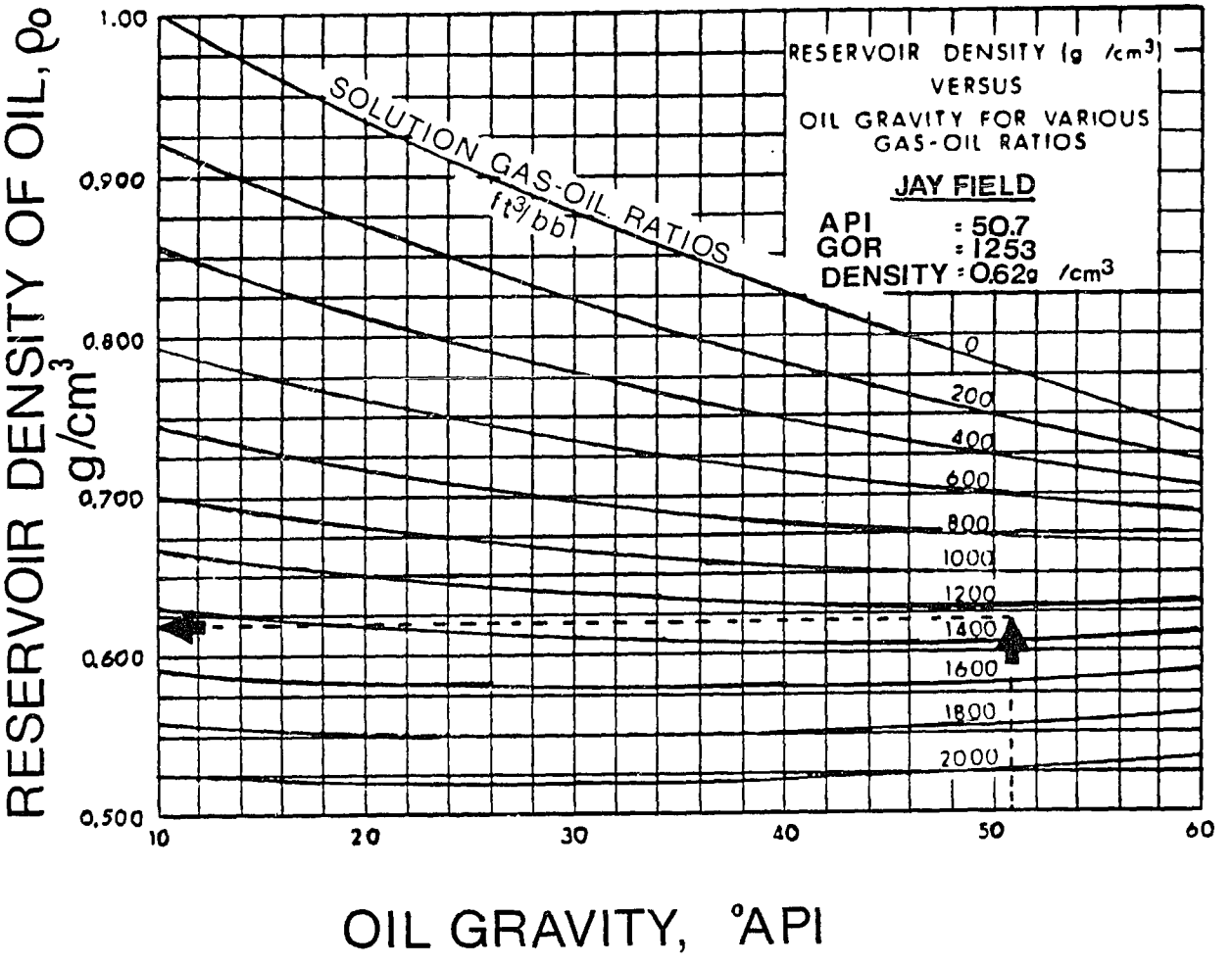
RESERVOIR DENSITY (g /cm³)
VERSUS
OIL GRAVITY FOR VARIOUS
GAS-OIL RATIOS
JAY FIELD
API : 50.7
GOR : 1253
DENSITY : 0.62g /cm³
SOLUTION GAS-OIL RATIOS
ft³/bbl
0
200
400
600
800
1000
1200
1400
1600
1800
2000
RESERVOIR DENSITY OF OIL, ρo
g/cm³
1.00
0.900
0.800
0.700
0.600
0.500
10
20
30
40
50
60
OIL GRAVITY, °API

TABLE 2. Jay field reservoir parameters.

RESERVOIR PROPERTIES (October, 1988; Florida Geological Survey, Personal Communication)

SUBSEA DATUM	15,400 ft (1,333 m)
TEMPERATURE	285°F (141°C)
ORIGINAL PRESSURE	7,850 psig (54 MPa)
CURRENT PRESSURE	7,150 psig (49 MPa)
PRODUCTION AREA	14,415 acres (58×10^6 m^2)
NET THICKNESS	95 ft (31.6 m)
ORIGINAL OIL IN PLACE (OOIP)	728×10^6 STB (116×10^6 stock-tank m^3)

ROCK AND FLUID PROPERTIES

OIL GRAVITY	50.7 °API (775 kg/cm^3)
OIL VISCOSITY	0.18 cp (0.00018 Pa.s)
GAS-OIL RATIO	1,253 ft^3/barrel (223)
ORIGINAL WATER SALINITY	192.4 ppm Cl^- x 10^3
CURRENT WATER SALINITY	20 ppm Cl^- x 10^3
TOTAL DISSOLVED SOLIDS (TTS)	317.8 ppm x 10^3
CONTACT ANGLE (θo/w)	45° (estimated)
WETTABILITY	partially oil-wet**
INTERFACIAL TENSION (To/w)	21 dynes/cm (estimated)
OIL DENSITY (Wo)	0.62 g/cm^3 (0.27 psi/ft)
WATER DENSITY (Ww)	1.155 g/cm^3 (0.499 psi/ft)
AVERAGE POROSITY	15%
AVERAGE PERMEABILITY	35 millidarcys
WATER SATURATION	12.7%
AVERAGE GRAIN SIZE	160 microns

PRODUCTION/INJECTION (July, 1984; Langston and Shirer, 1985)

OIL PRODUCTION RATE	25×10^3 STB/D (4×10^3 stock-tank m^3/D)
CUMULATIVE OIL PRODUCTION	359×10^6 STB (57×10^6 stock-tank m^3)
WATER INJECTION RATE	172×10^3 B/D (27×10^3 m^3/D)
CUMULATIVE WATER INJECTION	759×10^6 BBL (120×10^6 m^3)
GAS INJECTION RATE	61×10^6 scf/D (5.7×10^6 m^2/D)
CUMULATIVE GAS INJECTION	54×10^9 scf (5×10^9 m^2)

** Based on core flooding by Exxon petroleum company

Increasing temperature and pressure affect interfacial tension. Hocott (1938) and Livingston (1938) found a decrease in interfacial tension of approximately 0.10-0.15 dynes/cm/ F for natural crude oils and formation water, between the temperatures of 130-170°F.

The effect of increasing pressure on interfacial tension is complex. Crude oil-formation water interfacial tension tends to increase only 10-20% from atmospheric to saturation pressure, and then decrease slightly with increasing pressure (Hocott, 1938). Kusakov et al. (1954) found, however, that at pressures above 1,500 psi, continued increase in pressure had no effect on interfacial tension for crude oil-formation water systems. Thus, the effect of pressure on interfacial tension appears small enough that it can be considered negligible.

Values for interfacial tension at very high temperatures and pressures, as in the case of Jay field, are unknown. Cartmill (1976) suggested that oil-water interfacial tension may continue to decrease at high temperature and pressure and eventually become zero. He postulated that this reduction of interfacial tension at high temperature and pressure may be a mechanism for primary migration of oil from source rocks to reservoirs.

Schowalter (1979) suggested a value of 21 dynes/cm for interfacial tension can be used, with the values adjusted downward with increasing temperature by about 0.10 dynes/cm/°F. Jennings (1987), using capillary-pressure data from established fields with well-defined oil-columns, estimated interfacial tension values to range from 26 to 30 dynes/cm, giving an average of 28 dynes/cm, with an expected error of ±10% for the calculated oil column.

In the absence of measured data, an oil-water interfacial tension of 28 dynes/cm appears reasonable for depths up to 10,000 feet. For deeper reservoirs, such as Jay (approximately 15,000 feet), assuming an additional decrease in interfacial tension of 0.10 dynes/cm/ F, a value of 21 dynes/cm seems reasonable.

The height of the oil column for the Jay field reservoir was calculated using the Smith (1966) equation:

$$H = \frac{PdB - PdR}{(pw - ph) \times 0.433} = 88.6 \text{ feet } (29.5 \text{ m}) \qquad 6\text{-}3$$

Where H = maximum vertical hydrocarbon column in feet above the 100% water level (i.e., the oil/water contact),

PdB = subsurface hydrocarbon-water displacement pressure (psi) of the boundary bed,

PdR = subsurface hydrocarbon-water displacement

pressure (psi) of the reservoir rock,

pw = subsurface density (g/cm^3) of water = 1.155 (Table 2),

ph = subsurface density (g/cm^3) of oil = 0.62 (Table 2),

0.433 = a units conversion factor.

PdB and PdR were calculated to be 21.8 psi and 1.43 psi respectively using mercury-capillary-displacement values from Appendix 1, converted to subsurface oil-water capillary-pressure values. A conversion factor of 0.055 was used, which was determined using an interfacial tension of 21 dynes/cm and a simple graphic solution provided by Schowalter (1979; Figure 23).

Oil columns for 50% (marginal to fair wells) to 75% (good to excellent wells) saturations were calculated using equations 6-1 and 6-2. Calculations of vertical oil columns are important in quantifying secondary hydrocarbon migration and entrapment, in that they may be used to determine the minimum trap relief (structural or stratigraphic), needed to obtain a 50% or 75% oil saturation at the top of the trap (Schowalter, 1979; Jennings, 1987).

The oil column required for a 50% saturation provides an estimate of the minimum trap closure required to obtain a 50% oil saturation of the available

(effective) porosity. An average of 4 feet of oil is required for a 50% saturation in the sucrosic dolomite zone of Jay field. Shoal zones which are not pervasively dolomitized, such as parts of the Sam Watson and Brown wells, require 12-16 feet of oil.

The oil column required for a 75% oil saturation provides an estimate of the minimum trap closure required to obtain a 75% oil saturation of the available porosity. An average of 15 feet of oil is required for a 75% oil saturation in the sucrosic dolomite zone of the reservoir. Shoal zones which are not pervasively dolomitized require 25-62 feet of oil.

The calculated oil columns indicate that the height of the oil column reflects reservoir characteristics. Higher reservoir quality areas, associated with pervasive dolomitization, require 2-4 times less trap closure for 50 and 75% oil saturations than lower reservoir quality areas.

6.1.2 Total and Effective Porosity

Recognition of abrupt lateral and vertical heterogeneities of porosity in carbonate reservoirs and the need to understand and predict the type and amount of porosity for enhanced oil-recovery applications, were recognized early and by many workers (Imbt and Ellison,

1946; Dowling, 1970; Jardine et al., 1977; Reitzel and Callow, 1977).

Direct view of porosity is obtained by examining prepared samples under an optical or scanning electron microscope, as well as by examining resin-pore casts. In addition, porosity values (%) may be obtained from wireline logs and mercury porosimetry.

Mercury porosimetry-derived total porosity and effective porosity values were calculated using the formulas:

$$\text{Total Porosity } (\emptyset) = (D3 - D2)/(D3)(100) \qquad 6\text{-}4$$

$$\text{Effective Porosity } (\emptyset e) = (\emptyset)(SHg) \qquad 6\text{-}5$$

where: D3 = density of matrix

D2 = (M4)/(V3) = density of sample

M4 = mass of sample

V3 = (V2) - (V1) = volume of sample

V2 = volume of penetrometer

V1 = (M3)/(D1) = volume of mercury

D1 = density of mercury

M3 = (M1) - (M2) = mass of mercury

M1 = mass of penetrometer + sample + mercury

M2 = mass of penetrometer + sample

SHg = 1 - Swi

Swi = irreducible water saturation.

Mercury porosimetry-derived total porosity and

effective porosity values are listed in Appendix 1. Table 3 shows average total porosity and effective porosity for the reservoir and nonreservoir facies. Average reservoir porosity ranges from 13.7 - 16.0%, whereas nonreservoir porosity is 2.5 to 3.0 times lower: 4.7 - 6.4%.

Average porosity increases with increased dolomitization (Fig. 28), although there is considerable scatter of points. This trend, however, is not solemnly the result of increasing porosity through dolomitization. Some facies, such as the grainstones, were already quite porous when they were deposited. On the other hand, some of the diagenetically created porosity was occluded later by precipitation of anhydrite cement within the pore spaces.

A relationship exists between porosity and displacement efficiency, defined as the ratio (expressed as a percent) of the volume of mercury leaving the sample, as capillary pressure declines to a minimum value of 14 psi to the volume of mercury injected before the pressure was reduced (Wardlaw, 1976; Wardlaw and McKellar, 1981). The line was calculated using linear regression analysis.

Figure 29 illustrates that as porosity increases, mercury displacement efficiency increases. Although this

TABLE 3. Average Jay field petrophysical parameters obtained from mercury capillary-pressure data, listed in Appendix 1. Ø is the porosity in percent, Øe is the effective porosity in percent, Swi is the irreducible water saturation in percent, Pd is the displacement pressure in psi, CPT is the critical pore throat size in microns, and PTS is the pore-throat sorting.

WELL NAME	FACIES	Ø(%)	Øe(%)	Swi(%)	Pd(psi)	CPT(μ)	PTS
Bray	Reservoir	14.2	10.9	22.3	17.0	6.3	1.8
	Nonreservoir	6.4	3.9	53.8	363.3	0.3	4.1
Brown	Reservoir	13.7	11.6	16.9	57.6	2.0	1.4
	Nonreservoir	4.8	3.4	35.3	1074.2	0.1	1.4
Lizenby	Reservoir	----	----	----	-----	---	---
	Nonreservoir	4.7	2.5	53.0	463.0	0.2	3.6
McDavid	Reservoir	13.9	10.0	31.4	12.1	9.0	2.1
	Nonreservoir	6.3	4.2	34.8	451.4	0.2	3.0
Sam Watson	Reservoir	16.0	13.1	17.6	49.0	2.2	1.7
	Nonreservoir	5.1	2.7	52.7	320.0	0.3	6.7

FIGURE 28. Relationship between porosity and degree of dolomitization for all samples studied. The lower Smackover facies have low porosity and low dolomite-concentration values, whereas the upper Smackover grainstones have high porosity and high dolomite concentration-values. Dolomite concentration was obtained by point count from thin sections.

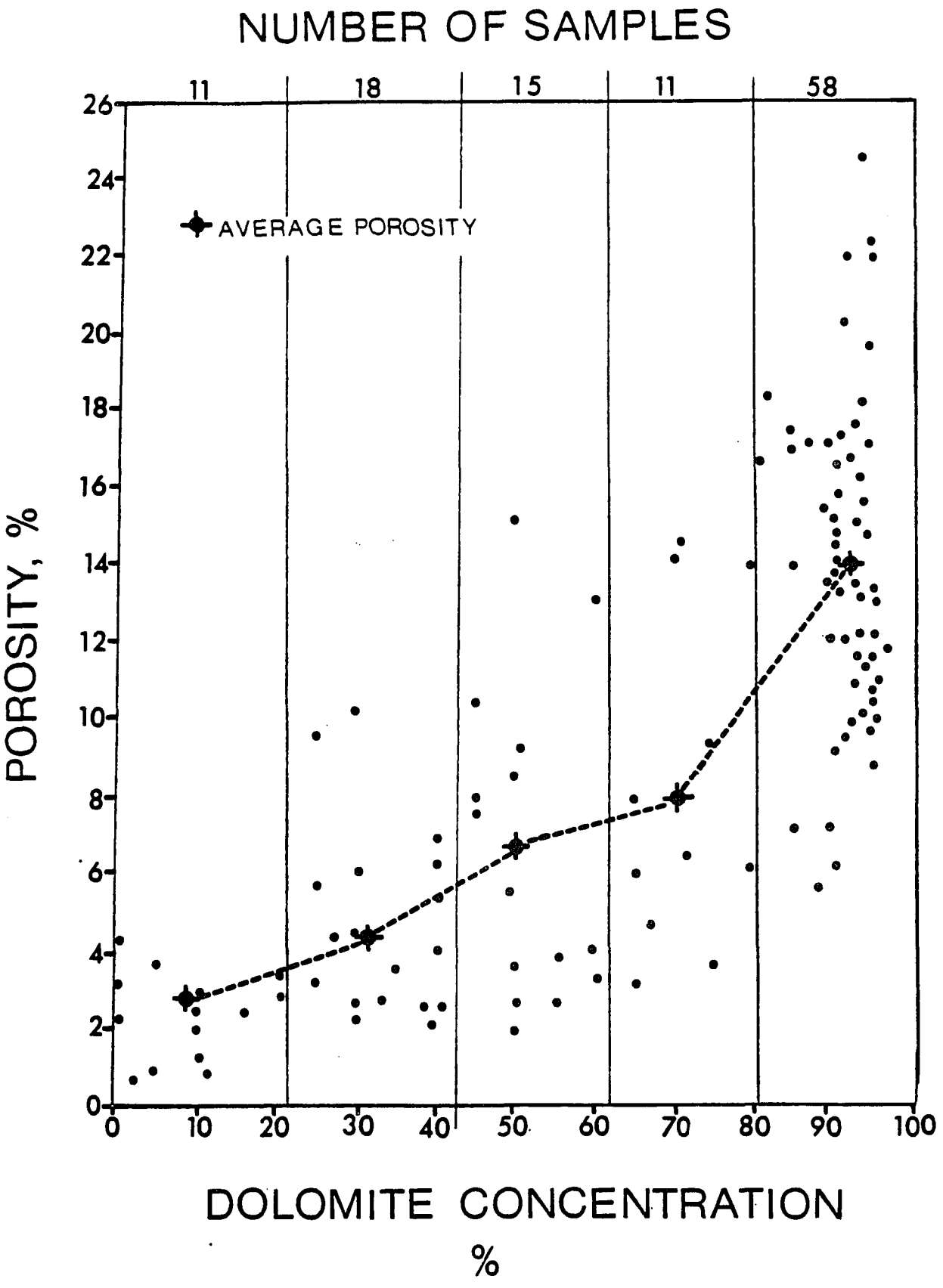
NUMBER OF SAMPLES
11
18
15
11
58
AVERAGE POROSITY
POROSITY, %
0
2
4
6
8
10
12
14
16
18
20
22
24
26
0
10
20
30
40
50
60
70
80
90
100
DOLOMITE CONCENTRATION
%

FIGURE 29. Displacement efficiency, expressed as a percentage of the volume of mercury leaving the sample (vol Hg ej) as capillary pressure declines to a minimum value, to the volume of mercury in the sample (vol Hg in) at maximum capillary pressure, versus porosity, for the three wells located within Jay field. A positive relationship exists between porosity and displacement efficiency. The equations are: (A) porosity (%) = 1.91 + 0.52(vol Hg ej/vol Hg in) x 100 and (B) porosity = 6.03 + 1.21 (vol Hg ej/vol Hg in) x 100.

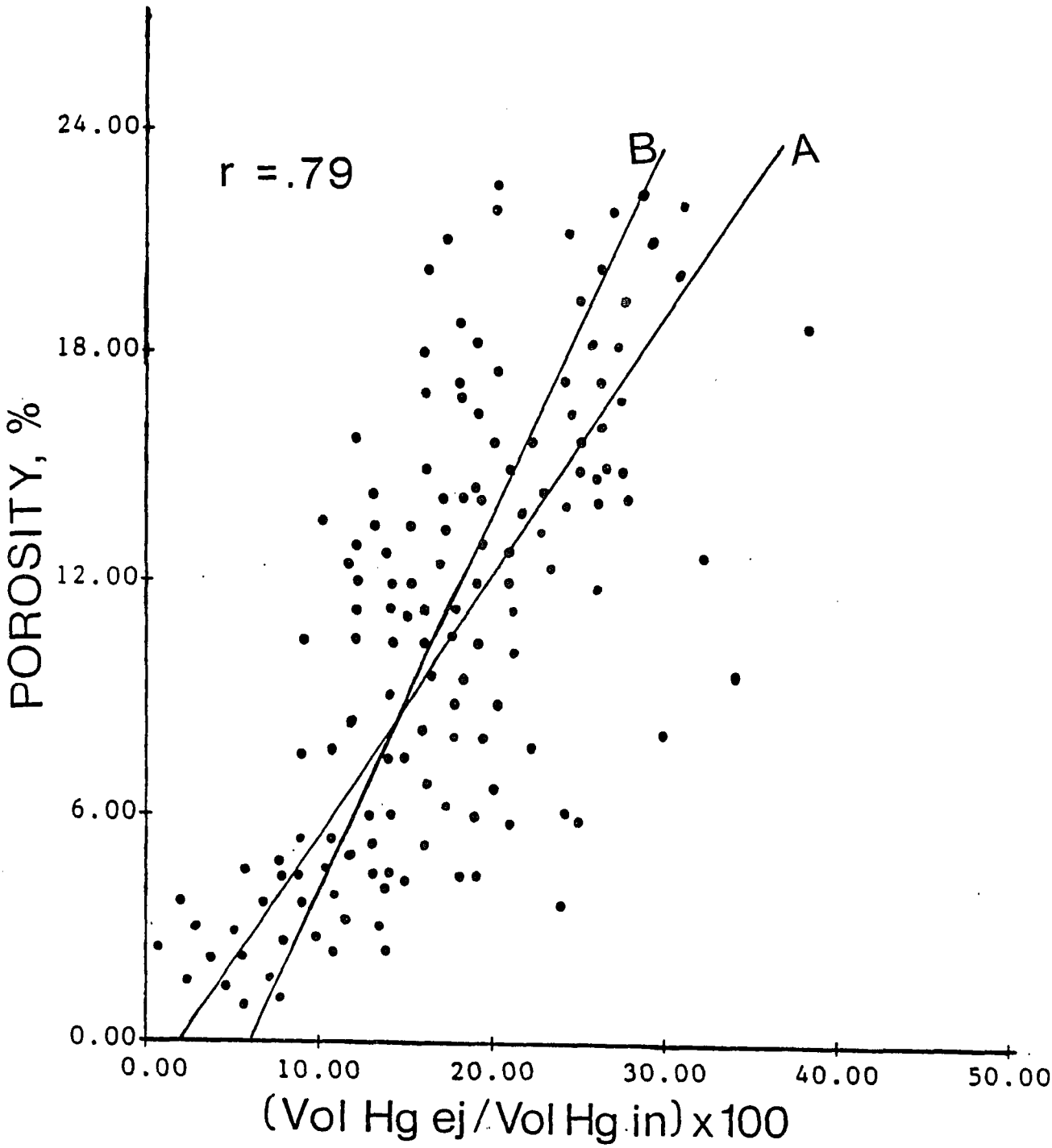
r =.79
B
A
24.00
18.00
12.00
6.00
0.00
POROSITY, %
0.00
10.00
20.00
30.00
40.00
50.00
(Vol Hg ej / Vol Hg in) x 100

relationship is not clear-cut, it is obvious that for a given porosity value there is a certain maximum displacement efficiency which never exceeds 40%. It is also clear that low-porosity rocks generally have low displacement efficiency (<20%), whereas high porosity rocks have variable displacement efficiency (5-35%).

Such positive relationship between porosity and displacement efficiency has been recorded by Wardlaw (1976, 1980) for Devonian dolostones. Larson (1977) suggested that at low porosity the number of throats connecting each pore (i.e., the degree of connectivity) is low, giving rise to high residual non-wetting phase saturations and, therefore, low displacement efficiency. At high porosity the above relationship is reversed and displacement efficiency is high.

Contrary to my results, Amthor et al. (1988) recorded, for the Ellenburger Dolomite, that porosity and displacement efficiency are inversely related.

The scattergram in figure 29 shows that for the Jay field reservoir, the difference in the values of displacement efficiency between low and high porosity is not great. In addition, some high porosity rocks have relatively low recovery efficiency values. Overall, recovery efficiency is low (<40%), most probably indicating that other parameters such as surface

roughness of pores and wettability, in addition to connectivity may be involved.

Wardlaw (1980) indicated that under conditions of intermediate wettability, as in the Jay field reservoir, pore geometry appears to be of reduced significance as a cause of trapping of the non-wetting phase and, under these conditions, displacement efficiency is greater. This does not appear to be the case here.

The Jay field reservoir facies combines favorable conditions for good displacement efficiency. The pores are well interconnected with numerous throats, the crystal surfaces lining the pores are smooth, and wettability is intermediate. However, although conditions are favorable, displacement efficiency never exceeds 40%. Low displacement efficiency may be caused by partial withdrawal of mercury from the surface complexities of larger pores as capillary pressure is lowered (Wardlaw and McKellar, 1988), as well as late anhydrite cementation.

Effective porosity is a function of mercury saturation, and as such its value is determined by the percent of irreducible water saturation (equation 6-5). Effective porosity values are thus, 72 - 85% of the total porosity values for the reservoir facies, and 53-71% for the nonreservoir facies which have higher irreducible

water saturation values (35.3 to 53.8%) versus 16.9 to 31.4% reservoir rocks.

The influence of rock and fluid properties on the magnitude of irreducible saturations was experimentally determined by Morrow (1970 and 1971). High irreducible wetting-phase saturations in porous media are caused mainly by random heterogeneities in pore structure. Fluids may be trapped as pendular rings or in clusters of fine pores because these regions lose their hydraulic continuity through the medium before the applied pressure is sufficient to effect drainage. Morrow (1970 and 1971) concluded that the magnitude of irreducible saturation is an index of packing heterogeneity, or local variation in pore-size distribution, which may reflect depositional environment and post-depositional history.

Pickell et al. (1966) showed that fluid distribution and residual non-wetting phase saturations are a function of pore-size distribution, pore configurations, interfacial properties, and initial saturation.

Melrose and Bradner (1974) reviewed factors controlling the distribution of immiscible fluids, such as oil and water, within the interstices of a porous medium. One such factor is small-scale packing heterogeneities, which, if present in a reservoir rock, increase the magnitude of residual wetting phase

saturation. In addition, experimental results for various porous systems showed that the broader the pore-size distribution, the larger the residual non-wetting phase saturation.

In Jay field, the magnitude of irreducible water saturation is clearly a function of pore geometry and pore-throat size sorting distribution, which are in turn related to depositional environment and kind and degree of dolomitization of the various facies.

Figure 30 illustrates the relationship between pore-throat size sorting (PTS) and irreducible water saturation (Swi) for both reservoir and nonreservoir facies. Although the relationship is not linear, for a certain pore-throat size sorting value there is a minimum percent of irreducible water saturation. In addition, low pore-throat size sorting values are associated with low irreducible water saturation values and vice versa.

The irreducible water saturation values used in figure 30 were obtained from mercury-porosimetry. S. K. Ghosh (personal communication, 1988) has compared Swi values of samples that were immersed in brine and centrifuged at 4000 RPM with Swi values of the same samples, obtained from mercury-porosimetry at 5000 psi (air-Hg), and found them similar. In addition, samples were sent to a core laboratory, in Dallas, to obtain

FIGURE 30. Plot of irreducible water saturation (Swi) versus pore- throat size sorting (PTS) for all data. The small dots represent reservoir facies, while the larger dots represent nonreservoir facies. The dashed line indicates the minimum percent irreducible water saturation for a certain pore-throat sorting value.

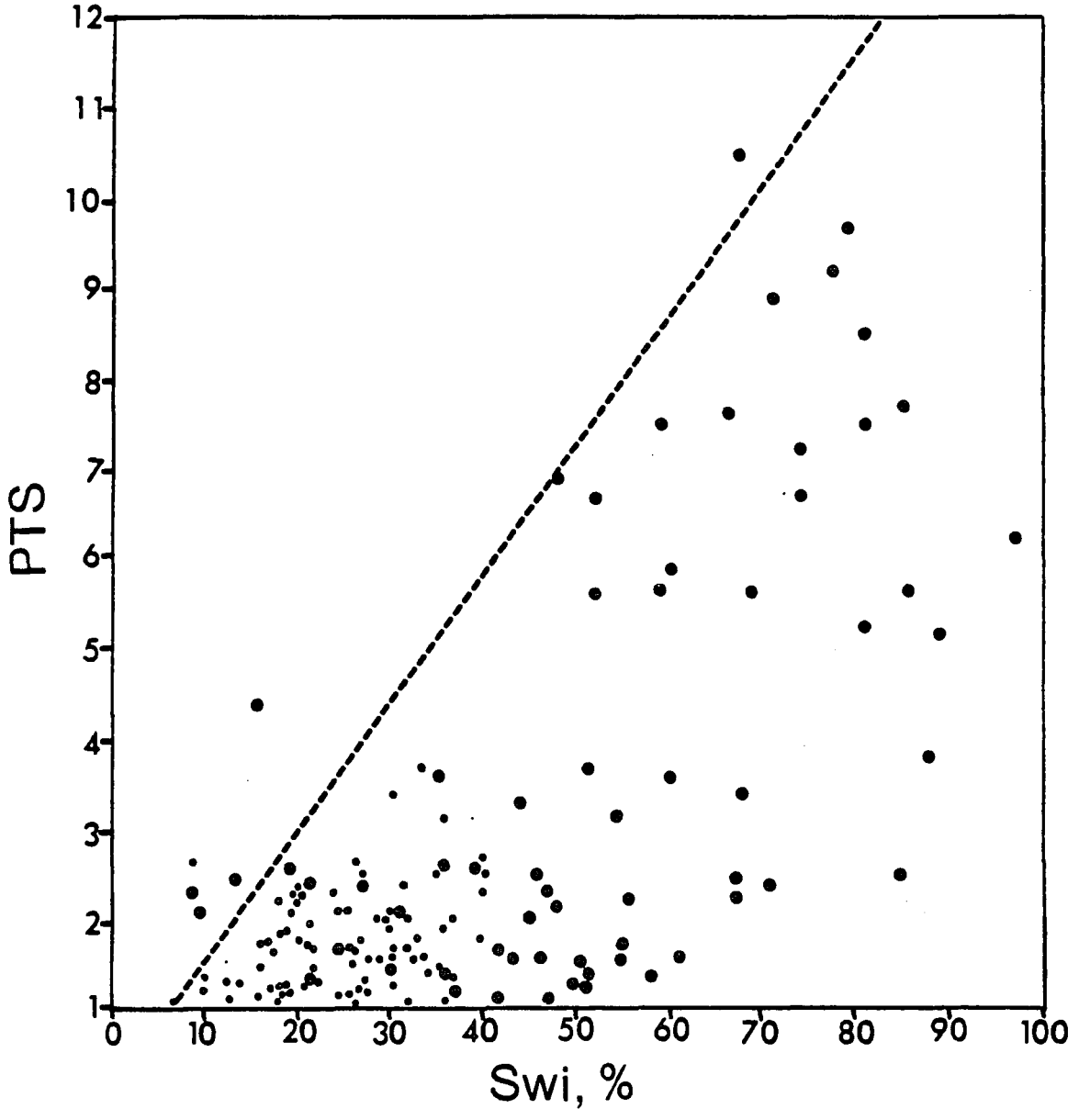
PTS
Swi, %
12
11
10
9
8
7
6
5
4
3
2
1
0
10
20
30
40
50
60
70
80
90
100

capillary-pressure-curves using the centrifuge method. The curves obtained were exact replicas of those obtained by the mercury-porosimetry method, proving that Swi values can be reliably obtained from mercury-porosimetry. Caution must be used, however, because the properties of mercury are not the same as those of brine.

The reservoir facies are moderate- to high-energy grainstones, now composed almost exclusively of medium-crystalline sucrosic dolomite. Porosity is diagenetic dolomite intercrystalline, exhibiting low irreducible water saturation values (never exceeding 40%; Fig. 30), average to good pore-throat size sorting (1.1-2.7), large critical pore-throat sizes (2-9 microns), and very low displacement pressures (12-57 psi), indicating the pores are homogeneous in size and well interconnected by numerous large pore throats.

Figures 31 and 32 show porosimeter-derived injection/withdrawal curves of the reservoir facies from two different wells. Both samples exhibit similar porosity, pore-throat size sorting and irreducible water-saturation values, indicating that irreducible water saturation is a function of pore-size distribution and pore configuration. The displacement pressures for the two reservoir samples are considerably different, indicating that although the pore throat sizes are well

FIGURE 31. Injection/withdrawal curves for dolomitized pelletal/peloidal packstone; McDavid Lands well (15524 ft). The sample has good porosity (Ø), permeability (K), and pore-throat size sorting ((PTS), and low displacement pressure (Pd) and irreducible water saturation (Swi).

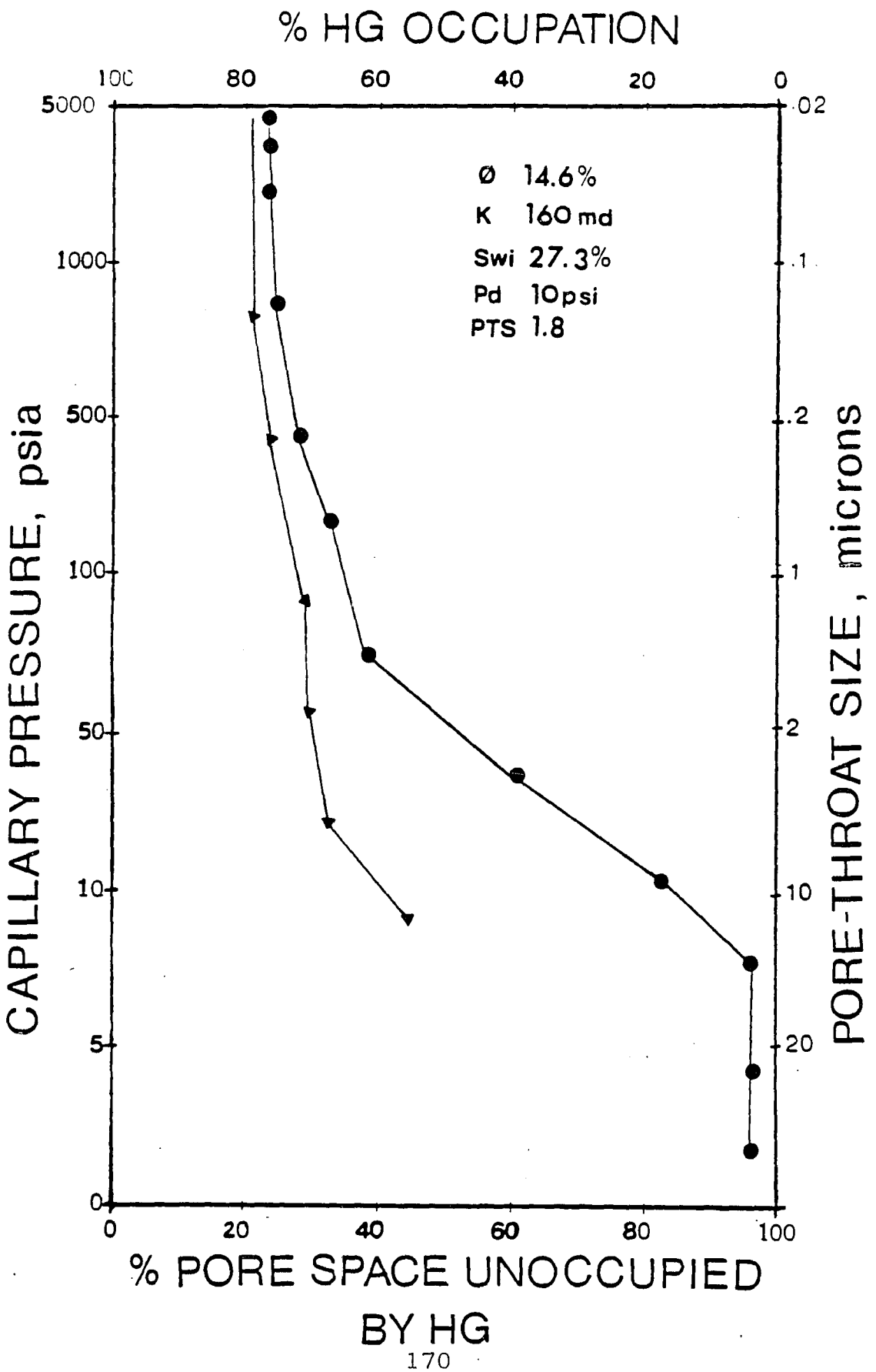
% HG OCCUPATION
100
80
60
40
20
0
5000
1000
500
100
50
10
5
0
.02
.1
.2
1
2
10
20
Ø 14.6%
K 160 md
Swi 27.3%
Pd 10psi
PTS 1.8
CAPILLARY PRESSURE, psia
PORE-THROAT SIZE, microns
0
20
40
60
80
100
% PORE SPACE UNOCCUPIED BY HG

FIGURE 32. Injection/withdrawal curves for sucrosic dolomite; C.H. Bray well (15550 ft). The sample has good porosity (Ø) and pore-throat size sorting (PTS), low irreducible water saturation (Swi), low permeability (K), and high displacement pressure (Pd).

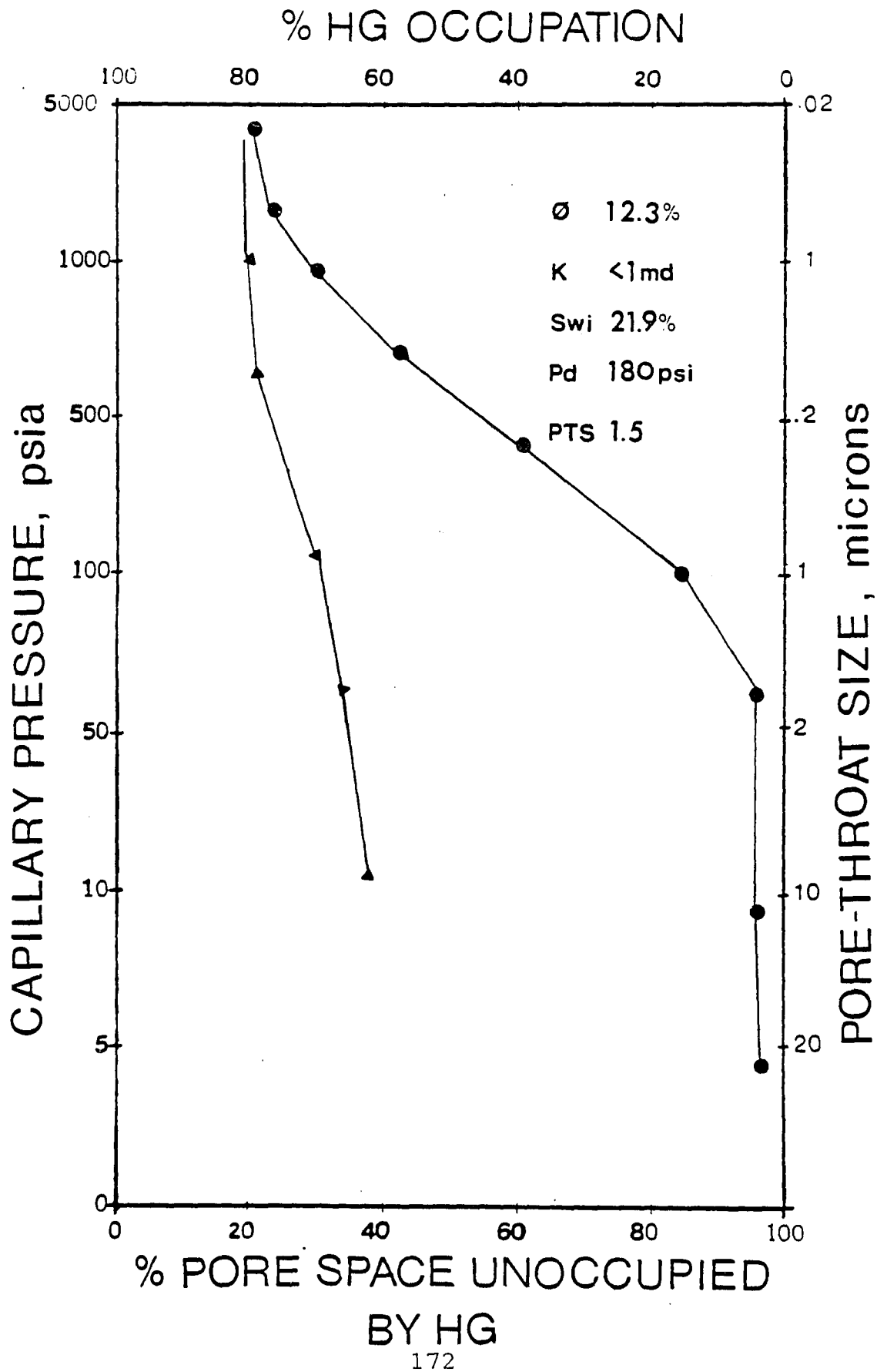
% HG OCCUPATION
100
80
60
40
20
0
5000
1000
500
100
50
10
5
0
.02
1
.2
1
2
10
20
Ø 12.3%
K <1md
Swi 21.9%
Pd 180psi
PTS 1.5
CAPILLARY PRESSURE, psia
PORE-THROAT SIZE, microns
0
20
40
60
80
100
% PORE SPACE UNOCCUPIED BY HG

sorted in both, their average size varies considerably. More specifically, in figure 31 the average pore-throat size ranges between 1.7 to 0.2 microns, whereas in figure 30 the average pore throat size ranges between 2 to 15 microns. This large variation in the average pore throat size between the two samples does not appear to have an effect on the value of the irreducible water saturation, or the mercury displacement efficiency of the two samples.

The nonreservoir facies are low-energy mudstones and wackestones, now partially composed of finely crystalline dolomite, with small intercrystalline pores in addition to larger moldic, vuggy, and some fracture pores. In general, irreducible water saturation values are highly variable (10-90%; Fig. 30), pore- throat size sorting is good to very poor (1.2->10), average critical pore-throat size (e.g., pore-throat size at which maximum intrusion of mercury occurs for relatively small pressure increase) is very small (0.1-0.3 microns), and displacement pressure values are highly variable, indicating highly variable critical pore-throat sizes. (see Appendix 1 and table 3), porosity is low, heterogeneous in nature, and pores are poorly interconnected by small, relatively long throats. Figure 33 shows an injection/withdrawal curve of the nonreservoir facies. Although the porosity of

FIGURE 33. Injection/withdrawal curves for partially dolomitized pelletal/peloidal wackestone; McDavid Lands well (15542). The sample has high porosity (Ø) and high irreducible water saturation (Swi), low permeability (K) and low displacement pressure (Pd), and poor pore-throat size sorting (PTS).

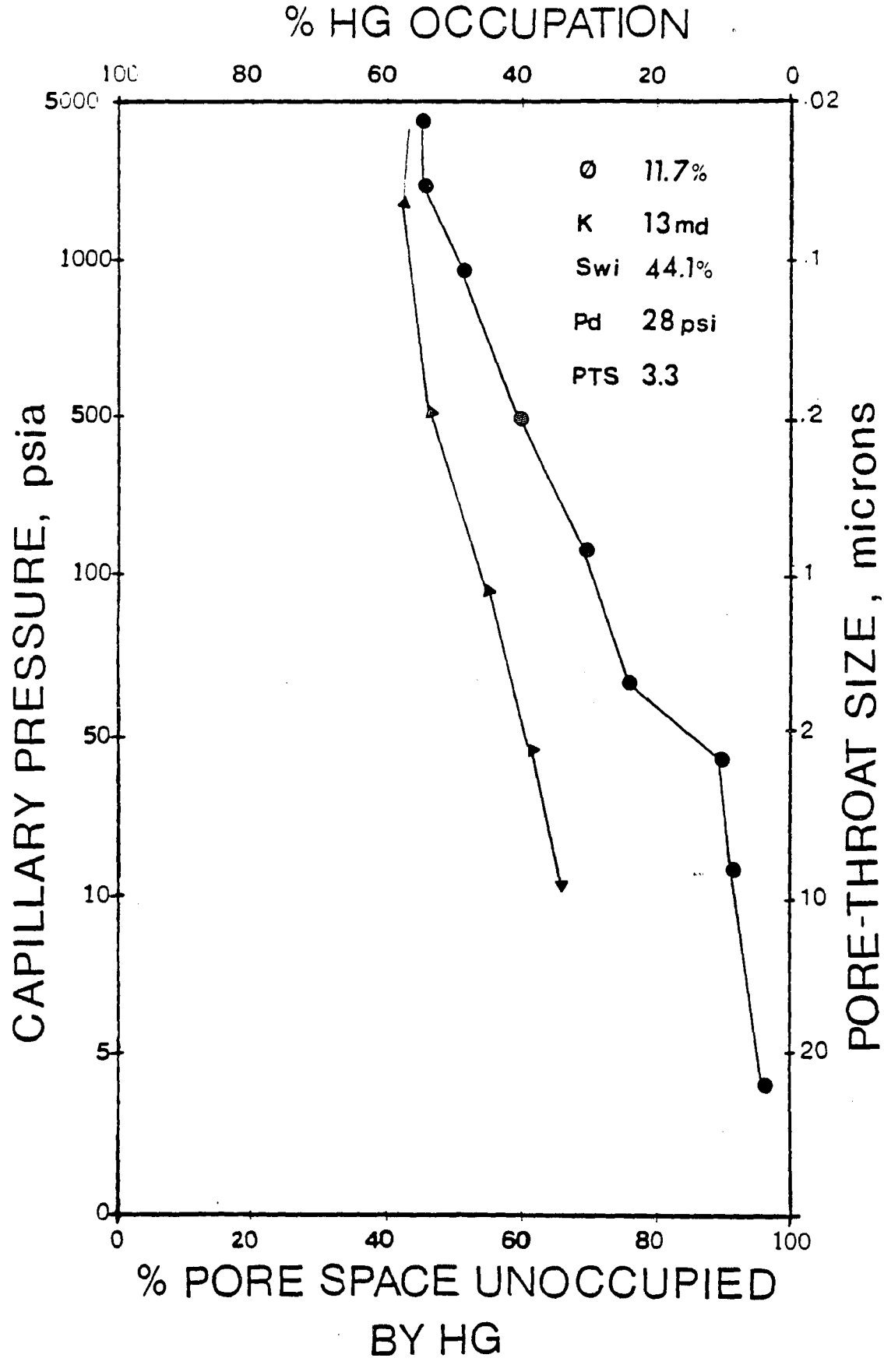
% HG OCCUPATION
100
80
60
40
20
0
5000
1000
500
100
50
10
5
0
.02
.1
.2
1
2
10
20
Ø 11.7%
K 13md
Swi 44.1%
Pd 28 psi
PTS 3.3
CAPILLARY PRESSURE, psia
PORE-THROAT SIZE, microns
0
20
40
60
80
100
% PORE SPACE UNOCCUPIED BY HG

this sample is very similar to those of the samples in figures 31 and 32, pore-throat size sorting is very poor, and as a consequence the irreducible water saturation is very high.

In conclusion, the amount of irreducible water saturation is a function of pore-throat size sorting, and is not affected by the amount of porosity or the average size of the pore throats.

6.1.3 Pore-Throat Size and Size Sorting

Reservoir quality and hydrocarbon-producing potential of a rock depend on the physical properties of the throats connecting the pores, the most important of which are pore throat size and size sorting.

Pore throats contribute little to the total pore volume of reservoir rocks, however, they are of great importance because they are the access to the pores (e.g., control permeability) and thus they are an important parameter when estimating hydrocarbon migration and recovery. The smaller the size of the pore throats in a rock, the greater the displacement pressure required for secondary hydrocarbon migration. In the case of dolomite reservoirs, pore throats are a function of the size, shape, and type of intercrystal boundaries of the dolomite crystals forming the rock matrix.

Visual and empirical estimates of pore-throat size are difficult to make. Mercury capillary-pressure curves offer the most common experimental method of determining pore-throat geometry in reservoir rocks, because the shape of the capillary-pressure curves is dependent on the size and size sorting of the pore throats through which the invading liquid must pass, and not on the size of the pores (Dullien and Dhawan, 1974, 1975).

Parameters such as pore-throat "radius" and size sorting are easily and efficiently estimated by mercury capillary-pressure tests. This method should be used with caution, however, because mercury penetration is never quite complete, and it takes practically infinite pressure to perfectly fill the pores (Dullien, 1979). In addition, filling of larger pores may be delayed because access through neighboring smaller throats is denied until their penetration pressures are attained (Morrow and Heller, 1985).

Figures 31 and 32 illustrate mercury capillary-pressure curves for two core samples which have essentially equal porosity, pore- throat size sorting and irreducible water-saturation values. Judging from these parameters, one might expect both samples to make good reservoir rocks. This is not the case, however. The porosity value of the core sample in figure 31 is

deceiving, because it is the small pore throats separating the pores which control productivity, requiring high pressures to allow oil movement. On the contrary, the pore throats in figure 32 are relatively large, and would allow oil to move at relatively low pressures, making this sample a better reservoir candidate.

Figure 33 illustrates a mercury capillary-pressure curve for a partially dolomitized wackestone. Observed under the microscope, this rock as well as the ones illustrated in figures 31 and 32 have the same visual porosity, and it may be assumed that all three samples have comparable producing capabilities. This again does not hold. Only 55% of the porosity of the sample in figure 33 could hold oil in a reservoir, and thus the sample could not be considered a good reservoir rock.

From the the above illustrations of capillary-pressure curves, it is obvious that the producing capabilities of the rocks are controlled not only by porosity and permeability but also by pore-throat geometry. The smaller the "radius" of a pore throat, the larger the displacement pressure required for penetration and vice versa. Thus, pore-throat size is critical in estimating displacement pressure in a reservoir.

The average displacement pressure values for

reservoir facies range from 12 to 57 psia (Appendix 1 and Table 3). This is equivalent to pore-throat sizes ranging from 2.0 to 9.0 microns. For nonreservoir facies average displacement pressures range from 364-1074 psia, which is equivalent to pore-throat sizes ranging from 0.1 to 0.3 microns.

In this study, displacement pressure (or critical pore- throat size) most commonly occurs when mercury saturation reaches 15 t0 20% of the pore space (see Q1 values in Appendix 1). Displacement pressure, which is directly related to pore-throat size, is the most important parameter, when differentiating reservoir from nonreservoir facies, because it is a parameter which shows considerable variation between reservoir and nonreservoir facies.

The large variation in the size of pore throats between reservoir and nonreservoir facies is the result of the difference in the nature and degree of dolomitization between the two facies, which is in turn influenced by the size of dolomite rhombs, and thus the size of the void spaces between the dolomite rhombs.

Pore throat size sorting (PTS) is a number that measures the sorting of the pore throats as follows:

$$PTS = \frac{(3rd\ Quartile\ Pressure)^{1/2}}{(1st\ Quartile\ Pressure)^{1/2}} \qquad 6\text{-}6$$

For the Jay field reservoir and nonreservoir facies

PTS ranges from 1.1 (near-perfect sorting) to 20.7 (extremely poor sorting). The higher PTS values are usually associated with the nonreservoir facies; however, no clear-cut relationship exists between the PTS values of the two facies (see Appendix 1).

6.1.4 Permeability

Purcell (1949) developed a method which provides a means of calculating the permeability of a porous medium from mercury injection capillary-pressure data, by measuring the area under a curve, defined by plotting 1/p2 (P2 is the second quartile pressure) vs. mercury saturations. The method, however, is laborious and permeability estimates are not reliable.

Jennings (1987) developed a simpler method of obtaining permeability estimates from samples possessing moderate- to well-sorted pore geometries, using a log-log plot of the second quartile pressure (P2) vs. permeability (K; Fig. 34). P2 is calculated by dividing the mercury saturation at 5,000 psi by 2, which provides the saturation where 50% of the effective porosity is filled with mercury.

A number of constraints are placed, however, on the capillary-pressure data to obtain results:

1) The capillary-pressure curve should display moderate

FIGURE 34. Log-log plot showing permeability (k) estimation using the second quartile pressure (P2), derived from porosimetry data (see Appendix 1). A strong negative correlation exists between permeability and second quartile pressure. The equations are (A) $K = 99.36 - 1.62(P2)$ and (B) $K = 61.69 - 0.59(P2)$.

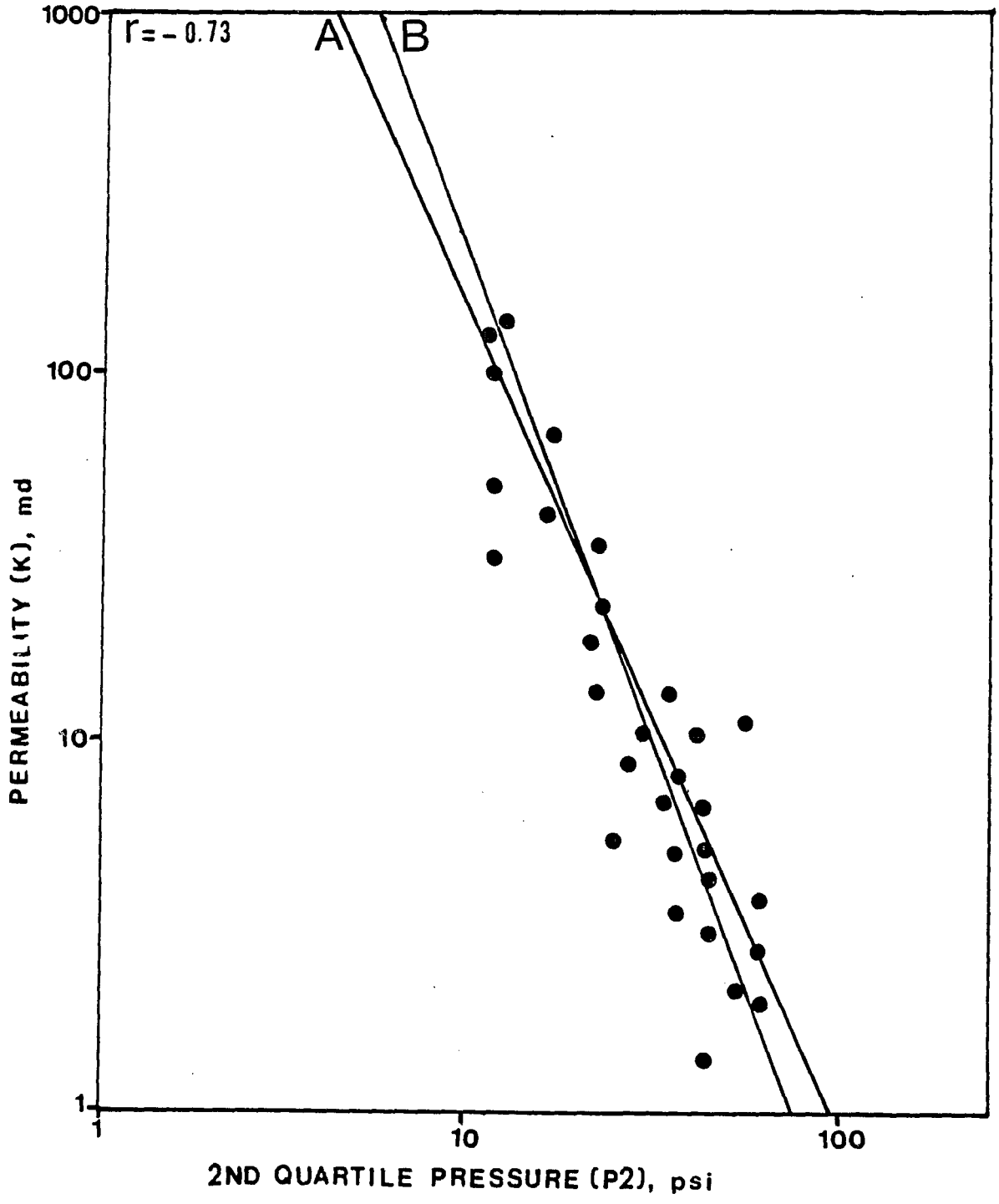
r = - 0.73
A
B
1000
100
10
1
PERMEABILITY (K), md
1
10
100
2ND QUARTILE PRESSURE (P2), psi

to well-sorted pore-throat sorting (less or equal to 2.0), because porosity and permeability exhibit an interdependence. As pore- throat sorting decreases in quality (i.e., gets poorer), porosity becomes less interdependent with permeability, and the rock begins to take on the characteristics of a dual-porosity reservoir, making permeability estimates less accurate.

2) Accuracy drops off considerably for permeabilities of less than 1 md, indicating smaller pore throats exhibit different relationships with permeability. Quartile pressures above 130 psi (80 psi in the case of Jay field) can only be categorized as having permeabilities of less than 1 md (Jennings, 1987).

3) The irreducible water saturation should be less than 25%, since high irreducible water saturations are indicators of poor pore-throat sortings. Calhoun (1953) concluded that irreducible water saturation is a function of permeability; i.e., irreducible water saturation increases as permeability decreases. This conclusion is based on the idea that lower permeabilities result from increasing nonuniformity of pore structure.

In the Jay field-reservoir facies, irreducible water saturations range from 17.6%-31.4%. No distinct relationship exists between permeability values and irreducible water saturations. When one considers,

however, reservoir versus nonreservoir facies, higher permeabilities are associated with lower irreducible water saturations and vice versa.

6.1.5 Relative Permeability

Hydrocarbon production commonly involves the simultaneous flow of two or more fluids. Relative permeability is defined as the permeability of a rock to one fluid when the rock is only partially saturated with that fluid. Relative permeability, therefore, may be used to describe the multiphase flow of fluids through porous media and to estimate water and oil production in a reservoir as well as the economic limits of the reservoir.

The relative permeability of a porous medium depends on its pore geometry, wettability, saturations of the wetting and non-wetting phases, saturation history, and capillary forces. Contact angle and pore geometry, however, control capillary forces for a given rock-fluid system. Thus, relative permeability is directly dependent upon saturations of wetting or non-wetting phases and capillary pressures, and as such, it is always reported as a function of both saturations and capillary pressure (Saraf and McCaffery, 1985).

Relative permeability can be determined using

laboratory data, mathematical models, and/or data published on similar porous media. Laboratory data, derived from mercury capillary- pressure curves, may be used to calculate relative permeabilities for two-phase fluid flow.

Capillary pressure is defined as the pressure drop across the interface of any two fluid phases (e.g., oil and water) in a capillary system (e.g., the reservoir rock), with both fluids being static (Arps, 1964). As such capillary-pressure curves can be used to determine relative permeability. This technique, however, is subject to a variety of uncertainties because conditions of saturation history and fluid-flow behavior generally differ for primary, secondary, and tertiary recovery regimes. In addition, it is assumed that the reservoir was originally filled with water which was later partly displaced by oil.

A typical relationship between relative permeability and capillary pressure, for a typical Jay field reservoir facies, is illustrated in figure 35, as suggested by Arps (1964). The upper part of figure 35 shows a set of oil-water relative permeability curves plotted against interstitial water saturation in percent. The lower part of figure 35 shows the depth interval (i.e., the transition zone) within which the water saturation

FIGURE 35. Relative permeabilities (Kro and Krw, oil and water respectively) and capillary-pressure curve (Pc) relationship for a typical Jay field-reservoir sample (adopted from Arps, 1964). The water-saturation scale in percent, on the horizontal axis, is the same for both graphs. Where water saturation is in excess of 95% (lower part of the transition zone), only water flows; where water saturation changes gradually from 95% to 32% (middle part of transition zone), both oil and water flow; where water saturation changes from 32% (critical water saturation) to 22% (irreducible water saturation, Swi), only oil flows.

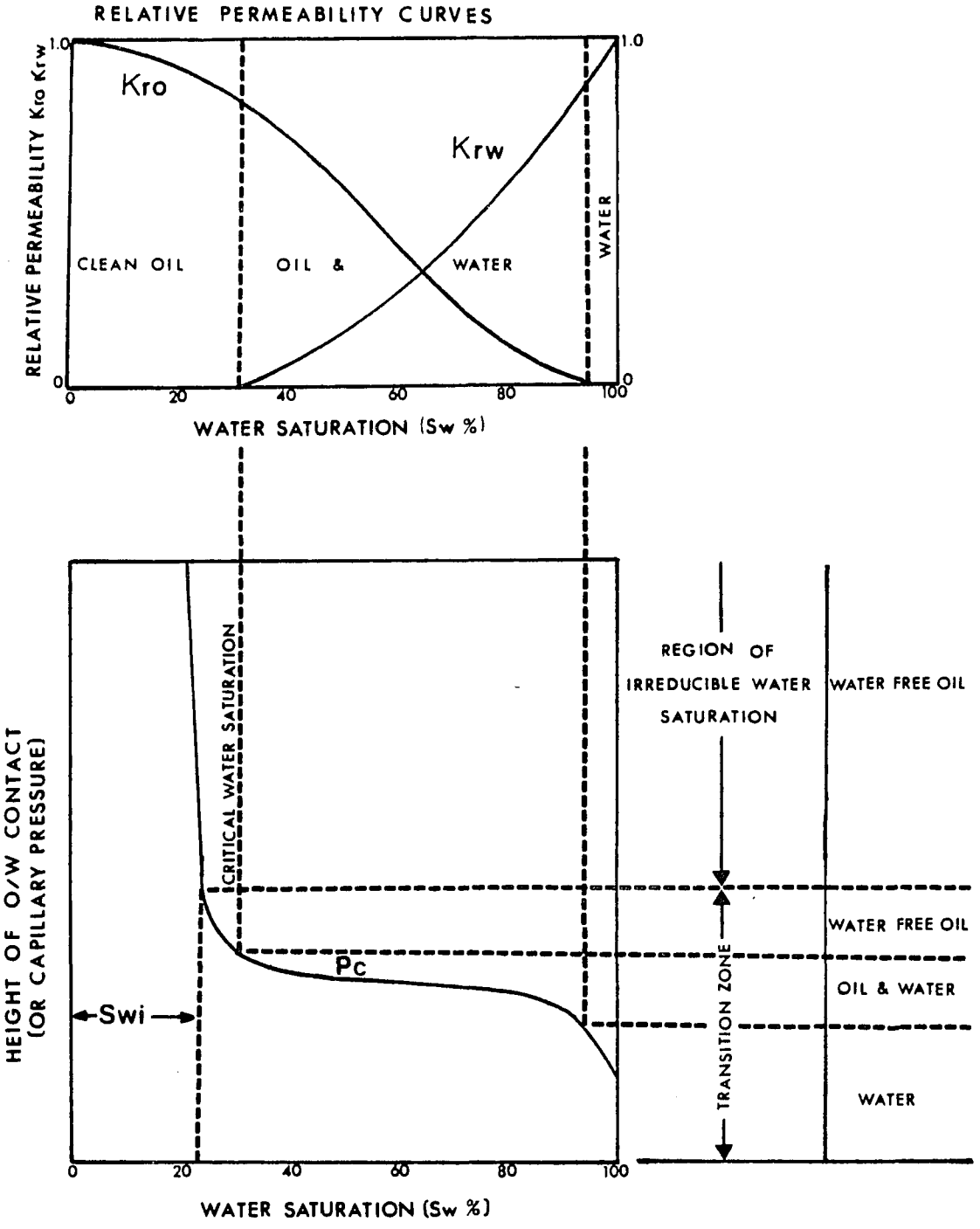
RELATIVE PERMEABILITY CURVES
RELATIVE PERMEABILITY Kro Krw
1.0
0
Kro
Krw
CLEAN OIL
OIL &
WATER
WATER
0
20
40
60
80
100
WATER SATURATION (Sw %)
HEIGHT OF O/W CONTACT (OR CAPILLARY PRESSURE)
CRITICAL WATER SATURATION
REGION OF IRREDUCIBLE WATER SATURATION
WATER FREE OIL
Pc
Swi
TRANSITION ZONE
OIL & WATER
WATER
WATER SATURATION (Sw %)

changes from 100% to 22%. Above this oil-water transition zone the reservoir is at irreducible water saturation, and will produce water-free oil. The curve labeled Kro (relative permeability of the formation to oil in the presence of varying amounts of interstitial water) begins at zero water saturation with a value of 1.0. The ability of oil to flow ceases when 95% or more of the pore space is occupied by water (i.e., at the lower boundary of the oil-water zone, of the capillary-pressure curve); only water flows.

The curve labeled Krw (relative permeability of the formation to water) reaches 1.0 when the pores are 100% saturated with water, and falls off sharply to the left reaching a zero value when the interstitial water saturation drops below 32% (critical water saturation for Jay field). Below this water saturation value of 32% there is no flow of water; only oil can move. In the part of the diagram representing the range of saturations from 32% to 95% there is permeability to both oil and water and both phases will appear in production.

The transition zone, whose thickness depends on the slope of the capillary pressure curve, is, therefore, divided into three parts as indicated by the dotted lines on figure 35: (a) A lower part, where capillary pressure causes water saturations in excess of 95%, and only water

flows; (b) a middle part, where water saturation changes gradually from 95% to 32%, and both oil and water flow; and (c) an upper part, characterized by water saturation values between the critical water saturation (32%; oil-water contact) and the irreducible water saturation (22%), where only oil flows. Of course what is actually measured here are mercury and air saturations and not oil and water.

6.2 Diagenetic Development and Petrophysical Characteristics of the Smackover Formation: A Summary

The reservoir characteristics of any rock depend on the depositional and diagenetic development of the rock, which in turn determine the petrophysical characteristics of the reservoir.

6.2.1 Diagenesis and Porosity Development of the Smackover Formation

The Smackover Formation of the studied area underwent extensive diagenetic alterations prior to significant burial, resulting in early, precompaction diagenetic fabrics. This preburial diagenetic history of the Smackover Formation played an important role in the porosity and permeability development within the sedimentary sequence. However, porosity distribution appears to be controlled by the original depositional

setting and as such, it is related to the location of the facies relative to sea level at the time of early diagenesis.

Porosity was maintained or enhanced in the most porous facies, in areas under the influence of a meteoric water system (i.e., high-energy intertidal facies). With the exception of some interparticle pores and some fabric-selective moldic and vuggy pores (Fig. 24a), porosity is almost exclusively secondary dolomite intercrystalline (Fig. 24b). In places stylolites and fracture pores are present in the low-energy, basal Smackover facies (Fig. 24c,d), but they are not significant.

The highest porosity values (up to 27%) are observed in the high-energy, intertidal oolitic and peloidal packstones and grainstones of the upper Smackover facies. This facies contains intercrystalline dolomite porosity, with some moldic pores where the original depositional fabric is preserved. With the exception of some thin zones, the original depositional fabric is, however, almost entirely destroyed by pervasive dolomitization, and the facies is now composed of hypidiotopic dolomite crystals (i.e., sucrosic texture), the result of piecemeal replacement of the precursor carbonate.

Dolomitization of the reservoir facies has proceeded

far enough to produce a well-sorted pore system, with large pores. Early dolomitization, when supporting framework was present, and later freshwater leaching have provided an extensive, complex, high quality reservoir in the upper Smackover facies. However, the irregular distribution of the facies presents difficult problems in hydrocarbon exploration, and extensive subsurface mapping of the facies is required in order to determine the lateral and vertical extent of the reservoir. In addition, the degree of dolomitization, within an otherwise homogeneous sequence poses additional problems, and detailed study of the facies is necessary.

Highly porous sucrosic dolostone (Figs. 22c,24b) alternates with lower porosity dolostone, in which dolomite growth has continued and compromise boundaries have formed (Fig. 22d). These moderately porous dolostones may act as barriers to fluid migration, and pose problems when one is trying to determine the migration path of oil and water, as well as hydrocarbon-recovery efficiency.

6.2.2 Petrophysical Characteristics of the Smackover Jay Field

More than 200 samples from the Jay field reservoir and vicinity were studied in an attempt to relate

geological parameters to petrophysical properties. The reservoir and nonreservoir facies are classified below using a variety of petrophysical properties such as porosity, effective porosity, displacement pressure (i.e., critical pore throat size), irreducible water saturation, and pore-throat sorting; easily calculated from mercury-capillary-pressure curves. These properties are summarized in Table 3.

In general, such classifications, together with geophysical logs and petrographic analyses, are helpful in identifying and mapping porous and permeable high-yield production zones in such a way that future drilling sites may be more accurately selected, and secondary and tertiary recovery strategies more easily planned, by petroleum engineers. In addition, they may be used to calculate the amount of oil and water expected from different zones (i.e., recovery efficiency) and the pressure necessary to produce oil from reservoir rocks.

A) Reservoir Facies--Well Sorted Pore Distribution

<u>High Porosity-Low Displacement Pressure.</u> Figure 36a is a photomicrograph of an oolitic grainstone composed of finely-crystalline dolomite, in which original depositional texture is preserved. This lithofacies is present only in the upper parts of the C.H. Bray and Sam

FIGURE 36. Photomicrographs (plane polarized light) of the dolomitized oolitic grainstone facies present in the upper few feet of C.H. Bray and Sam Watson wells. a. Highly porous, dolomitized oolitic grainstone (Humble C.H. Bray well #10-4; 15410 ft or 5137 m). The dominant types of pores are moldic (m) and interparticle (i). b. Dolomitized oolitic grainstone, where most available porosity was occluded by late anhydrite cementation (Humble Sam Watson well #23-4; 15600 ft or 5200 m).

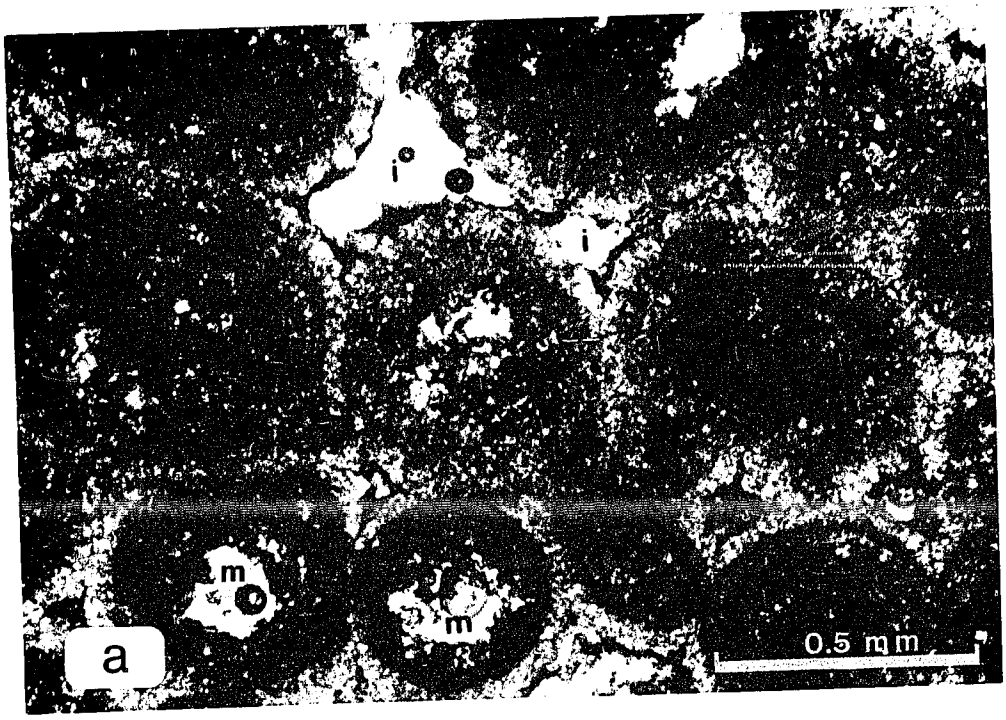
i
i
m
m
a
0.5 mm


0.5 mm
a
a
a
a
a
b

Watson wells. Porosity is high (22-27%) and is moldic, interparticle, and fine dolomite intercrystalline. The pores are well interconnected by numerous pore throats.

In places, however, late anhydrite cement was precipitated, occluding some of the porosity and modifying the petrophysical properties of the lithofacies. Figure 36b is a photomicrograph of the same dolomitized grainstone, where anhydrite cement has reduced the porosity by as much as 73%.

The mercury-capillary-pressure curves illustrated in figure 37 show the petrophysical characteristics of the two rock samples. The sample shown in figure 36a (solid symbols in figure 37) has high porosity, well-sorted pore-size distribution, low irreducible water saturation, and low displacement pressure indicative of .pn196 large pore throats. This is an excellent reservoir rock. The sample shown in figure 36b has low porosity, well-sorted pore-size distribution, high irreducible water saturation, and very high displacement pressure. This is a poor reservoir rock.

It is clear from these two examples that identical lithofacies may possess entirely different petrophysical characteristics when altered during their diagenetic history. The the sample in figure 36b has approximately 1/4 the porosity of the sample in figure 36a. The high

FIGURE 37. Mercury-capillary-pressure curves corresponding to core samples in Figure 36. Although the two samples had undergone the same depositional and diagenetic history until burial, late anhydrite cement in one of the samples (Sam Watson 15600') modified its petrophysical properties greatly. The curve corresponding to sample Bray 15410' has high porosity (Ø) and effective porosity (Øe), low displacement pressure (Pd) and irreducible water saturation (Swi), and good pore-throat sorting (PTS), whereas the curve corresponding to sample Sam Watson 15600' has low porosity and effective porosity, high displacement pressure and irreducible water saturation, and good pore-throat sorting.

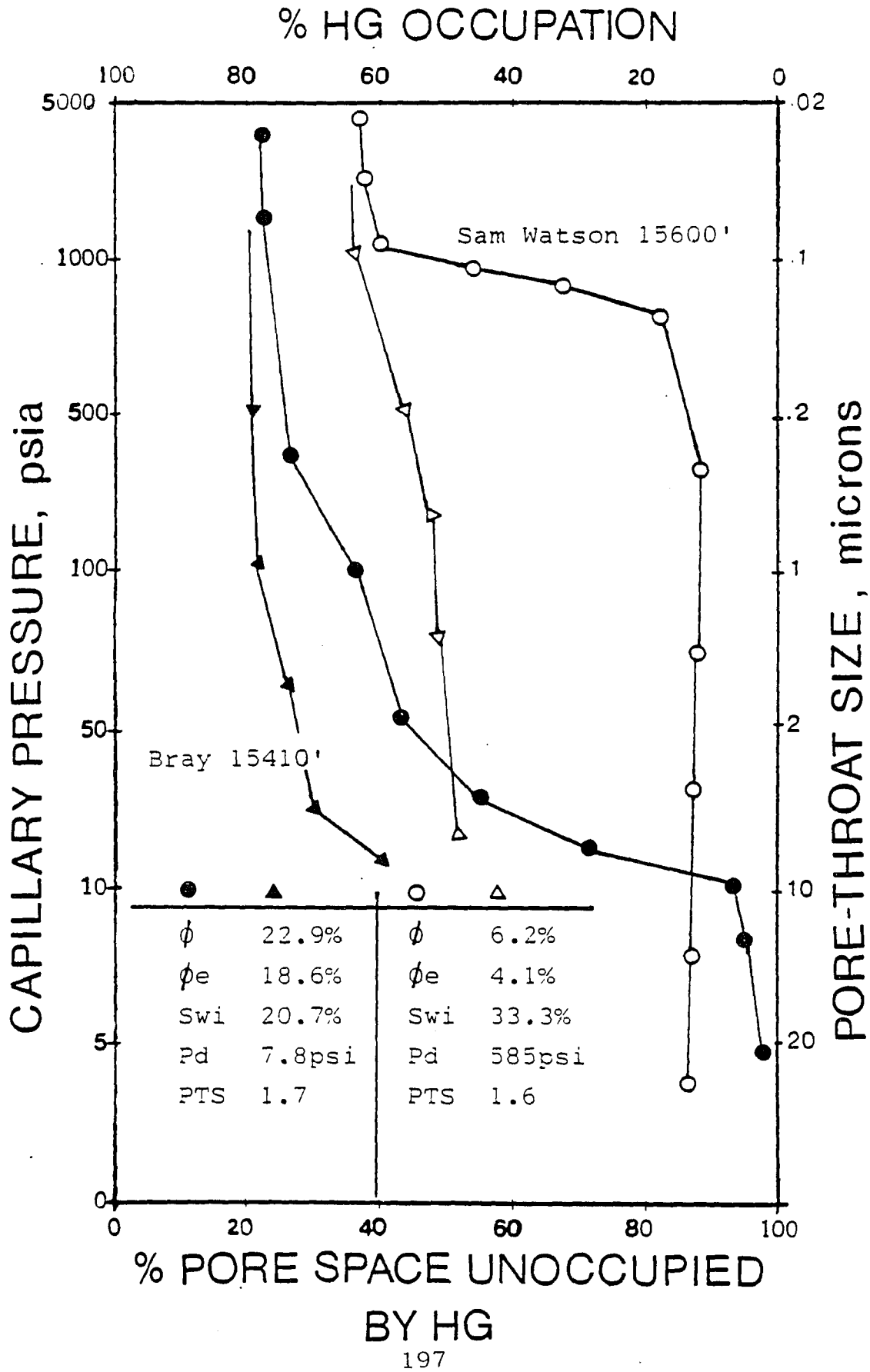
% HG OCCUPATION
100
80
60
40
20
0
5000
1000
500
100
50
10
5
0
.02
.1
.2
1
2
10
20
Sam Watson 15600'
Bray 15410'
CAPILLARY PRESSURE, psia
PORE-THROAT SIZE, microns
ϕ 22.9%
ϕe 18.6%
Swi 20.7%
Pd 7.8psi
PTS 1.7
ϕ 6.2%
ϕe 4.1%
Swi 33.3%
Pd 585psi
PTS 1.6
0
20
40
60
80
100
% PORE SPACE UNOCCUPIED BY HG

displacement pressure associated with the sample in figure 36b indicates that anhydrite cement not only occluded half of the porosity but it also blocked or reduced the size of all large pore throats. Increased pressure is, therefore, required to saturate effective pores with oil.

Intermediate Porosity-Low Displacement Pressure. Figure 38 is a photomicrograph of a typical Jay field-reservoir dolomitized grainstone. Porosity of this facies is intermediate (9-17%) and consists of large, well interconnected, uniformly shaped dolomite-intercrystalline pores.

The mercury-capillary-pressure curve illustrated in figure 39 shows a well-sorted pore-size distribution and low displacement pressure, indicative of uniformly sized, relatively large pore throats connecting the pores. The irreducible water saturations in this lithofacies range from 13-31%, relatively low.

Effective porosity, which is a function of irreducible water saturation, is 72-85% of the total porosity (i.e., 72-85% of total porosity is available to oil saturation). The low displacement pressure and the well sorted pore-size distribution of this sample mean that the effective porosity may be saturated to more than 60% with oil, with slightly increased oil column.

FIGURE 38. Photomicrograph of pervasively dolomitized grainstone comprising the Jay-field reservoir facies (Humble C.H. Bray well #10-4; 15418 ft or 5139 m). The intercrystalline pores are large, well interconnected by numerous pore throats, resulting in good reservoir quality.


0.5 mm

FIGURE 39. Mercury-capillary-pressure curve corresponding to the core sample in Figure 38. This curve represents typical petrophysical characteristics of the Jay field reservoir facies; i.e., high porosities (Ø) and effective porosities (Øe), relatively low irreducible water saturations (Swi), low displacement pressures (Pd), and good pore throat sortings (PTS).

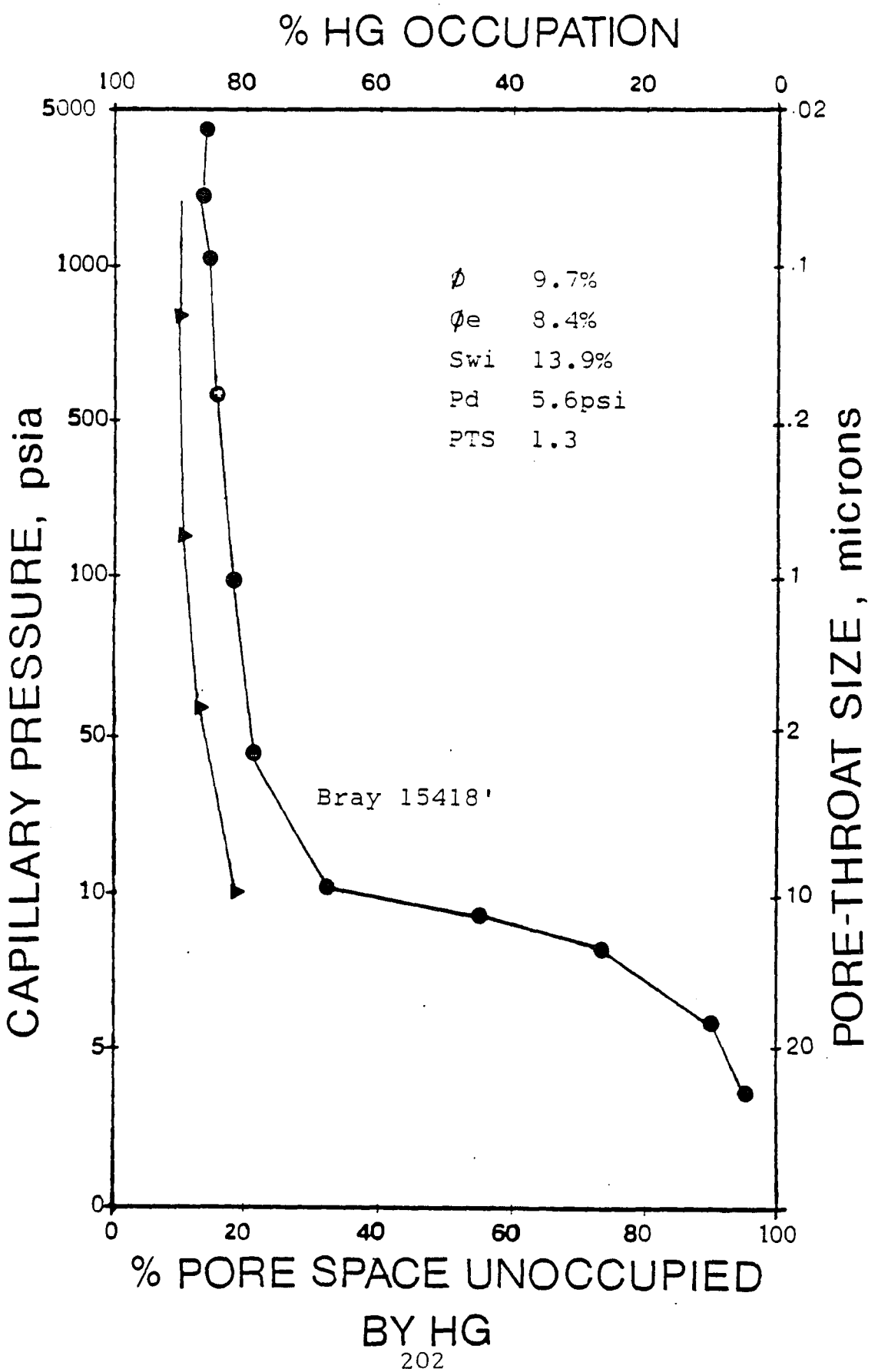
% HG OCCUPATION
100
80
60
40
20
0
5000
1000
500
100
50
10
5
0
.02
.1
.2
1
2
10
20
ϕ 9.7%
ϕe 8.4%
Swi 13.9%
Pd 5.6psi
PTS 1.3
Bray 15418'
CAPILLARY PRESSURE, psia
PORE-THROAT SIZE, microns
0
20
40
60
80
100
% PORE SPACE UNOCCUPIED BY HG

Overall, the petrophysical properties of this lithofacies are indicative of a very good reservoir. Caution must be used, however, because some of the porosity was occluded by late anhydrite cement.

Low Porosity-High Displacement Pressure. The continuity of the reservoir lithofacies described above is often disrupted by thin layers of carbonate whose petrophysical properties differ significantly. Figure 40 shows two photomicrographs of a dolomitized peloidal packstone (40a) and a crystalline dolomite where compromise boundaries have formed (40b). These two lithofacies are commonly interlayered within the reservoir rock.

Porosity of these lithofacies is low (less than 7%) and consists of poorly interconnected dolomite intercrystalline pores. The effective porosity is also low, averaging 40-60% of total porosity. The mercury-capillary-pressure curves illustrated in figure 41 show well-sorted pore distributions and high irreducible water saturations. The small pore throats (averaging less than 1 micron) cause high displacement pressures (greater than 100 psi) which in turn reduce the possibility of the rock containing oil.

Such lithofacies, when interlayered within the reservoir rock, can result in altered oil migration paths or act as barriers to oil migration, causing problems

FIGURE 40. Photomicrographs (plane polarized light) of the thin carbonate layers commonly interlayered within the reservoir facies. a. Dolomitized peloidal packstone (Humble McDavid Lands well #7-1; 15422 ft or 5141 m). b. Crystalline dolomite, where dolomitization was continued and compromise boundaries formed between the dolomite crystals (Humble C.H. Bray well #10-4; 15573 ft or 5191 m).

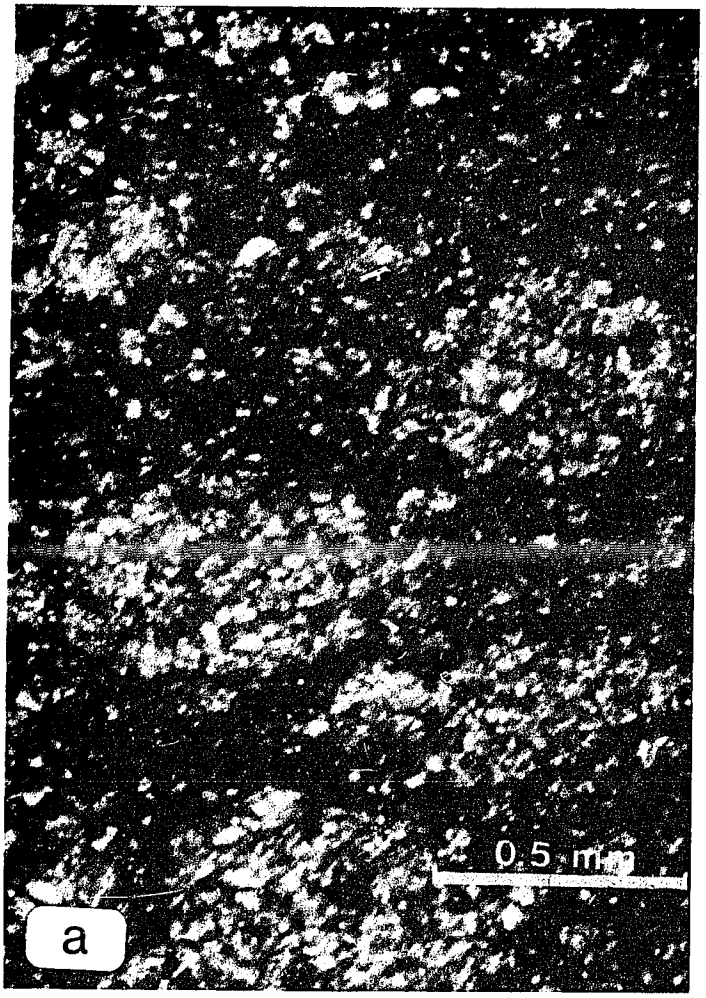
0.5 mm
a

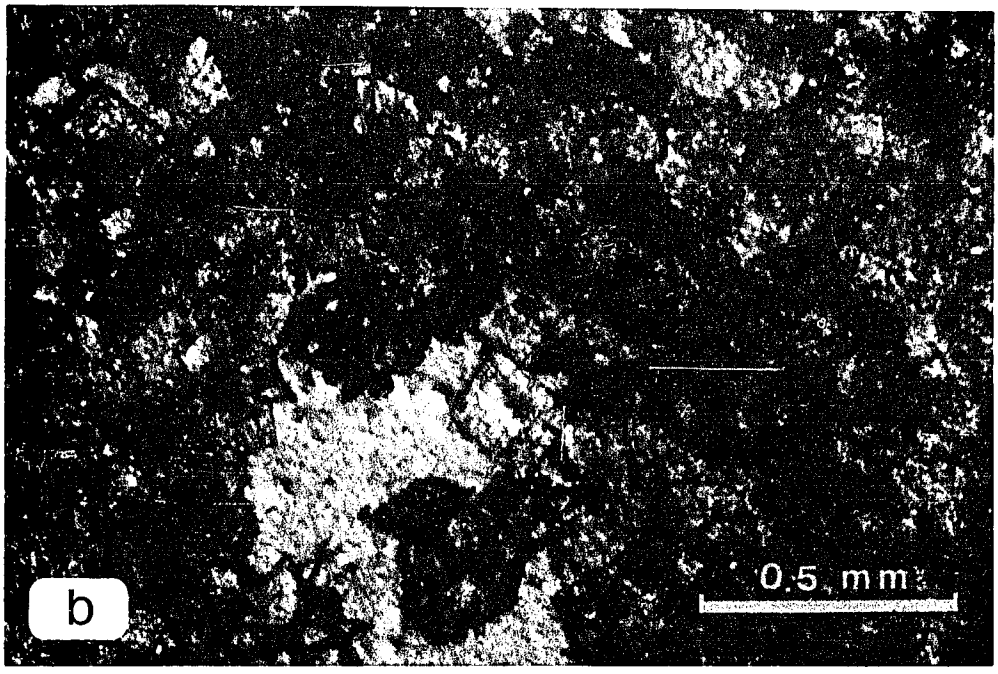
0.5 mm
b

FIGURE 41. Mercury-capillary-pressure curves corresponding to core samples in Figure 40. Both curves posses similar petrophysical characteristics such as low porosities (ϕ), low effective porosities (ϕe), high irreducible water saturations (Swi), and high displacement pressures (Pd), indicative of poor reservoir rocks. Pore-throat sorting (PTS) is good.

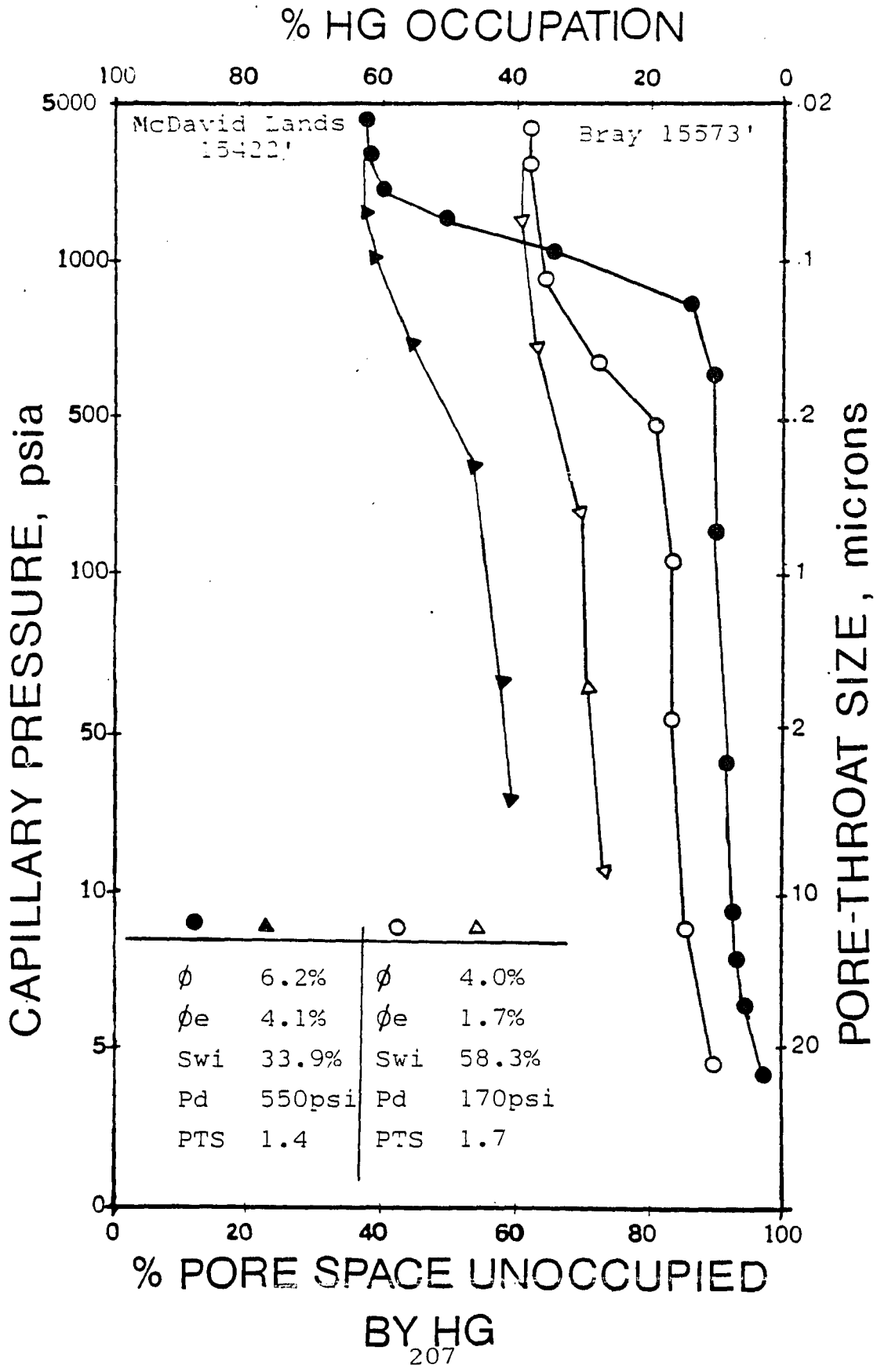
% HG OCCUPATION
100
80
60
40
20
0
5000
1000
500
100
50
10
5
0
.02
.1
.2
1
2
10
20
McDavid Lands
15422'
Bray 15573'
CAPILLARY PRESSURE, psia
PORE-THROAT SIZE, microns
ϕ 6.2%
ϕe 4.1%
Swi 33.9%
Pd 550psi
PTS 1.4
ϕ 4.0%
ϕe 1.7%
Swi 58.3%
Pd 170psi
PTS 1.7
0
20
40
60
80
100
% PORE SPACE UNOCCUPIED
BY HG

when one is trying to determine hydrocarbon recovery efficiency. Careful three-dimensional subsurface mapping is required.

B) Nonreservoir Facies--Poorly Sorted Pore-Size Distribution

Negligible Porosity-Nonclear-Cut Displacement Pressure. This lithofacies includes very tight (less than 1%) supratidal bedded, nodular, and massive anhydrites which cap Jay field and act as barriers to fluid migration (Fig. 42). This facies continuously overlies the Smackover reservoir grainstones all along the United States Gulf Coast. Three-dimensional subsurface mapping of this impermeable facies may thus help the identification of otherwise undetected stratigraphic traps.

The negligible porosity consists of tiny fractures most probably created during drilling. No clear-cut displacement pressure exists and no imbibition curve is obtainable (Fig. 43).

Low Porosity-Nonclear-Cut Displacement Pressure. This lithofacies group includes low porosity, generally on the order of 0.5-4%, laminated mudstones and pelletal-oncoidal wackestones present in the lower part of the Smackover Formation (Fig. 44). Bed thickness varies from

FIGURE 42. Photomicrograph (plane polarized light) of interpreted supratidal bedded anhydrite capping the Jay field reservoir facies (Humble C.H. Bray well #10-4; 15376 ft or 5125 m).


0.5 mm

FIGURE 43. Mercury-capillary-pressure curve corresponding to the anhydrite caprock facies sample in Figure 42. The curve is almost vertical, indicating very tight rock where fluids cannot penetrate.

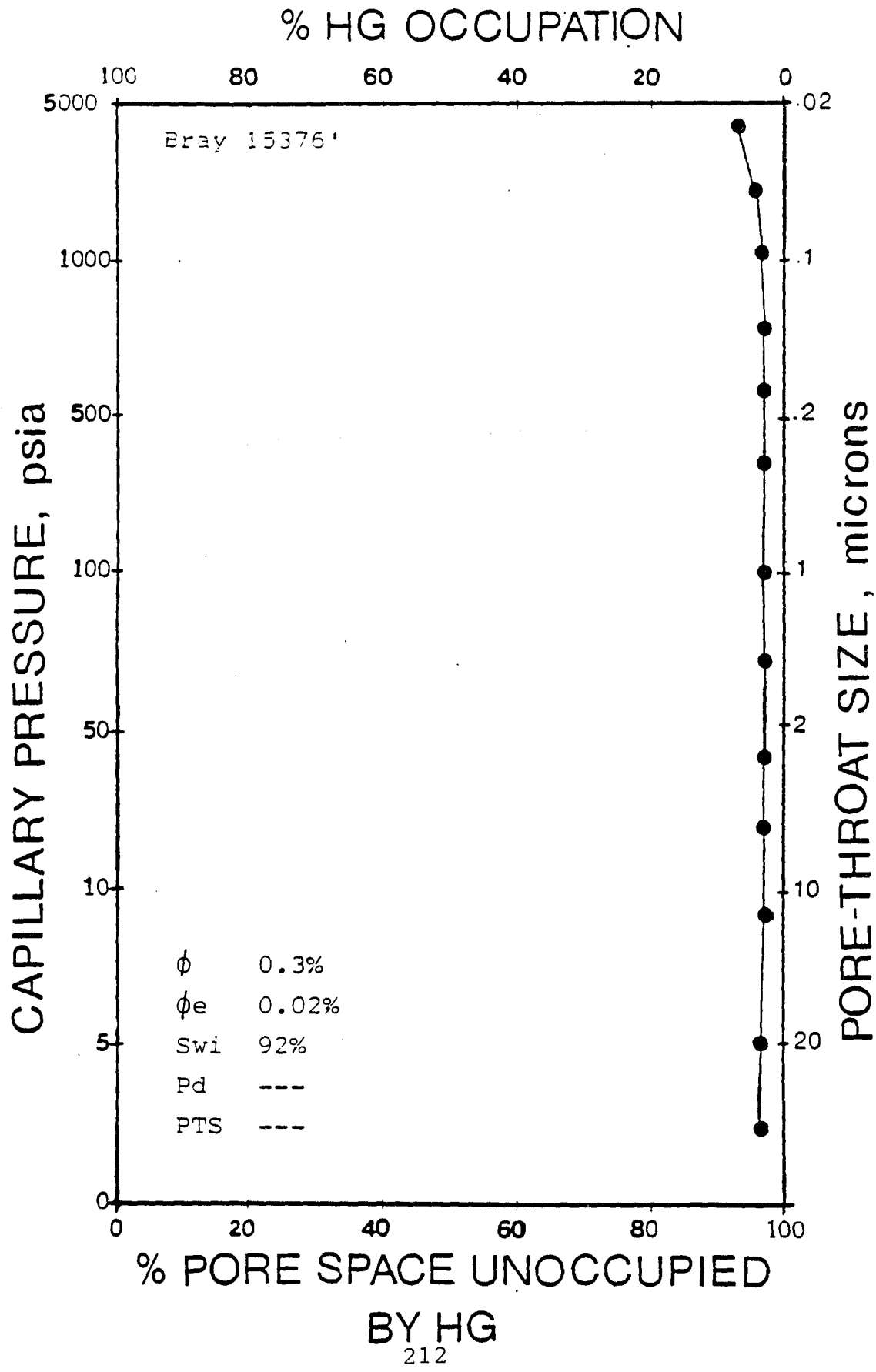
% HG OCCUPATION
100
80
60
40
20
0
5000
1000
500
100
50
10
5
0
.02
.1
.2
1
2
10
20
Bray 15376'
CAPILLARY PRESSURE, psia
PORE-THROAT SIZE, microns
ϕ 0.3%
ϕe 0.02%
Swi 92%
Pd ---
PTS ---
0
20
40
60
80
100
% PORE SPACE UNOCCUPIED BY HG

FIGURE 44. Photomicrographs (plane polarized light) of the lower Smackover lithofacies. a. Algal laminated mudstone (Humble C.H. Bray well #10-4; 15737 ft or 5246 m). b. Pelletal wackestone (Humble C.H. Bray well #10-4; 15676 ft or 5225 m).

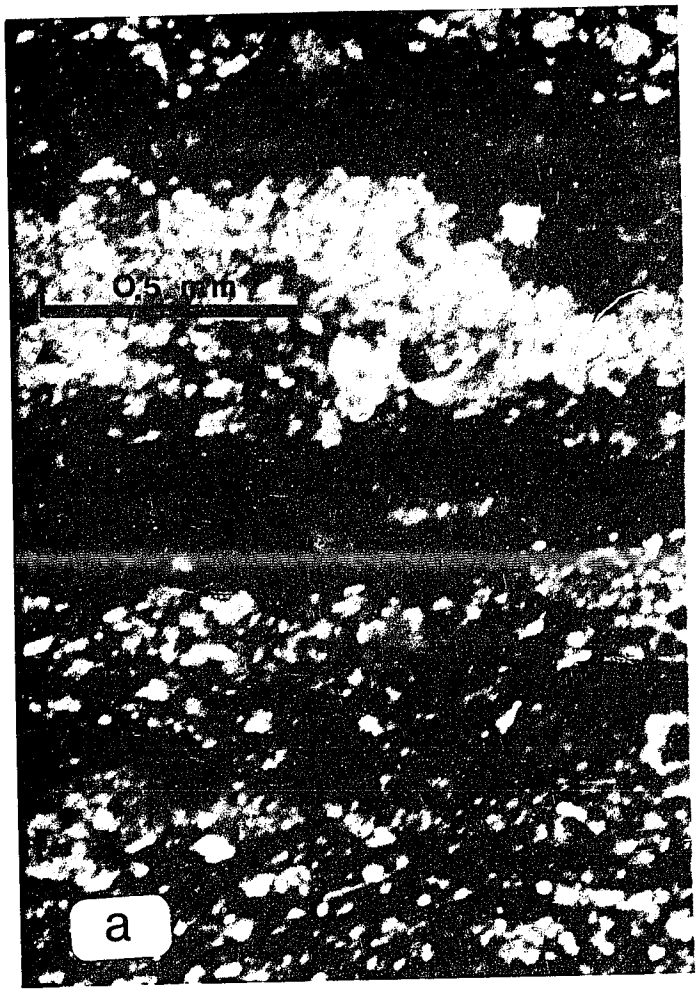
0,5 mm
a

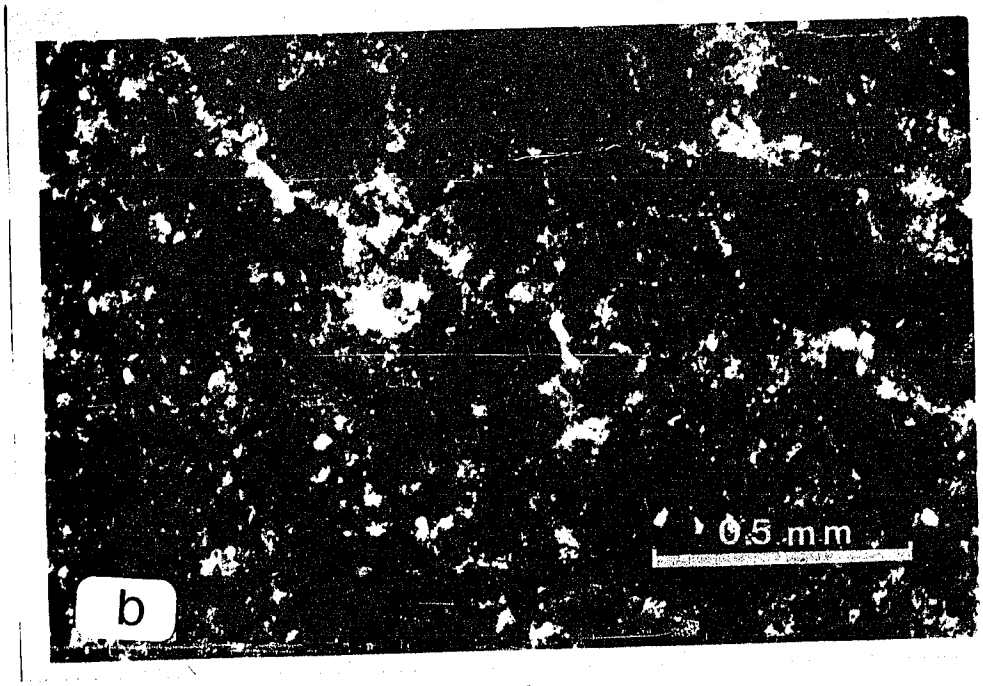
0.5 mm
b

several inches to several feet thick; beds alternate with more porous pelletal/peloidal wackestones described below.

The dolomite content of these rocks ranges from 0-55% and consists of fine rhombs. The mercury capillary-pressure curves illustrated in figure 45 show high irreducible water saturations (more than 40%), and negligible effective porosity values (less than 40%) indicative of poor pore interconnections. The displacement pressure is not clear cut in either of the curves, suggesting highly variable pore throat sizes.

These lithofacies are very poor reservoir rocks. They are considered by many workers to be the source rocks of the Smackover reservoirs.

Intermediate Porosity-High Displacement Pressure. This type of lithofacies is composed of partially dolomitized pelletal/peloidal wackestones in the lower part of the Smackover Formation (Fig. 46). These wackestones differ from the ones described above in that they do not contain algal oncoids and are more extensively dolomitized.

Porosity of this lithofacies is intermediate, ranging from 3.7-16.5%; averaging about 10%. The mercury-capillary-pressure curves illustrated in figure 47 show fairly sorted pore distributions, high

FIGURE 45. Mercury-capillary-pressure curves corresponding to core samples in Figure 44. Both samples have low porosities (Ø) and effective porosities (Øe), high irreducible water saturations (Swi), and nonclear-cut displacement pressures (Pd), indicative of poorly sorted pore throats (PTS).

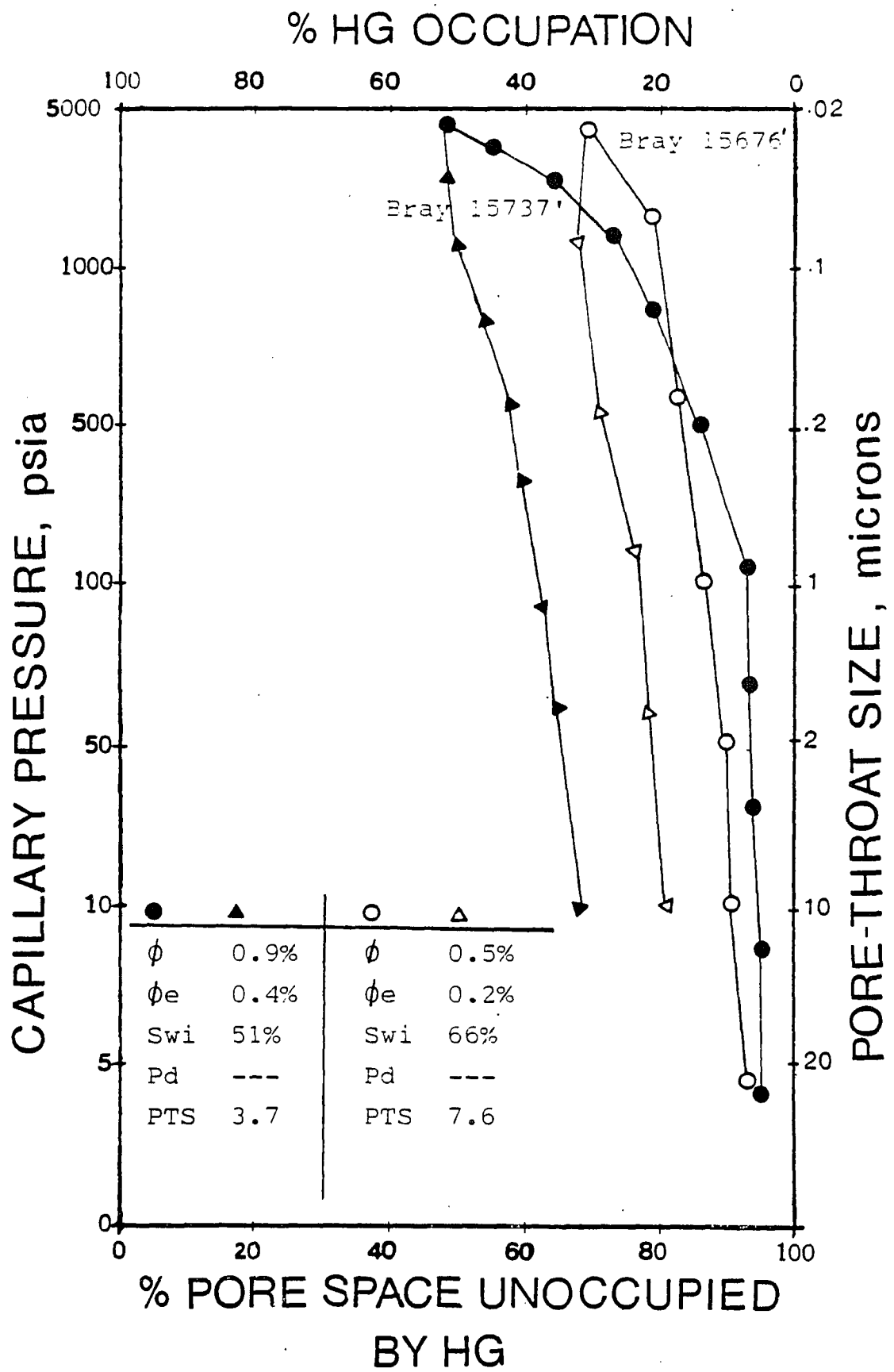
% HG OCCUPATION
100
80
60
40
20
0
5000
1000
500
100
50
10
5
0
CAPILLARY PRESSURE, psia
.02
.1
.2
1
2
10
20
PORE-THROAT SIZE, microns
Bray 15676'
Bray 15737'
● ▲ ○ △
ϕ 0.9% ϕ 0.5%
ϕe 0.4% ϕe 0.2%
Swi 51% Swi 66%
Pd --- Pd ---
PTS 3.7 PTS 7.6
0
20
40
60
80
100
% PORE SPACE UNOCCUPIED BY HG

FIGURE 46. Photomicrographs (plane polarized light) of the lower Smackover pelletal/peloidal wackestones. a. Pelletal wackestone composed of fine-crystalline dolomite. Some anhydrite cement (a) is present (Humble McDavid lands well #7-1; 15534 ft or 5177 m). b. Peloidal wackestone where allochems where allochems were selectively replaced by coarse-crystalline dolomite (Humble sam watson well #23-4; 15713 ft or 5238 m).

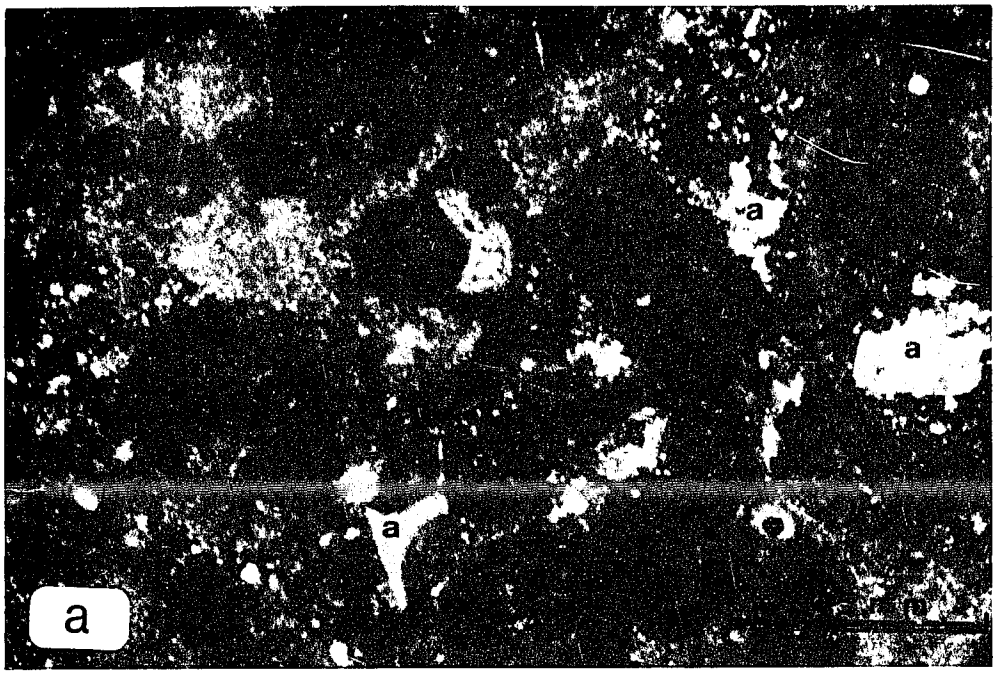
a
a
a
a

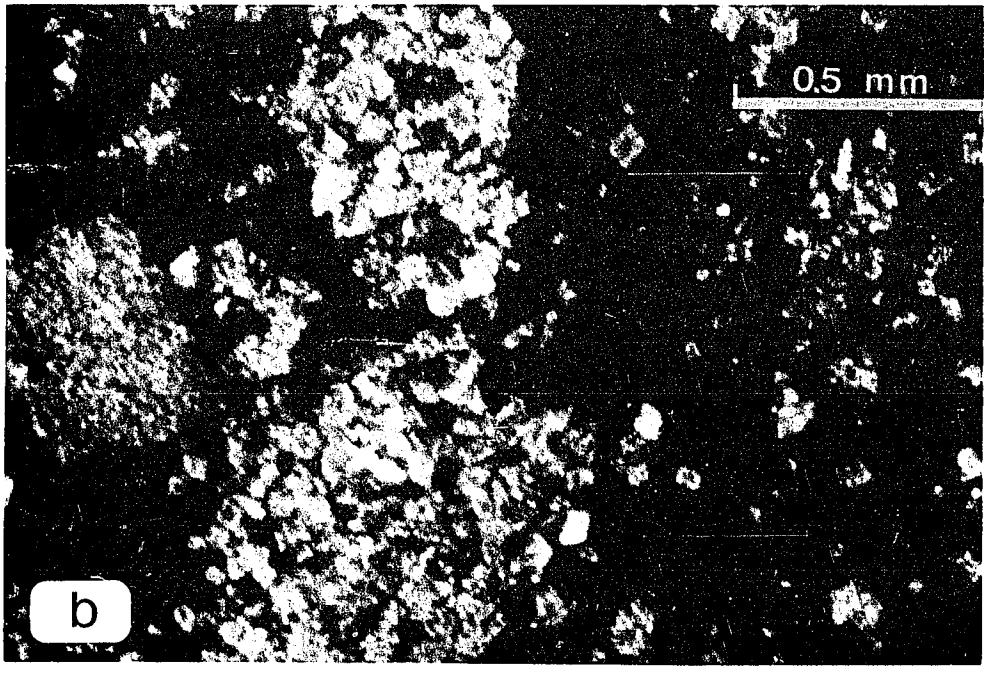
0.5 mm
b

FIGURE 47. Mercury-capillary-pressure curves corresponding to core samples in Figure 46. Both samples have intermediate porosities (Ø) and effective porosities (Øe), high irreducible water saturations (Swi) and displacement pressures (pd), and intermediate pore-throat sortings (PTS).

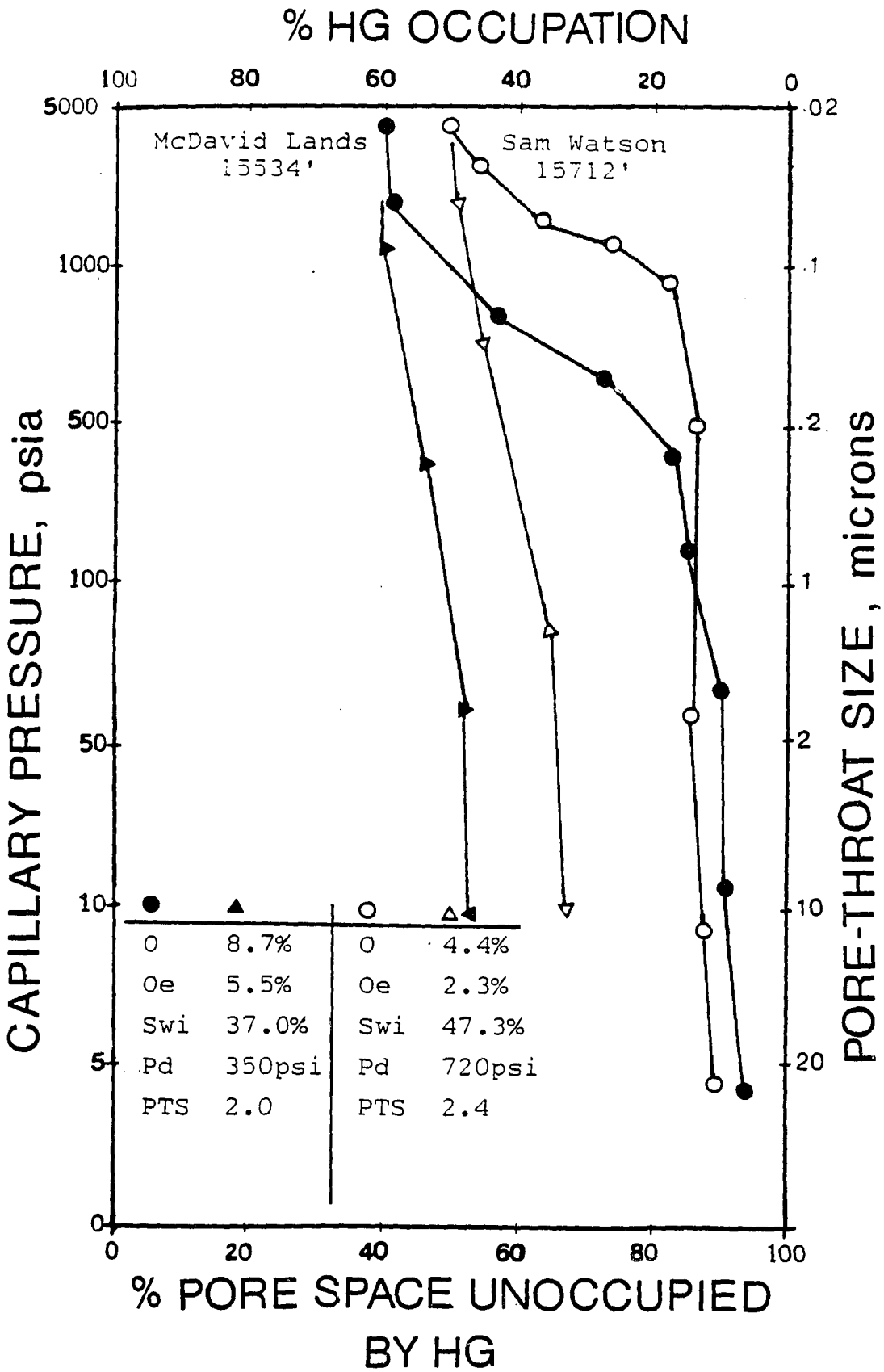
% HG OCCUPATION
100
80
60
40
20
0
5000
1000
500
100
50
10
5
0
.02
.1
.2
1
2
10
20
McDavid Lands
15534'
Sam Watson
15712'
CAPILLARY PRESSURE, psia
PORE-THROAT SIZE, microns
O 8.7%
Oe 5.5%
Swi 37.0%
Pd 350psi
PTS 2.0
O 4.4%
Oe 2.3%
Swi 47.3%
Pd 720psi
PTS 2.4
0
20
40
60
80
100
% PORE SPACE UNOCCUPIED BY HG

irreducible water saturations (greater than 35%), and high displacement pressures (greater than 500 psia) indicative of small pore throats (less than 0.2 microns in diameter) connecting the pores.

In the following section I will show how the above petrophysical classification of the Jay field carbonates can be related to log-derived petrophysical properties.

6.3 Textural Analysis Based on Wire-Line Logs

The evolution, preservation, and distribution of porosity in the subsurface is very important, especially when dealing with carbonate reservoirs, such as Jay field, where there is enormous regional and temporal variation in the diagenetic history. Geophysical well logs are valuable tools in subsurface exploration in that they provide a continuous recording of all measurable physical properties of the rocks and the fluids they contain. In addition, they can be used to determine the geometry and orientation of the reservoir and to map the three-dimensional subsurface distribution of reservoir and nonreservoir lithofacies, once these lithofacies and their petrophysical characteristics are defined using petrographic and facies analyses, and mercury-porosimetry. No log motif, however, is specific to a particular environment. A combination of two or more log profiles along with information on the composition of well samples is necessary to describe and interpret the various lithofacies.

A complete package consisting of gamma-ray, neutron (CNL), density, dual-induction spontaneous potential (SP) and resistivity, and some sonic logs was available for 13 wells in Jay field. Density, neutron, and gamma-ray logs

are traditionally used to determine lithology and obtain lithologic correlations between wells. Sonic logs afford an excellent way of estimating porosity within ranges of 5-35%. Resistivity logs in combination with sonic logs can be used to measure hydrocarbon saturation in "clean" formations, whereas resistivity logs in combination with spontaneous potential logs are used to make correlations between neighboring wells using "electrical marker beds", and to determine the hydrocarbon-water contact.

The most important use of neutron logs is for estimating porosity where production is from shale-free carbonates, in which porous and impervious zones alternate. Gamma-ray and neutron logs are always combined for estimating porosity, because shaly and porous strata show alike on neutron logs, and the gamma-ray log is needed to distinguish shaly from porous zones (Russel, 1952).

A variety of crossplots derived from two or more logs may be used to determine various parameters. Subsurface units with simple mineralogies (e.g., clean limestones and sandstones), logged by two or three porosity logs, can be crossplotted and their trends compared to the theoretical limestone, dolomite, and sandstone (Doveton, 1986). The selection of the

crossplots depends on the specific information sought and the available information. Density-neutron crossplots are used to derive porosity values from apparent limestone porosity and determine the quartz content in carbonate rocks. Sonic-density and M-N crossplots are used to determine the presence of evaporite minerals as well as possible trends toward secondary porosity.

6.3.1 Textural Well Log Analysis of the Smackover Formation

For this study, a variety of crossplots were generated using uncorrected log-derived porosity as well as log porosities corrected for matrix density and volume of shale (clay minerals). Lithology plots were developed and compared with the known lithologies defined by core and thin section analysis. This provided a characteristic log response for each lithology encountered.

Neutron, density, and sonic logs are influenced by porosity, lithology, clay content, and the presence of gas. When used in combination, the logs give a more accurate indication of porosity, as well as other useful information about formation characteristics.

Combination neutron, density, and gamma-ray logs are

illustrated in figure 48 as they correlate to different lithofacies of the Humble C.H. Bray #10-4 core. The relationship between all three logs and rock type is characteristic. The log motif of the reservoir, nonreservoir, and caprock facies is distiguishable, and with the aid of key lithologic control it may be correlated throughout the field. In addition, porosity correlates well with the percentage of dolomite present within each facies, determined by thin-section analysis; the higher the dolomite concentration, the higher the porosity value registered by the logs.

The combination neutron-density log is a combination porosity log, used to determine lithology and detect gas-bearing zones, in addition to accurate determination of true porosity. When apparent limestone porosities from neutron porosity (CNL) and bulk density curves were crossplotted on a neutron-density porosity chart (Fig. 49), representative points plotted below the limestone line, according to the porosity and lithology of the various facies. Log-derived lithofacies classification is confirmed by core and thin section analysis. Reservoir facies data points cluster nearest the dolomite curve within the 12-15% porosity range. Data points corresponding to the lower Smackover nonreservoir facies show a considerable scatter of both porosity and

FIGURE 48. Typical well logs (gamma-ray, caliper, density, and neutron) for Humble C.H. Bray #10-4 well, as they relate to the various lithofacies and dolomite content of the core. The dolomite content was determined by point count.

C.H. BRAY

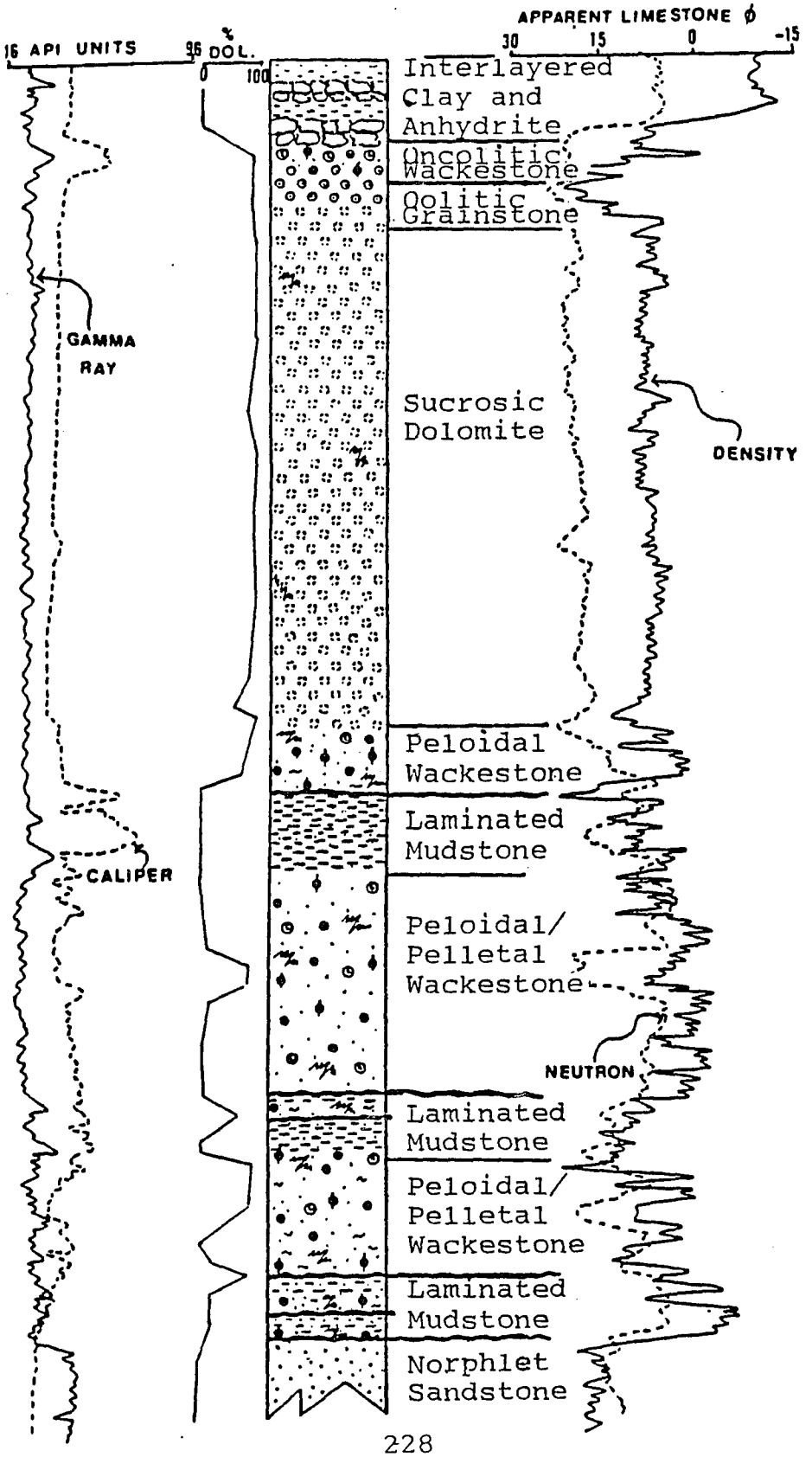
16 API UNITS
% DOL.
0
100
APPARENT LIMESTONE ϕ
30
15
0
-15
GAMMA RAY
CALIPER
DENSITY
NEUTRON
Interlayered Clay and Anhydrite
Oncolitic Wackestone
Oolitic Grainstone
Sucrosic Dolomite
Peloidal Wackestone
Laminated Mudstone
Peloidal/ Pelletal Wackestone
Laminated Mudstone
Peloidal/ Pelletal Wackestone
Laminated Mudstone
Norphlet Sandstone

FIGURE 49. Neutron-density crossplot for the Smackover lithofacies in Jay field. The clustering of points between the dolomite and limestone lines suggest a limy dolomite. Furthermore the clustering of points near the 10 to 17% interval of the dolomite line support the previous conclusions, that the lithology of this facies is dolomite with high porosity values. pf is suggested fluid density of salt muds (adopted from Schlumberger, 1972a).

POROSITY AND LITHOLOGY DETERMINATION FROM
FORMATION DENSITY LOG AND
COMPENSATED NEUTRON LOG (CNL)

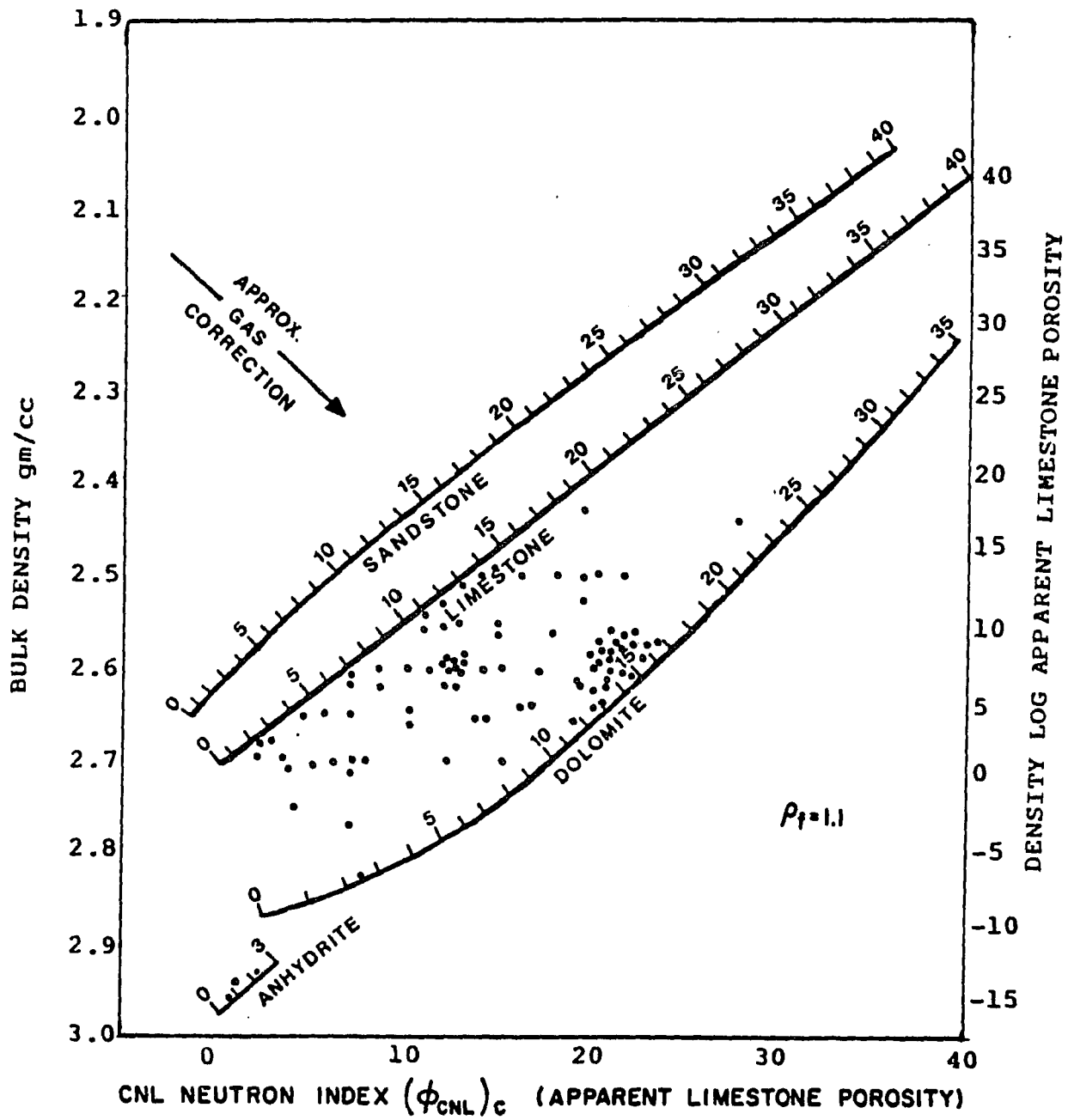

lithology, whereas caprock facies points, corresponding to the sabkha anhydrites, plot near the anhydrite curve.

When log-derived porosity, corrected for lithology, was compared to mercury-porosimetry-derived porosity (Fig. 50), a close approximation was evident, even though values may be slightly different on a foot-by-foot basis. This similarity in porosity values confirms the validity of the mercury-porosimetry experimental method in reservoir analysis. The foot-by-foot porosity variations are most probably the result of such factors as changing lithology, changing hole size, and variations of porosity types, which all affect porosity logs. Inn addition, microporosity cannot be detected by mercury porosimetry, underestimating porosity (Kopaska-Merkel and Amthor, 1988).

In carbonate rocks, resistivity logs are a function of pore geometry and the presence of hydrocarbons, and are very important in determining water saturation. Water saturations may be calculated using the standard Archie equation for a carbonate reservoir containing only intergranular or intercrystalline porosity:

$$Sw = (1/\phi^2(Rw/Rt))^{1/2} \qquad 6\text{-}8$$

where Rt = true formation resistivity (uninvated zone)

ϕ = porosity

Rw = formation water resistivity = 0.024 for Jay

FIGURE 50. Scattergram of log-derived and mercury-porosimetry-derived porosities. A strong positive relationship exists between the two porosities. The equations are: (A) log porosity = 1.72 + 0.81(Hg-porosimetry porosity) and (B) log porosity = 2.08 + 0.85(Hg-porosimetry porosity).

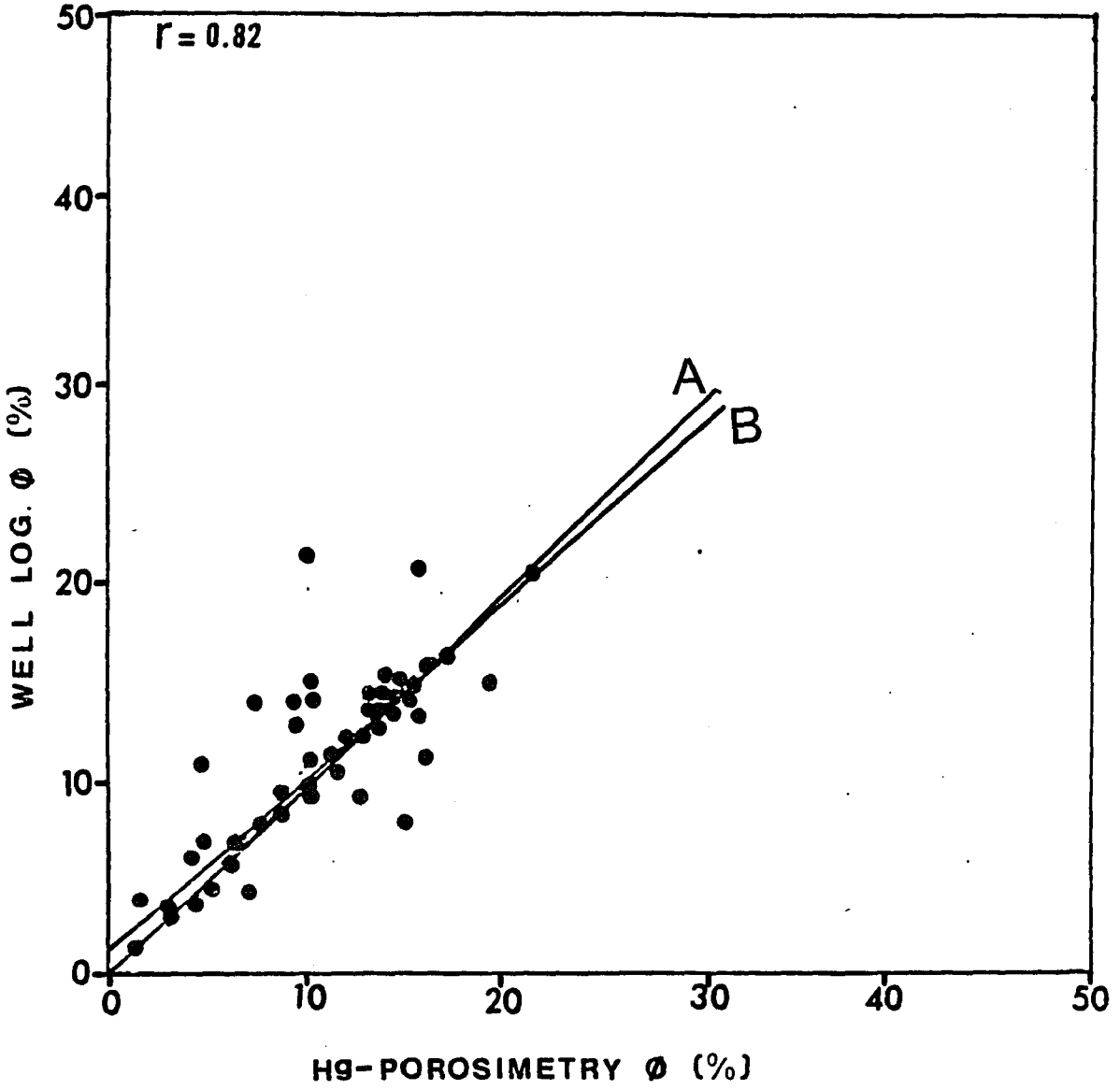
r = 0.82
A
B
WELL LOG. Ø (%)
Hg-POROSIMETRY Ø (%)
0
10
20
30
40
50

field at formation temperature (Tf = 285° F).

Porosity versus water saturation crossplots may be used to determine the bulk volume water and permeability of a reservoir. The bulk volume water (BVW) in a reservoir is the product of the water saturation (Sw) times the porosity (ϕ): $BVW = Sw\phi$. BVW is one of the most important parameters that we can use to evaluate a carbonate reservoir's potential because it indicates whether or not a reservoir is at irreducible water saturation (Swi). At Swi, a reservoir produces water-free hydrocarbons because all the formation's water is held through surface tension or capillary pressure by the grains. A reservoir at irreducible water saturation exhibits bulk volume water values that are constant throughout (Dewan, 1983; Asquith, 1985).

The BVW chart (Fig. 51) has hyperbolic lines representing lines of constant BVW. When a reservoir is at irreducible water saturation data should crossplot on or parallel to one of the hyperbolic lines. When the data points exhibit a scatter from the lines, then the reservoir is not at irreducible water saturation and will produce water, possibly with some hydrocarbons.

Values for bulk volume water (BVW) were calculated at several depths in the Jay field reservoir (Fig. 51). The values plot almost parallel to the 0.01-0.02 (i.e.,

FIGURE 51. Bulk volume water (BVW) crossplot of water saturation (Sw) versus porosity from the Smackover Formation, Jay field (reproduced from Schlumberger, 1987). Data points plot parallel to the 0.1 to 0.2 lines of constant BVW, indicating the reservoir is at irreducible water saturation.

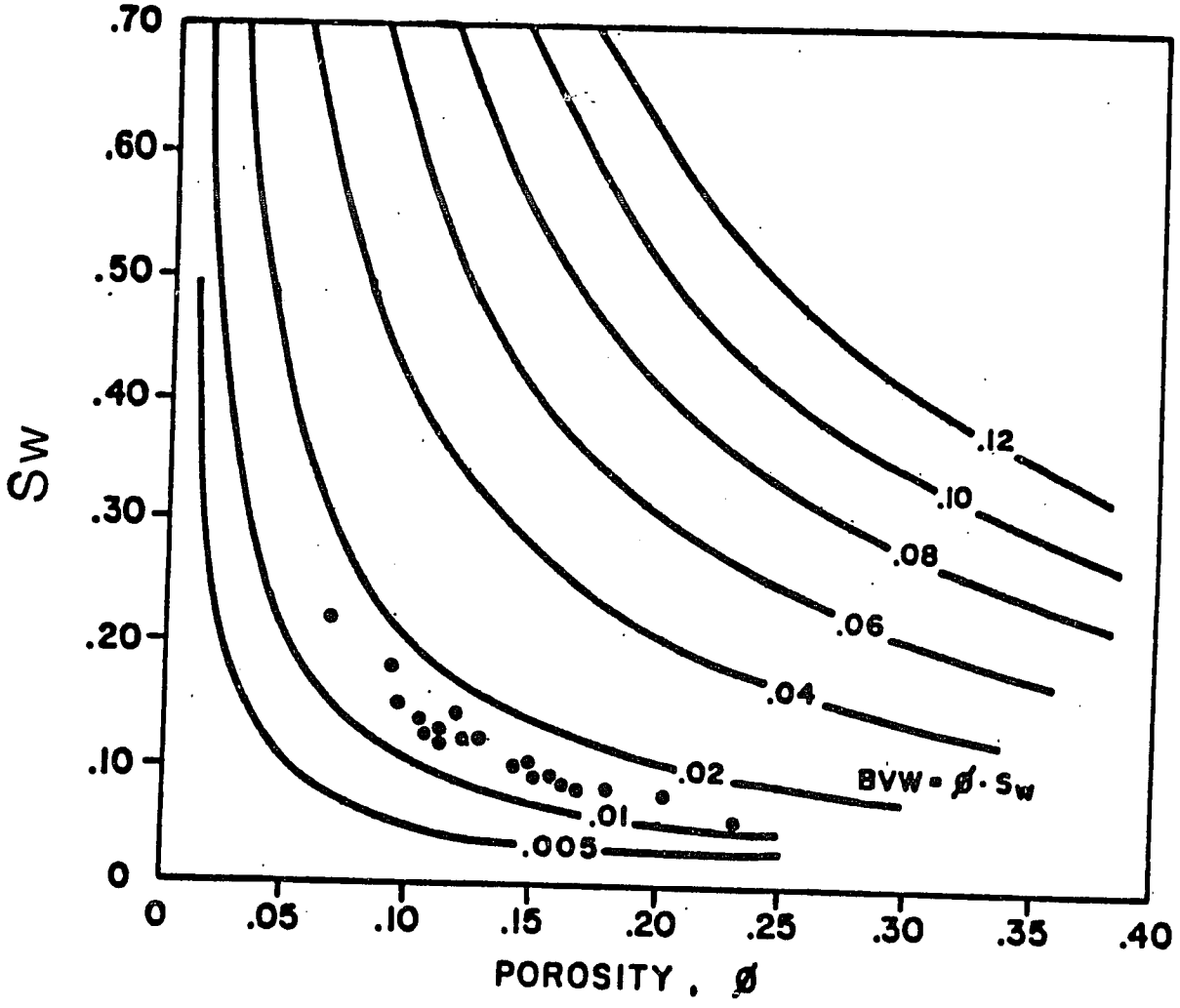
.70
.60
.50
.40
.30
.20
.10
0
Sw
0
.05
.10
.15
.20
.25
.30
.35
.40
POROSITY , ø
.12
.10
.08
.06
.04
.02
.01
.005
BVW = ø · Sw

0.015) hyperbolic lines, indicating that the reservoir was at or near irreducible water saturation during its early production history (i.e., prior to 1974 when water flooding was first introduced). Conditions are different today, however, because the reservoir is at a secondary and early tertiary recovery stage, in which energy is furnished by a combination of water flooding and injection of nitrogen gas.

Permeability values are provided when porosity versus water saturation at irreducible water saturation are crossplotted. Most of the data points for the Jay field reservoir plot in the range of 2.5-100 millidarcies (Fig. 52), with an average of 30-50 md, indicating a very good reservoir.

Water saturation (Sw) versus irreducible water saturation (Swi) crossplots compare the relative permeability to water (Krw), relative permeability to oil (Kro), and percent water-cut. Relative permeabilities to water of different zones within the Jay field reservoir (Fig. 53) show, with some exceptions, clustering below the zero permeability to water line, indicating water-free production during the early development of Jay field prior to waterflooding. Data points above the zero line represent zones which will produce some water, the amount of which depends on how far away they are from the zero

FIGURE 52. Irreducible water saturation versus porosity crossplot for permeability determination, Jay field Smackover reservoir (reproduced from Schlumberger, 1987).

PERMEABILITY: SANDSTONES, SHALY SANDS

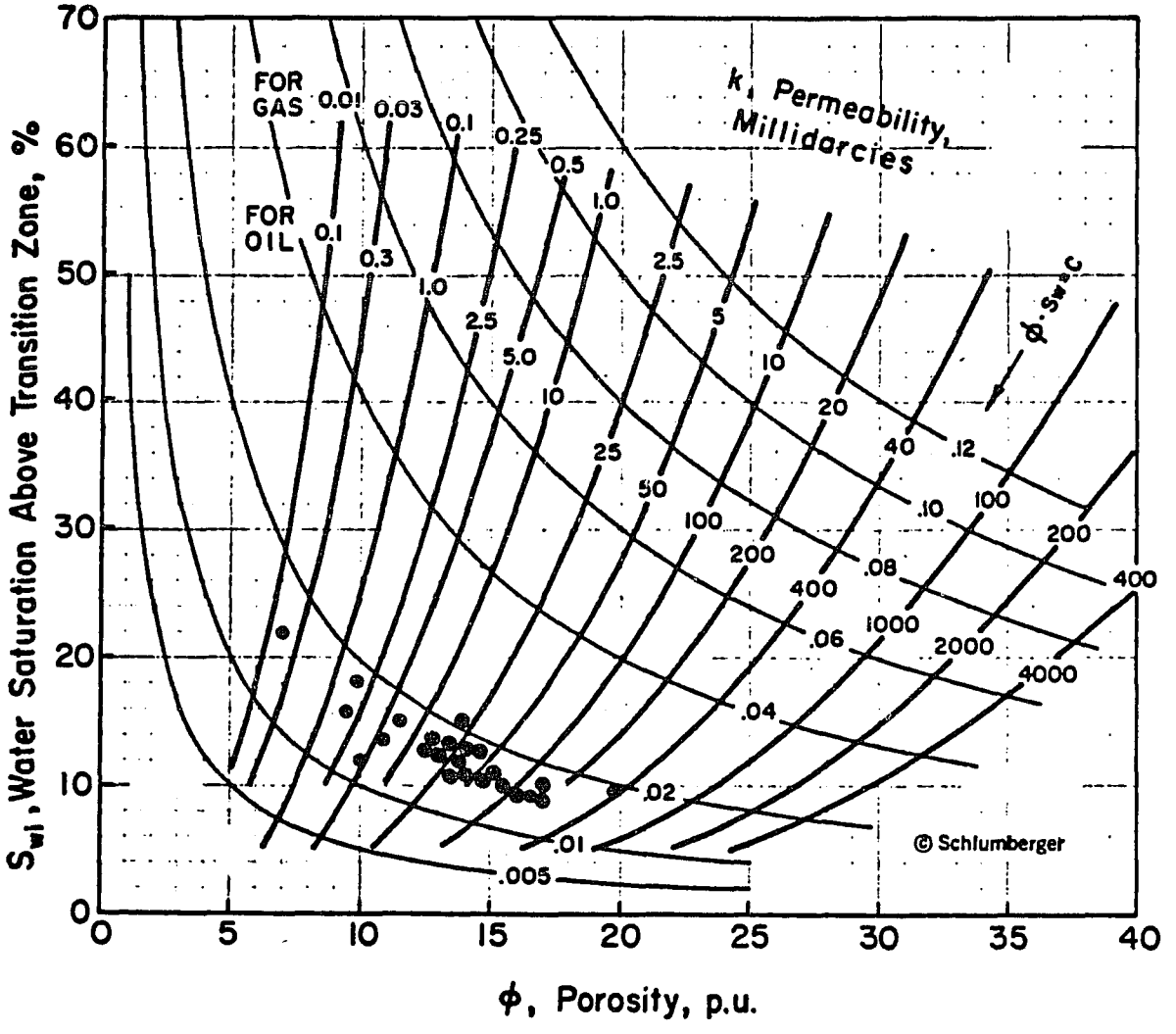

FIGURE 53. Irreducible water saturation (Swi) versus water saturation (Sw) crossplot for determining relative permeability to water (Krw), Smackover Formation, Jay field (reproduced from Schlumberger, 1987).

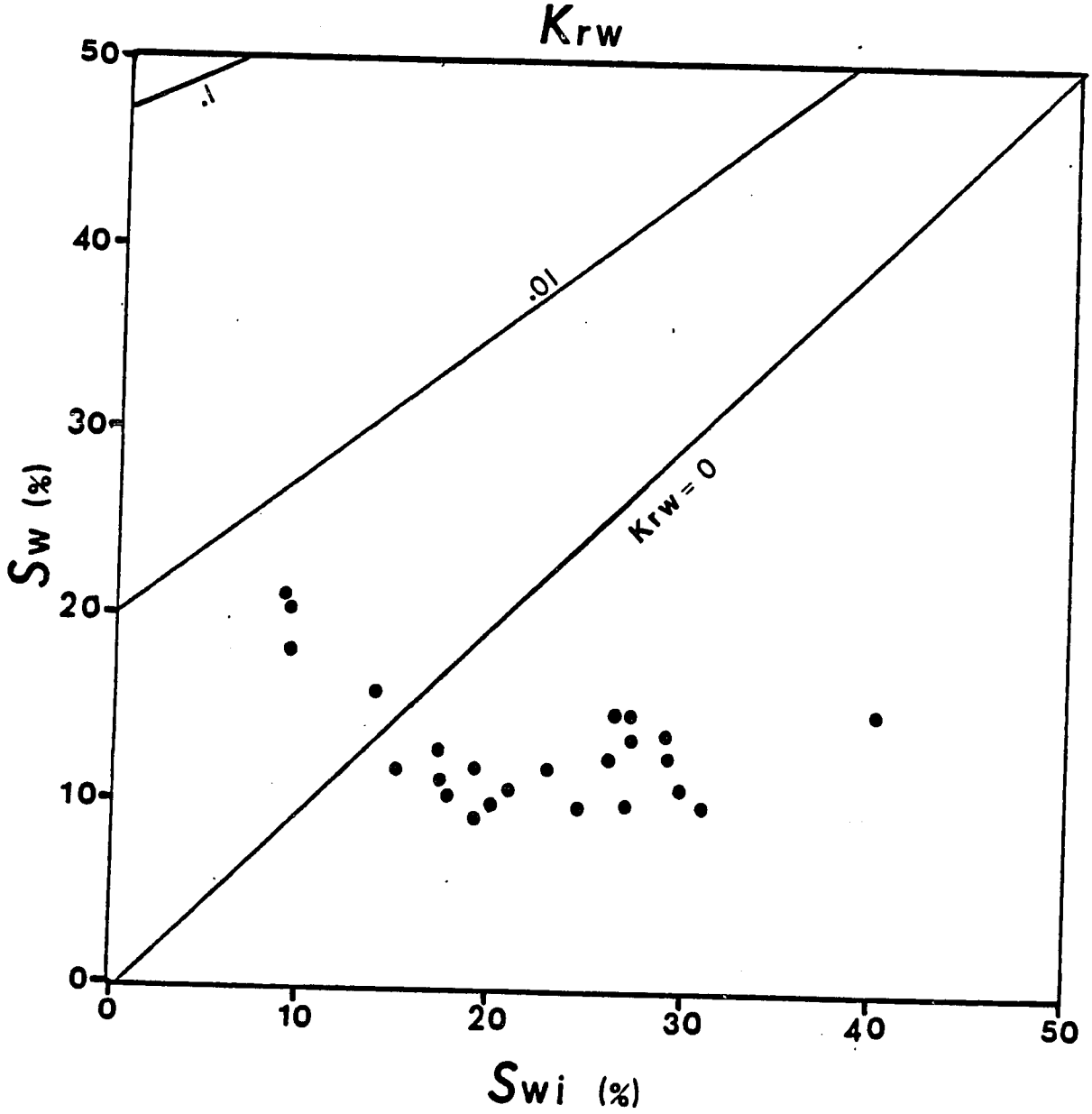
Krw
50
40
30
20
10
0
.1
.01
Krw=0
Sw (%)
0
10
20
30
40
50
Swi (%)

Krw line.

Relative permeabilities to oil of different zones within the Jay field reservoir (Fig. 54) show data points clustering mostly below the 100% permeability to oil (Kro = 1) line, representing zones which should produce 100% oil. data points plotting above the 100% line represent zones which will produce some water, the amount of which increases with increasing distance away from the 100% line.

The water-cut crossplot may be used to determine the amount of water produced in different zones within the reservoir, prior to secondary and tertiary stimulation. The water-cut crossplot for the Jay field reservoir (Fig. 55) reveals a 0% water-cut. The outcome of this crossplot is supported by the BVW crossplot (Fig. 51), in which all data points plot below the 0.035 line, indicating production from high-intercrystalline porosity zones at irreducible water saturation.

FIGURE 54. Irreducible water saturation (Swi) versus water saturation (Sw) crossplot for determining relative permeability to oil (Kro), Smackover Formation, Jay field (reproduced from Schlumberger, 1987).

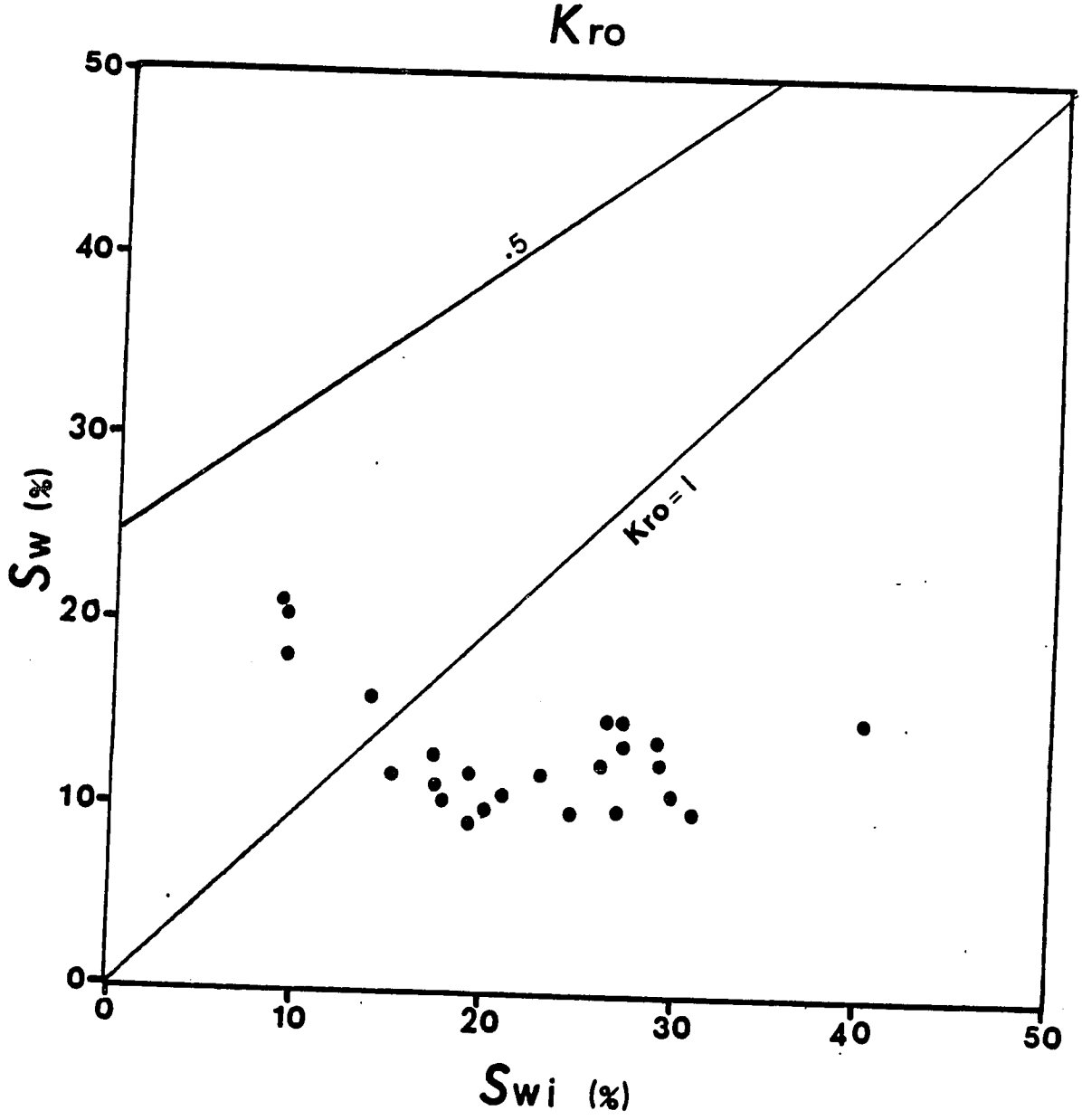
Kro
50
40
30
20
10
0
Sw (%)
.5
Kro=1
0
10
20
30
40
50
Swi (%)

FIGURE 55. Irreducible water saturation (Swi) versus water saturation (Sw) crossplot for determining percent water cut, Jay field Smackover reservoir (Fertl and Vercellino, 1978). Most data points plot above the 0% water-cut line indicating water-free oil production.

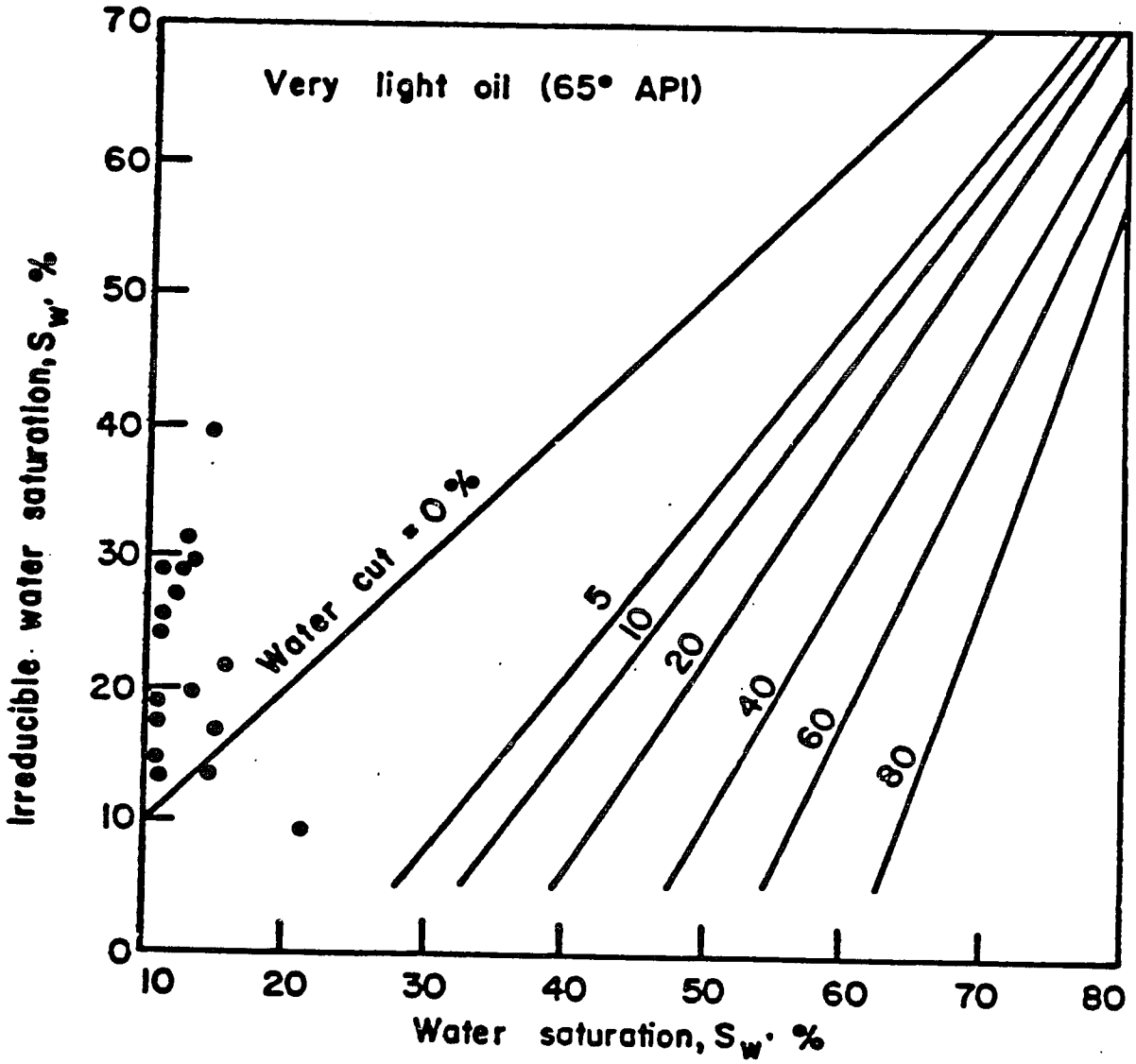
Very light oil (65° API)
Water cut = 0 %
5
10
20
40
60
80
Irreducible water saturation, $S_{w'}$, %
Water saturation, $S_{w'}$, %
0
10
20
30
40
50
60
70
80

7.CONCLUSIONS

The upper Jurassic Smackover grainstones are reservoir rocks which produce in many areas around the Gulf Coast.

Jay field is a combination stratigraphic, diagenetic, and structural trap, in which oil accumulation is caused by facies change from a more permeable reservoir facies to an impermeable caprock facies.

The Smackover grainstones in the Conecuh Embayment are part of a shoaling-upward carbonate sequence, capped by an evaporite interval. They were deposited in a moderate- to high- energy intertidal shoal located on a local paleobathymetric high, most probably produced by salt movements. Diagenetic recrystallization and dolomitization of these grainstones created a porous and permeable, high-yield reservoir. The reservoir facies is pervasively dolomitized, and characterized by medium- to coarsely-crystalline hypidiotopic turbid dolomite crystals with an average porosity of 15% and average permeability of 35 md.

The accurate and complete characterization of the pore system of the Smackover carbonates was the goal of this research. A conceptual and quantitative, combined study of the geological, petrophysical, and logging data

of these carbonates provided a thorough understanding of reservoir and nonreservoir characteristics of the cores studied.

The reservoir produces from a layered section with high porosity and permeability contrasts among its layers. The various lithofacies are largely defined and their depositional environments deduced from petrography. Mercury-porosimetry defines the pore characteristics as they relate to the various carbonate lithofacies. Geophysical well logs, in addition to providing an alternative method for petrophysical characteristics determination, show the subsurface distribution of the various lithofacies as defined by petrography and mercury-porosimetry.

Because the pore-system characteristics, derived from mercury-porosimetry relate to the lithofacies present, a better understanding of the reservoir properties, from the microscopic to the reservoir scale, is possible.

Early dolomitization of the carbonate grainstones had an extremely beneficial effect on the production of the reservoir: Pores and pore throats are well sorted, indicating very thin oil-water transition zones; pore throats are enlarged, indicating that production is possible with minimal oil columns; the lining of the

pores became smooth crystal phases lowering the irreducible water saturation values.

8. GLOSSARY

Absolute Permeability-Permeability of a rock saturated completely with one fluid.

Available Porosity-The amount of pore volume connected by throats.

Aspect Ratio-The ratio between pore size and throat size. The smaller the ratio, the larger the relative size of the pore throats, the easier the intrusion of mercury.

Breakthrough Pressure-See displacement pressure.

Capillary Pressure-(a) The pressure difference across the interface created by two immiscible fluids, also called "interface pressure" (dynes/cm^2); (b) the pressure necessary to inject liquids into the pore spaces of a specific rock (psi; Berg, 1975).

Connectivity-The degree to which a pore is multiply connected. As the number of connections between pores increases, so does permeability. Connectivity is important in defining displacement pressure.

Coordination Number (CN)-See connectivity.

Critical Oil Column-Oil column required to cause oil to displace the interstitial water.

Critical Pore-Throat Size-See displacement pressure.

Displacement Pressure-(a) The minimum pressure required to establish a connected hydrocarbon filament through the

largest interconnected water-saturated pore throats of the rock; (b) the capillary pressure at which maximum intrusion of mercury occurs for relatively small pressure increase.

Drainage-Displacement of a wetting phase by a nonwetting phase.

Drainage Curve-Curve obtained by measuring the volume of mercury entering the pore system when pressure is increased.

Effective Porosity-Total porosity reduced by irreducible water saturation.

Free-Oil Level-The point at which enough oil saturation exists (normally more than 70%) to allow 100% oil production.

Free-Water Level-The point of zero capillary pressure with oil; i.e., oil globules moving freely within large open pores.

Imbibition Curve-Curve obtained by measuring the volume of mercury leaving the pore system when pressure is reduced.

Injection Curve-See drainage curve.

Interfacial Tension-The stress between two liquids or a solid and a liquid caused by Van der Waal forces. It is dependent on the temperature, pressure, and chemical composition of the fluid and rock.

Interstitial Water-A thin film of water around grains.

Irreducible Water Saturation (Swi)-The part of interstitial water not effectively displaced by oil.

Oil-Column-The vertical dimension of a continuous oil accumulation, with its bottom located at the free-water level and extending to the top of the trap.

Oil-Water Contact-See free-water level.

Oil-Water transition Zone-The interval from water production at the base of the oil-saturated reservoir to water-free oil production higher in the reservoir. The thickness of the oil-water transition zone depends on the capillary properties of the rock and fluid properties of the system.

Porosity-Portion of bulk volume composed of voids (pores).

Productive Oil-Water Contact-The point at which oil first can be produced.

Recovery Curve-See imbibition curve.

Relative Permeability-Permeability of a rock to one fluid, when the rock is only partially saturated with that fluid. Residual Mercury Saturation-The percent volume of mercury (of the total volume) retained in the pore system when pressure is reduced to a minimum.

Saturation-The percentage of total pore space filled with the fluid in question.

Surface Tension-The stress on the surface of a liquid (when in contact with air or its own vapor) caused by Van der Waal forces that are not opposed by intermolecular agitation.

Threshold Pressure-See displacement pressure.

Total Porosity-The ratio of the rock's void space to its bulk volume.

Wettability-The tendency of a fluid to spread on or adhere to a solid surface in the presence of other immiscible fluids.

Withdrawal Curve-See imbibition curve.

9. APPENDIX 1

Experiments were carried out in a micromeritics mercury porosimeter according to procedures outlined in the methods section. Data gathered for each sample were first separately plotted by computer on semilog paper.

Mercury capillary-pressure data were used to evaluate and calculate petrophysical characteristics of reservoir rocks. In addition, oil migration and entrapment are a function of capillary pressure characteristics and fluid dynamics.

A linear, inverse relationship exists between pressure and pore throat diameter: i.e., the higher the pressure, the smaller the diameter of the pore throats which may be intruded by mercury. With each increment of pressure increase, therefore, smaller pore throat diameters were consistently invaded by mercury. 5,000 psia was chosen as an upper limit to represent sufficiently high pressure under which the pore system will become saturated with mercury. When pressure is reduced, progressive ejection or withdrawal from the smaller to the larger pore spaces occurs.

A capillary-pressure curve indicates the percentage of the total pores in a rock that is connected by pore throats of sufficient size to allow oil entry at a given capillary pressure.

A typical mercury injection curve representing typical Jay field reservoir facies is shown on figure 56. For each sample plotted, the shape of the curve is characteristic of the petrophysical properties of that sample, and may be used to determine several parameters, including porosity, effective porosity, pore throat sorting, irreducible water saturation, mercury saturation, and displacement pressure.

We may, therefore, describe the shape of the curve, and thus, the petrophysical properties of each sample quantitatively. This appendix contains quantitative description of the petrophysical properties of each sample , derived from capillary pressure curves. Quantitative description was preferred because it saves a lot of space and allows comparison between the samples.

The symbols in the following tables are explained in figure 56. For well location, refer to Table 1 and figure 8 in text.

FIGURE 56. Typical mercury injection curve, obtained from mercury porosimetry. The shape of the curve is used to determine pore throat size sorting (PTS), irreducible water saturation (Swi), mercury saturation (SHg), and displacement pressure (Pd) of the reservoir and nonreservoir facies of the cores studied. In addition, the curve is used to calculate effective porosity (Øe) from porosity (Ø) and mercury saturation. Q1 and Q3 are the first and third quartile, while P1 and P3 are their injection pressures respectively. Q2 is the mercury saturation at 5,000 psi divided by 2, while P2 is its pressure respectively.

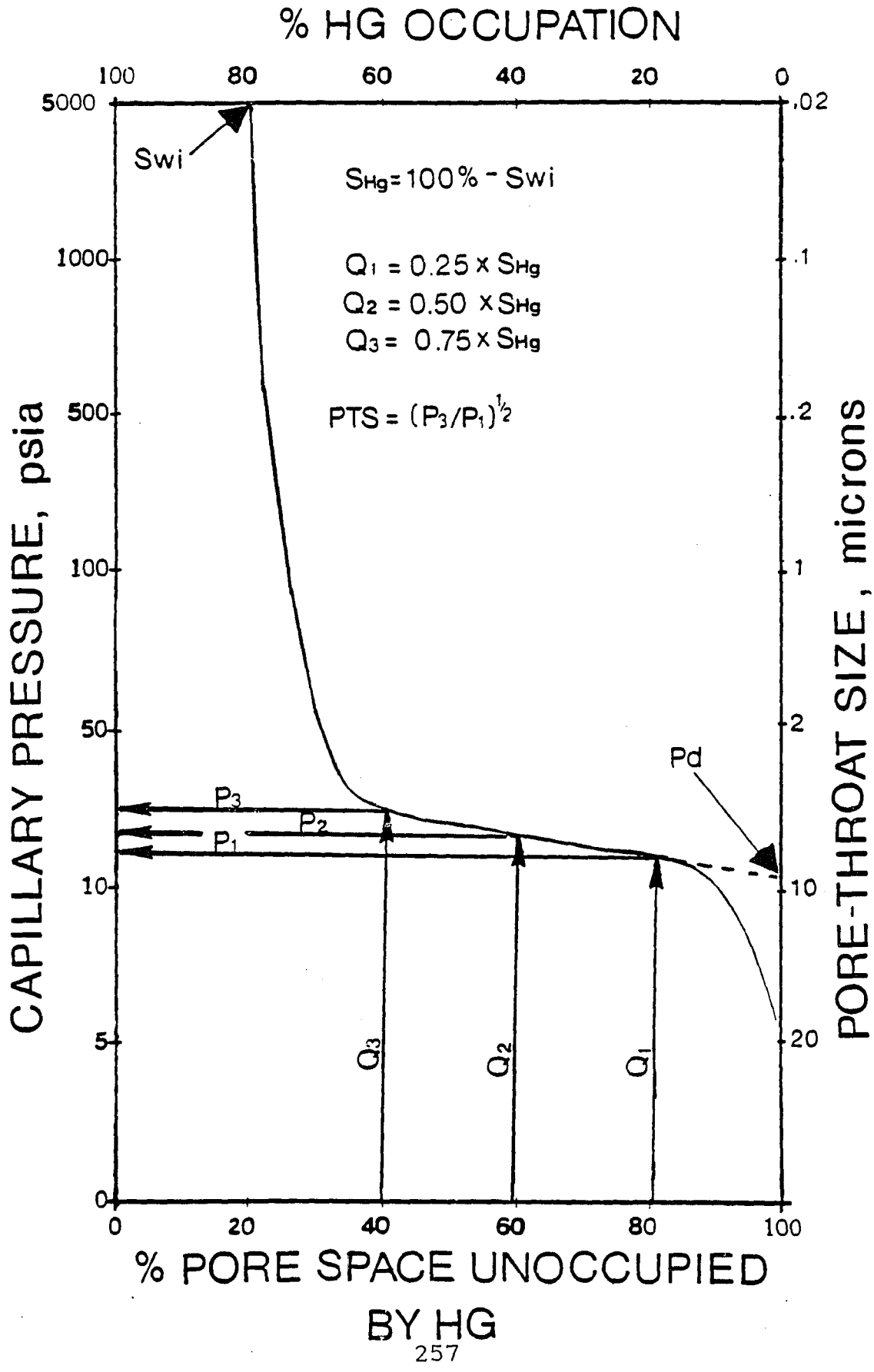
% HG OCCUPATION
100
80
60
40
20
0
5000
1000
500
100
50
10
5
0
.02
.1
.2
1
2
10
20
Swi
SHg=100% - Swi
Q1 = 0.25 x SHg
Q2 = 0.50 x SHg
Q3 = 0.75 x SHg
PTS = (P3/P1)1/2
Pd
P3
P2
P1
Q3
Q2
Q1
CAPILLARY PRESSURE, psia
PORE-THROAT SIZE, microns
0
20
40
60
80
100
% PORE SPACE UNOCCUPIED BY HG

BRAY WELL (Jay Field)

Sample (ft)	Φ (%)	Swi (%)	Φe (%)	Pd (psi)	Q1 (%)	Q2 (%)	Q3 (%)	P1 (psi)	P2 (psi)	P3 (psi)	PTS
15376	0.3	74.0		___	6.5	13.0	19.5	3.0	___	___	___
15385	0.6	83.5		___	4.1	8.3	12.4	1.0	___	___	___
15395	9.8	22.0	8.6	66	19.5	39.0	58.5	150	610	354	2.0
15402	5.9	30.6	4.1	220	17.4	34.7	52.0	390	890	1010	1.6
15410	22.9	20.7	18.6	7.8	19.8	39.7	59.4	22	32	66	1.7
15418	9.7	13.9	8.4	5.6	21.5	43.1	64.6	6.5	10	12	1.3
15427	7.0	8.4	6.4	5.8	22.9	45.8	68.7	9.8	14.5	68	2.6
15436	11.4	26.6	8.4	8.2	18.4	36.7	55.1	10	32	73	2.6
15446	16.2	19.7	13.0	10.1	20.1	40.2	60.2	9.7	13	23	2.4
15454	17.2	18.3	14.1	10.0	20.4	40.9	61.3	9.7	14	14	1.2
15467	16.3	20.6	12.9	9.7	19.9	39.7	59.6	10	12	50	2.2
15480	13.9	29.2	9.8	8.7	17.7	35.4	53.1	10	12	26	1.6
15491	15.6	15.8	13.1	9.6	21.1	42.1	63.2	10	12	14	1.2
15500	12.3	32.6	8.3	23.0	16.9	33.7	50.6	17	55	69	2.0
15511	10.8	16.7	9.0	40.0	20.8	41.7	62.5	58	85	125	1.5
15518	13.0	27.7	9.4	23.0	18.1	36.2	54.2	38	48	67	1.3
15525	13.2	28.0	9.5	13.0	18.0	36.0	54.0	23	32	61	1.6
15530	15.0	26.2	11.1	9.0	18.5	36.9	55.4	10	12	13	1.1
15537	10.1	22.5	7.8	50.0	19.4	38.8	58.1	58	58	92	1.3
15543	13.7	40.1	8.2	35.0	15.0	30.0	44.9	51	71	180	1.8

15550	14.6	27.3	10.6	10.0	18.2	36.5	54.5	20	30	65	1.8
15559	20.2	24.3	15.3	8.5	18.9	37.9	56.8	12	30	56	2.1
15569	16.9	18.9	13.7	37.0	20.3	40.6	60.8	42	45	62	1.2
15573*	4.0	58.3	1.7	170	10.4	20.9	31.3	503	110	1380	1.7
15575**	10.4	9.5	9.4	50.0	22.6	45.5	67.9	57	95	270	2.2
15579**	9.3	12.7	8.1	120	21.8	43.7	65.5	260	210	640	1.8
15593	3.2	76.9	0.8	___	5.9	11.6	17.8	3.5	850	960	9.2
15600	4.1	67.5	1.3	___	10.5	16.3	31.5	45	4200	5000	10.5
15609	6.9	52.5	3.3	___	11.9	23.6	35.6	58	1130	1800	5.6
15619	3.0	88.7	0.3	___	2.8	5.7	8.5	2.0	2.7	55	5.2
15627	2.5	73.8	0.7	___	6.6	13.1	19.7	58	760	3000	7.2
15635	16.5	9.4	15.0	61	22.7	45.1	68.0	90	180	380	2.1
15640	5.1	54.5	2.3	675	11.4	22.8	34.1	910	1800	2650	1.7
15646	3.4	84.3	0.5	___	3.9	7.9	11.8	75	250	475	2.5
15657	1.6	66.3	0.5	___	8.4	16.9	25.3	67	205	565	2.9
15661	1.9	68.0	0.6	___	8.0	16.0	24.0	57	240	670	3.4
15676	0.5	66.0	0.2	___	8.5	17.0	25.5	52	2000	3000	7.6
15683	11.9	55.1	5.3	870	11.2	22.5	33.7	1030	2100	2650	1.6
15689	3.7	51.7	1.8	610	12.1	24.2	36.2	1075	2000	2850	1.6
15694	11.9	58.5	4.9	630	10.4	20.8	31.1	840	1250	1550	1.4
15702	3.7	84.9	0.6	___	3.8	7.6	11.3	4.5	158	270	7.7
15709	14.3	7.7	13.2	68.0	23.1	46.2	69.2	100	190	520	2.3
15717	7.8	66.7	2.6	1000	8.4	16.7	25.2	520	2600	2750	2.3
15723	15.2	12.8	13.3	57.0	21.8	43.6	65.4	75	170	475	2.5
15728	1.5	14.4	1.3	48.0	21.4	42.8	64.2	57	430	1100	4.4

15737	0.9	51.0	0.4	___	12.3	24.5	36.8	205	2680	2850	3.7
15742	15.3	19.8	12.3	10.0	20.1	40.1	60.2	12	28	67	2.4
15809**	18.6	23.2	14.3	8.0	19.2	38.4	57.6	11	65	230	4.6

* Inequigranular textured sucrosic dolomite.

** Calcite cement partially filling intercrystalline pores.

*** Quartz sandstone (Norphlet Formation).

BROWN WELL

Sample (ft)	Ø (%)	Swi (%)	Øe (%)	Pd (psi)	Q1 (%)	Q2 (%)	Q3 (%)	P1 (psi)	P2 (psi)	P3 (psi)	PTS
15573	4.6	97.2	0.1	___	0.7	1.4	2.1	62	660	2350	6.2
15577	20.1	9.8	18.1	54	22.6	45.1	67.7	54	71	92	1.3
15586	14.6	20.5	11.6	52	19.9	39.8	59.6	63	100	95	1.3
15589	5.8	32.2	3.9	560	17.0	33.9	50.9	590	710	670	1.1
15593	2.6	61.6	1.0	1850	9.6	19.2	28.8	1650	3350	4010	1.6
15595	3.8	25.3	2.8	1980	18.7	37.35	56.0	580	2280	2650	2.1
15598	9.4	18.2	7.7	380	20.5	40.9	61.4	500	580	620	1.1
15601	12.0	18.2	9.8	260	20.5	40.9	61.4	340	395	540	1.3
15606	7.1	25.6	5.3	540	18.6	37.2	55.8	545	610	730	1.2
15609	4.9	25.5	3.7	540	18.6	37.3	55.8	620	810	900	1.2
15611	9.6	26.2	7.1	68	18.5	36.9	55.4	105	173	250	1.5
15615	9.6	18.0	7.9	62	20.5	41.0	61.5	70	110	120	1.3
15617	14.6	10.2	13.1	52	22.5	44.9	67.4	60	75	120	1.4
15621	3.0	49.9	1.5	1800	12.7	25.1	38.2	2200	2950	3700	1.3
15624	3.3	36.7	2.1	990	15.8	47.5	31.7	1136	2550	2250	1.4
15626	2.3	50.4	1.1	1130	12.4	24.8	37.2	1580	2450	2650	1.3
15629	1.2	30.0	0.8	1850	17.5	35.0	52.5	1750	3280	4150	1.5

LIZENBY WELL

Sample (ft)	Ø (%)	Swi (%)	Øe (%)	Pd (psi)	Q1 (%)	Q2 (%)	Q3 (%)	P1 (psi)	P2 (psi)	P3 (psi)	PTS
16329	2.8	85.8	0.4	___	3.6	7.1	10.7	65	1000	2150	5.6
16336	4.5	87.9	0.6	___	3.0	6.1	9.1	180	1710	2650	3.8
16343	2.7	56.4	1.2	290	10.9	21.8	32.7	350	510	1785	2.3
16354	4.1	78.9	0.9	___	5.3	10.6	15.8	14	500	1320	9.7
16358	3.9	70.3	1.2	___	7.4	14.9	22.3	1.4	2.7	8.2	2.4
16366	6.7	43.1	3.8	380	14.2	28.5	42.7	425	750	1025	1.6
16372	6.2	21.8	4.9	210	19.6	39.1	58.7	410	640	780	1.4
16378	2.3	19.0	1.9	520	20.3	40.5	60.8	500	1690	3250	2.6
16381	3.6	26.5	2.7	620	18.4	36.8	55.1	400	1010	1130	1.7
16392	5.7	35.5	3.7	640	16.1	32.3	48.4	110	1390	1415	3.6
16395	13.1	47.1	6.9	295	13.2	26.5	39.7	515	530	595	1.1
16398	9.4	41.3	5.5	520	14.7	29.4	44.0	540	640	650	1.1
16413	6.0	37.3	3.8	830	15.7	31.4	47.0	880	1050	1250	1.2
16420	2.2	45.5	1.2	130	13.6	27.3	40.9	395	870	2450	2.5
16422	1.9	39.8	1.1	530	15.1	30.1	45.2	610	1310	3950	2.6
16427	9.2	26.8	6.7	590	18.3	36.6	54.9	645	1755	3750	2.4
16432	2.2	74.1	0.6	___	6.5	13.0	19.4	8.5	103	380	6.7
16437	2.2	60.1	0.9	___	10.0	20.0	30.0	120	430	4100	5.9
16442	2.4	81.3	0.5	___	4.7	9.4	14.0	38	350	2150	7.5
16448	2.6	81.2	0.5	___	4.7	9.4	14.0	39	1060	1060	5.2

McDAVID LANDS WELL (Jay Field)

Sample (ft)	Φ (%)	Swi (%)	Φe (%)	Pd (psi)	Q1 (%)	Q2 (%)	Q3 (%)	P1 (psi)	P2 (psi)	P3 (psi)	PTS
15299	24.2	19.8	19.4	8.5	20.1	40.1	60.2	18.0	35	95	2.3
15304	18.3	23.7	14.0	8.0	19.1	38.2	57.2	10.0	23	55	2.3
15312	14.5	39.9	8.7	8.0	15.1	30.1	45.1	8.5	12	63	2.7
15322	13.7	40.1	8.2	8.0	15.0	30.0	44.9	12.5	12	80	2.3
15330	14.4	28.9	10.2	7.5	17.8	35.6	53.3	10.0	12	40	2.0
15346*	6.2	33.9	4.1	550	16.5	33.1	49.6	800	1480	1550	1.4
15355	17.0	30.3	11.9	8.5	17.4	34.9	52.3	9.0	12	40	2.1
15361	15.7	27.0	11.5	8.0	18.3	36.5	54.8	10.0	14	60	2.5
15374	13.2	36.4	8.4	8.0	15.9	31.8	47.7	65.0	42	75	1.1
15384	14.5	31.5	9.9	8.0	17.1	34.3	51.4	10.0	14	57	2.4
15391	9.3	60.1	3.7	35.0	10.0	20.0	30.0	55.0	72	730	3.6
15404	14.3	26.9	10.5	8.8	18.3	36.6	54.8	10.0	12	18	1.3
15414	17.5	30.3	12.2	8.5	17.4	34.9	52.3	10.0	12	38	1.9
15422	11.6	35.2	7.5	9.0	16.2	32.4	48.6	9.5	14	60	2.5
15429	11.3	31.8	7.7	17.0	17.1	34.1	51.2	25.0	38	70	1.7
15442	11.6	36.6	7.4	20.0	15.9	31.7	47.6	38.0	39	70	1.4
15455	13.1	35.6	8.4	9.0	16.1	32.2	48.3	19.0	36	68	1.9
15465	17.0	18.6	13.8	7.5	20.4	40.7	61.1	9.3	12	33	1.9
15475	14.6	40.5	8.7	9.0	14.9	29.8	44.6	10.0	12	60	2.5
15484	12.3	21.3	9.3	28.0	19.7	39.4	59.0	42.0	43	125	1.7
15493	10.7	30.0	7.5	38.0	17.5	35.0	52.5	60.0	120	680	3.4
15510	8.6	32.8	5.8	65.0	16.8	33.6	50.4	65.0	480	900	3.7

15518	10.9	36.2	7.0	37.0	16.0	31.9	47.9	60.0	125	620	3.2
15524	12.3	21.9	9.6	180	19.5	39.1	58.6	310	480	680	1.5
15534	8.7	37.0	5.5	350	15.8	31.5	47.3	380	460	1550	2.0
15542	11.7	44.1	6.5	28.0	14.0	28.0	42.0	50.0	70	540	3.3
15546	4.8	48.4	2.5	560	12.9	25.8	38.7	600	1300	2800	2.2
15560	6.1	41.7	3.6	500	14.6	29.2	43 7	680	150	2530	1.9
15576	4.8	51.5	2.3	900	12.1	24.3	36.8	2300	3400	5000	1.5
15584	6.1	30.7	4.2	450	17.3	34.7	52.0	475	1240	2050	2.1
15590	4.2	45.5	2.3	500	13.6	27.3	40.9	490	2020	3400	2.6
15594	2.6	59.1	1.1	___	10.2	20.3	30.7	75	85	4200	7.5
15602	1.7	14.9	1.5	___	21.3	42.6	63.8	115	270	3950	5.9
15608	3.9	46.4	2.1	1050	13.4	26.8	40.2	1000	2700	3850	2.0
15622	4.2	26.9	3.1	680	18.3	36.6	54.8	500	540	1220	1.6
15630	2.9	12.7	2.5	___	21.8	43.7	65.5	780	2100	4050	7.2
15637	7.16	19.6	5.6	100	20.1	40.7	60.3	180	380	670	1.9
15643**	18.6	22.0	14.5	7.5	19.5	39.0	58.5	10.0	12	58	1.9
15664**	15.0	33.5	10.0	8.0	16.6	33.3	49.9	10.5	12	63	2.5

* Peloidal packstone layer, incorporated within the sucrosic dolomite.

** Quartz sandstone (Norphlet Formation).

SAM WATSON WELL (Jay Field)

Sample (ft)	Ø (%)	Swi (%)	Øe (%)	Pd (psi)	Q1 (%)	Q2 (%)	Q3 (%)	P1 (psi)	P2 (psi)	P (psi)	PTS
15583	10.4	1.3	10.3	53.0	24.7	49.4	74.0	54.0	63	115	1.5
15586	11.7	13.3	10.1	65.0	21.7	43.4	65.0	69.0	103	125	1.3
15590	22.0	13.3	19.1	38.0	21.7	43.4	65.0	50.0	51	65	1.1
15597*	6.0	54.5	2.7	645	11.4	22.8	34.1	101	940	1040	3.2
15600*	6.2	33.3	4.1	585	16.8	33.4	50.0	380	830	920	1.6
15604	22.0	18.9	17.8	9.0	20.3	40.6	60.8	16.0	18	56	1.9
15613	14.0	17.7	11.5	13.0	20.6	41.2	61.7	13.0	53	63	2.2
15617	14.2	16.9	11.8	38.0	20.8	41.6	62.3	50.0	53	67	1.2
15622	4.6	68.5	1.5	___	7.9	15.8	23.6	120	3130	3800	5.6
15634	13.1	33.4	8.7	78.0	16.7	33.3	50.0	160	285	520	1.8
15640	13.9	25.1	10.4	105	18.7	37.5	56.2	190	280	520	1.7
15646	8.6	32.9	5.8	350	16.8	33.6	50.3	360	825	900	1.6
15650	5.7	35.6	3.8	330	16.1	32.2	48.3	770	1580	1795	1.5
15666	6.9	45.5	3.8	380	13.6	27.3	40.9	600	1000	1500	1.6
15670	8.4	27.0	6.1	240	18.3	36.5	54.8	330	385	570	1.3
15679	4.3	81.4	0.8	___	4.7	9.3	14.0	8.0	13	640	8.5
15686	4.5	6.6	4.2	360	23.4	46.7	70.1	480	490	640	1.2
15688	17.0	16.9	14.1	13.0	20.8	41.6	62.3	22.0	30	68	1.8
15694	20.2	19.5	16.3	12.5	20.1	40.3	60.4	12.5	16	55	2.1
15700	18.8	17.4	15.5	66.0	20.7	41.3	62.0	66.0	102	190	1.7
15706	14.2	17.4	11.7	100	20.7	41.3	62.0	104	165	330	1.8
15712	4.4	47.3	2.3	780	13.2	26.4	39.5	570	2200	3400	2.4

15722	8.0	52.4	3.8	___	11.9	23.8	35.7	88	3750	3900	6.7
15726	3.4	69.3	1.0	___	7.8	15.4	23.0	120	2550	3900	5.7
15735	5.0	70.9	1.5	___	7.3	14.6	21.8	52.0	1020	4200	8.9
15745	3.0	62.9	1.1	___	9.3	18.6	27.8	3.4	3.9	670	14.0
15757	3.1	76.9	0.7	___	5.8	11.6	17.3	2.0	3.3	650	18.0
15763	3.3	80.4	1.0	___	4.9	9.8	14.7	2.0	3.2	860	20.7
15774	6.9	20.1	5.5	115	20.0	40.0	60.0	210	690	700	1.8
15779	3.1	39.9	1.9	6.5	15.0	30.1	45.1	6.8	10	735	10.4

* Anhydrite cement partially occludes porosity.

10. REFERENCES

Adams, N.K., 1941, The Physics and Chemistry of Surfaces, Oxford University Press, London.

Ahr, W.M., 1973, Carbonate ramp-an alternative to the shelf model: Gulf Coast Assoc. Geol. Soc. Trans., v. 23, p. 221-225.

Amthor, J.E., Kopaska-Merkel, D.C., and Friedman, G.M., 1988, Reservoir characterization, porosity, and recovery efficiency of deeply-buried Paleozoic carbonates: Examples from Oklahoma, Texas and New Mexico: Carbonates and Evaporites, v. 3, p. 33-52.

Anderson, W.G., 1986a, Wettability literature survey-Part 1: Rock/oil brine interaction and the effects of core handling on wettability: Jour. Pet. Tech., v. 48, p. 1125-1144.

Anderson, W.G., 1986b, Wettability literature survey-Part 2: Wettability measurment: Jour. Pet. Tech., v. 48, p. 1246-1262.

Anderson, W.G., 1986c, Wettability literature survey-Part 3: The effects of wettability on the electrical properties of porous media: Jour. Pet. Tech., v. 48, p. 1371-1378.

Archie, G.E., 1950, Introduction to petrophysics of reservoir rocks: Am Assoc. Pet. Geol. Bull., v. 34, p. 943-961.

Archie, G.E., 1952, Classification of carbonate reservoir rocks and petrophysical considerations: Am. Assoc. Pet. Geol. Bull., v. 36, p. 278-298.

Arps, J.J., 1964, Engineering concepts useful in oil finding: Am. Assoc. Pet. Geol. Bull., v. 48, p. 157-165.

Aschenbrenner, B.C., and Achauer, C.W., 1960, Minimum conditions for migration of oil in water-wet carbonate rocks: Am. Assoc. Pet. Geol. Bull., v. 44, p. 235-243.

Asquith, G.B., 1979, Subsurface carbonate depositional models-a concise review, Tulsa, Pennwell, 121pp.

Asquith, G.B., 1985, Handbook of log evaluation techniques for carbonate reservoirs, Am. Assoc. Pet. Geol., Methods in Exploration Series No. 5, 47pp.

Asquith, G.B., and Gibson, C., 1982, Basic well log analysis for geologists, Am. Assoc. Pet. Geol., Methods in Exploration, Tulsa Oklahoma, 216pp.

Ball, M.M., 1967, Carbonate sand bodies of Florida and the Bahamas: Jour. Sed. Pet., v. 37, p. 556-591.

Badiozamani, K., 1973, The dorag dolomitization model-Application to the Middle Ordovician of Wisconsin: Jour. Sed. Pet., v. 43, p. 965-984.

Bathurst, R.G.C., 1975, Carbonate sediments and their diagenesis, In Developments in Sedimentology, v.12, Elsevier Scientific Publ. Comp., New York, 568pp.

Barrett, M., 1989, Stratigraphy of the Smackover Formation (U. Jurassic), Southeast Alabama: Eustatic and tectonic influences on depositional patterns: Shereveport Geological Society, v. 27, p. 4-5.

Beall, R., 1973, Plate tectonics and the origin of the Gulf Coat Basin: Gulf Coast Assoc. Geol. Soc. Trans., v. 23, p. 109-114.

Benner, F.C., and Bartell, F.E., 1941, The effect of polar impurities upon capillary and surface phenomena in petroleum production: Drill and prod. Prac., API, New York City, p. 341-348.

Benson, D.J., and Mancini, E.A., 1984, Porosity development and reservoir characteristics of the Smackover Formation in southwest Alabama, p.1-17, In The Jurassic of the Gulf Rim, Proceedings of the Third Annual Research Conference, Gulf Coast Section, Soc. Econ. Paleont. Mineral. Foundation, Ventress, W.P.S., Bebout, D.G., Perkins, B.F., and Moore, C.H. (Eds.), 408pp.

Berg, R.R., 1975, Capillary pressures in stratigraphic traps, Am. Assoc. Pet. Geol. Bull., V. 59, No. 6, p 939-956.

Bishop, W.F., 1968, Petrology of upper Smackover Limestone in North Haynesville Field, Claiborne

Parish, Louisiana: Am. Assoc. Pet. Geol. Bull., v. 52, p. 92-128.

Bradford, C.A., 1984, Transgressive-regressive carbonate facies of the Jurassic Smackover Formation, Big Escambia Creek and Flomaton Fields, Escambia County, Alabama, p. 27-40, In The Jurassic of the Gulf Rim, Proceedings of the Third Annual Research Continental, Gulf Coast Section, Soc. Econ. Paleo. Min. Foundation, Ventrees, W.P.S., Bebout, D.G., Perkins, B.F., and Moore, C.H., (Eds.) 408 pp.

Brown, H.W., 1951, Capillary pressure investigations: Petroleum Trans. AIME, v. 192, p. 67-74.

Buchbinder, L.G., and Friedman, G.M., 1980, Vadose, phreatic, and marine diagenesis of Pleistocene-Holocene carbonates in a borehole: Mediterranean coast of Israel: Jour. Sed. Pet., v. 50, p. 395-408.

Budd, D.A., and Loucks, R.G., 1981, Smackover and Lower Buckner formations, South Texas: Depositional Systems on a Jurassic carbonate ramp: Bureau of Economic Geology, Report of Investigations No. 112, 38pp.

Burdine, T.N., Cournay, L.S., and Reichertz, P.P., 1950, Pore size distribution of petroleum reservoir rocks: Petroleum Trans. AIME, v. 189, p. 195-204.

Calhoun, J.C., Jr., 1953, Fundamentals of Reservoir Engineering, University of Oklahoma Press, 417pp.

Cartmill, J.C., 1976, Obscure nature of petroleum migration and entrapment: Am. Assoc. Pet. Geol. Bull., v. 60, p. 1520-1530.

Chilingar, G.V., and Yen, T.F., 1983, Some notes on wettability and relative permeabilities of carbonate reservoir rocks, 11: Energy Sources, v. 7, p. 442-448.

Craig, F.F., 1971, The Reservoir Engineering Aspects of Waterflooding, Monograph Series 3, Petroleum Engineers of AIME, Dallas Texas, 134pp.

Crevello, P.D., and Harris, P.M., 1984, Depositional models for Jurassic reefal buildups, p. 57-102, In The Jurassic of the Gulf Rim, Proceedings of the Third Annual Research Conference, Gulf Coast

Section, Soc. Econ. Paleont. Mineral. Foundation, Ventrees, W.P.S., Bebout, D.C., Perkins, B.F., and Moore, C.H., 408pp.

Crevello, R.D., Harris, P.M., Stoudt, D.L., and Baria, L.P., 1985, Porosity evolution and burial diagenesis in a Jurassic reef-debris reservoir, Smackover Formation, Hico Knowles Field, Louisiana, p. 387-406, In Carbonate Petroleum Reservoirs, Roehl, P.O., and Choquette, P.W. (Eds.), Springer-Verlag Publ. Comp., New York, 622pp.

Davies, G.R., 1970, Algal-laminated sediments, Gladstone Embayment, Shark Bay, Western Australia, p. 169-205, In Carbonate Sedimentation and Environments, Shark Bay, Western Australia, Am. Assoc. Pet. Geol., Memoir #13, 223pp.

Dewan, J.T., 1983, Essentials of modern open-hole log interpretation, Penn Well Publ. Comp., Tulsa, Oklahoma, 361pp.

Doveton, J.H., 1986, Log analysis of subsurface geology; Concepts and computer methods. John Wiley and Sons Publ. Comp., New York, 273pp.

Dowling, P.L., Jr., 1970, Application of carbonate environmental concepts to secondary recovery projects: Soc. Petrol. Engr., AIME, Paper No. SPE 2987.

Dullien, F.A.L., and Dhawan, G.K., 1975, Bivariate pore-size distributions of some sandstones, Jour. Colloid. and Interface Sciences, p. 129-135.

Dullien, F.A.L., 1979, Porous Media, fluid transport and pore structure, Academic Press Publ. Comp., 396 pp.

Dullien, F.A.L., and Dhawan, G.K., 1974, Characterization of pore structure by a combination of quantitative photomicrography and mercury porosimeter, Jour. colloidal and Interface Science, v. 47, p. 337-349.

Dunham, R.J., 1965, Vadose pisolite in the Capitan Reef, (abs.): Am. Assoc. Pet. Geol. Bull., v. 49, p. 338.

Dunham, R.J., 1969, Vadose pisolite in the Capitan Reef (Permian), New Mexico and Texas, p. 182-191, In

Depositional Environments in Carbonate Rocks, Friedman, G.M. (Ed.), Soc. Econ. Paleont. Mineral., Sp. Pub. # 14, 209pp.

Esposito, R.A., Jr., and King, D.T.., Jr., 1987, Facies analysis, sea-level history, and platform evolution of the Jurassic Smackover Formation, Conecuh Basin, Escambia County, Alabama: Trans. Gulf Coast Assoc. Geol. Soc., v. 37, p. 335-336.

Esteban, M.C., 1976, Vadose pisolite and caliche: Am. Assoc. Pet. Geol. Bull., v. 60, p. 2048-2057.

Esteban, M.C., and Pray, L.C., 1977, Origin of the pisolite facies of the shelf crest, p. 479-484, In Upper Guadalupian Facies Permian Reef Complex, Guadalupe Mountains New Mexico and West Texas, 1977 Field Conference Guidebook, Permian Basin Section, Soc. Econ. Paleont. Mineral., Pub. 77-16.

Esteban, M.C., and Pray, L.C., 1983, Pisoids and pisolite facies (Permian), Guadalupe Mountains, New Mexico and West Texas, p. 503-537, In Coated Grains, Peryt, T.M. (Ed.), Springer-Verlag Publ. Comp., New York, 655pp.

Fatt, I., and Klikoff, W.A., 1959, Effect of fractional wettability on multiface flow through porous media: AIME Petroleum Trans., v. 216, p. 71-77.

Fertl, W,H, and Vercellino, W.C., 1978, Predict water cut from well logs, In Practical Log Analysis-4: Oil and gas Jour., May 15, 1978-Sept. 19, 1979.
Folk, R.L., and Land, L.S., 1975, Mg/Ca ratio and salinity: Two controls over crystallization of dolomite: Am. Assoc. Pet. Geol. Bull., v. 59, p. 60-68.

Friedman, G.M., 1959, Identification of carbonate minerals by staining methods: Jour. Sed. Pet., v. 29, p. 87-97.

Friedman, G.M., 1964, Early diagenesis and lithification of carbonate sediments: Jour. Sed. Pet., v. 34, p. 777-813.

Friedman, G.M., Amiel, A.J., Braun, M., and Miller, D.S., 1973, Generation of carbonate particles and laminites in algal mats-Example from sea-marginal hypersaline pool, Gulf of Agaba, Red Sea: Am. Assoc.

Pet. Geol. Bull., v. 57, p. 541-557.

Friedman, G.M., and Sanders, J.E., 1967, Origin and occurrence of dolostones, p. 267-348, In Developments in Sedimentology 9A-Carbonate Rocks; Origin, Occurrence and Classification, Chilingar, G.V., Bissell, H.J., and Fairbridge, R.W. (Eds.), Elsevier Publ. Comp., New York, 471pp.

Friedman, G.M., Sneh, A., and Owen, R.W., 1985, The Ras Muhammad Pool: Implications for the Gavish Sabkha, p. 218-237, In Hypersaline ecosystems: The Gavish Sabkha, Friedman, G.M., and Krumbein, W.E. (Ed.), Springer-Verlag, New York.

Gebelein, C.D., 1969, Distribution, morphology, and accretion rate of recent subtidal algal stromatolites, Bermuda: Jour. Sed. Pet., v. 39, p. 49-69.

Ghosh, S.K., and Friedman, G.M., 1989, Petrophysics of a dolostone reservoir: San Andres Formation (Permian), West Texas: Carbonates and Evaporites, v. 4, in press.

Handford, C.R., Kendall, A.C., Prezbindowski, D.R., Dunham, J.B., and Logan, B.W., 1984, Salina-margin tepees, pisoliths, and aragonite cements, Lake MacLeon, Western Australia: Their significance in interpreting anchient analogs: Geology, v. 12, p. 523-527.

Hardie, L.A., 1987, Dolomitization: A critical review of some current views: Jour. Sed. Pet., v. 57, p. 166-183.

Hjelmeland, O.S., and Larrondo, L.E., 1986, Experimental investigation of the effects of temperature, pressure, and crude oil composition on interfacial properties: Society of Petroleum Engineers Reservoir Engineering, v. 1, p. 321-328.

Hobson, D.G., 1954, Some Fundamentals of Petroleum Geology, Oxford University Press, London, 139pp.

Hocott, C.R., 1938, Interfacial tensions between water and oil under reservoir conditions: AIME Petroleum Trans., v. 32, p. 184-190.

Hubbert, M.K., 1953, Entrapment of petroleum under

hydrodynamic conditions: Am. Assoc. Pet. Geol. Bull., v. 37, p. 1954-2026.

Hsu, K.J., and Siegenthaler, C., 1969, Preliminary experiments on hydrodynamic movement induced by evaporation and their bearing on the dolomite problem: Sedimentology, v. 12, p. 11-25.

Imbt, W.C., and Ellison, S.P., 1946, Porosity in limestone and dolomite petroleum reservoirs: Drilling and production practice: Amer. Petrol. Inst., New York, p. 364-372.

James, N.P., and Choquette, P.W., 1984, Diagenesis 9-. Limestones-The meteoric diagenetic environment: Geoscience Canada, v. 11, p. 161-194.

Jardine, D., Andrews, D.P., Wishart, J.W., and Young, J.W., 1977, Distribution and continuity of carbonate reservoirs, Jour. Pet. Tech., July issue, p. 873-885.

Jay-LEC Fields unit Geological Committee, 1974, Structure Map-Top of Smackover-Norphlet Oil Pool: Exhibit No. G-1 for Florida Department of Natural Resources Hearing No.36.

Jennings, J.B., 1987, Capillary pressure techniques: Application to exploration and development: Am. Assoc. Pet. Geol. Bull., v., 71, p. 1196-1209.

Jodry, R.L., 1972, Pore geometry of carbonate rocks (Basic Geologic concepts), p. 35-82 In Oil and Gas Production from carbonate rocks, Chillingar, G.V., Mannon, R.W., Rieke, H.H. (Ed.), Elsevier, New York, 408 pp.

Johnson, J.H., 1942, Permian lime secreting algae from Guadalupe Mountains, New Mexico: Geol. Soc. Am. Bull., v. 53, p. 195-226.

Jones, F.G. and Wilkinson, B.H., 1978, Structure and growth of lacustrine pisoliths from recent Michigan Marl Lakes: Jour. Sed. Pet., v. 48, p. 1103-1110.

Kendall, C.G.St.C., and Skipwith, S.P.A.D'E., 1969, Holocene shallow-water carbonate and evaporite sediments of Khor al Bazam, Abu Dhabi, Southwest Persian Gulf: Am. Assoc. Pet. Geol. Bull., v. 53, p. 841-869.

Kinsman, D.J.J., 1969, Modes of formation, sedimentary associations, and diagenetic features of shallow-water and supratidal evaporites: Am. Assoc. Pet. Geol. Bull., v. 53, p. 830-840.

Kopaska-Merkel, D.C., and Amthor, J.E., 1988, Very high-pressure mercury porosimetry as a tool in reservoir characterization: Carbonates and Evaporites, v. 3, p. 53-63.

Kusakov, M.M., Lubman, N.M., and Koshevnik, A. Yu., 1954, Oil-water and oil-gas interfacial tensions under in-situ conditions: Neftyanoye Khozyaystvo, v. 32, p. 62-69 (transl. by Assoc. Tech. Series, Inc.).

Land, L.S., 1973, Holocene meteoric dolomitization of Pleistocene limestones, North Jamaica: Sedimentology, v. 20, p. 411-424.

Land, L.S., 1982, Dolomitization: Am. Assoc. Pet. Geol., Educ. Course Note #24, 20pp.

Lang, W.B., 1942, The Carlsbad dolomite amd pisolites of the Guadalupe Mountains of New Mexico (abs.): Am. Assoc. Pet. Geol. Bull., v. 26, p. 901.

Logan, B.W., rezak, R., and Ginsburg, R.N., 1964, Classfication and environmental significance of algal stromatolites: Jour. Geol., v. 72, p. 68-83.

Langston, E.P., and Shirer, J.A., 1985, Performance of the Jay/LEC fields unit under mature waterflood and early tertiary operations: Jour. Pet. Tech., v. 37, p. 261-268.

Langston, E.P., Shirer, J.A., and Nelson, D.E., 1981, Innovative reservoir managment-key to highly successful Jay/LEC waterflood: Jour. Pet. Tech., v. 33, p. 783-791.

Larson, R., 1977 Percolation in porous media with application to enhanced oil recovery, M.Sc. thesis, Chemical Engineering, University of Minnesota, Minneapolis, 103pp.

Leja, J., 1982, Surface chemistry of froth flotation, Plenum Press Publ. Comp., New York.

Levorson, A.L., 1967, Geology of Petroleum, Freeman Press, New York, 724pp.

Livingston, H.K., 1938, Surface and interfacial tension of oil-water systems in Texas oil sands: AIME Petroleum Technology, v. 1, Paper 1001.

Logan, B.W., Rezak, R., and Ginsburg, R.N., 1964, Classification and environmental significance of algal stromatolites: Jour. Geol., v. 72, p. 68-83.

Longman, M.W., 1980, Carbonate diagenetic textures from nearsurface diagenetic environments: Am. Assoc. Pet. Geol. Bull., v. 64, p. 461-487.

Loucks R.G., and Budd, D.A., 1984, Diagenesis and reservoir potential of the Upper Jurassic Smackover Formation of south Texas, p. 195-205, In The Jurassic of the Gulf Rim, Proceedings of the Third Annual Research Conference, Gulf Coast Section, Soc. Econ. Paleont. Nineral, Foundation, Ventrees, W.P.S., Bebout, D.C., Perkins, B.F., and Moore, C.H. (Eds.), 408pp.

Lowenstein, T.K., 1987, Evaporite depositional fabrics in the deeply buried Jurassic Buckner Formation, Alabama: Jour. Sed. Pet., v. 57, p. 108-116.

Mancini, E.A., and Benson, D.J., 1980, Regional stratigraphy of Upper Jurassic Smackover carbonates of southwest Alabama: Gulf Coast Assoc. Geol. Soc. Trans., v. 30, p. 151-165.

Mancini, E.A., Mink, R.M., Bearden, B.L., and Wilkerson, R.P., 1985, Norphlet Formation (Upper Jurassic) south-western and offshore Alabama: Environments of deposition and petroleum geology: Am. Assoc. Pet. Geol. Bull., v. 69, p. 881-898.

McCaslin, J.C., 1987, Jurassic success spreads to NW Florida: Oil and Gas Journal, August issue, p. 78.

McKenzie, J.A., Hsu, K.J., and Schneider, J.F., 1980, Movement of subsurface waters under the sabkha, Abu Dhabi, UAE, and its relation to evaporative dolomite genesis, p. 11-30 In Concepts and Models of Dolomitization, Zenger, D.H., Dunham, J.B., and Ethington, R.L. (Eds.), Soc. Econ. Paleont. Mineral, Spec. Publ. #28, 320pp.

Melas, F.F., and Friedman, G.M., 1987, Pisoids in the Jurassic Smackover Formation (Alabama-Florida) evidence of marine vadose diagenesis: Am. Assoc. Pet. Geol. Bull., v. 71, p. 1119.

Melas, F.F., and Friedman, G.M., 1987a, Pisoids in the Jurassic Smackover Formation (Alabama-Florida) evidence of marine vadose diagenesis: Trans. Gulf Coast Assoc. Geol. Soc., v. 37, p. 405-414.

Melrose, J.C., Brandner, C.F., 1974, Role of capillary forces in determining microscopic displacement efficiency for oil recovery by waterflooding, Jour. Canadian Pet. Tech., v. 13, p. 54-62.

Mink, R.M., Bearden, B.L., and Mancini, E.A., 1985, Regional Jurassic geologic framework of Alabama Coastal waters area and adjacent federal waters, Oil and Gas Report 12, Geological Survey of Alabama and State Oil Gas Board, 57pp.

Mitchell-Tapping, T.J., 1984, Depositional environment of the updip Smackover area of East Texas, p. 69-86, In The Jurassic of East Texas, Presley M.W. (Ed.), East Texas Geological Society, 304 pp.

Monty, C.L.V., 1983, recent algal stromatolitic deposits, Andros Island, Bahamas. Preliminary Report, p. 113-149, In Modern Carbonate Environments, Bhattacharya, A., and Friedman, G.M. (Eds), Hutchinson Ross Publ. Comp., Stroudsburg Pennsylvania, 376pp.

Moore, C.H., and Druckman, Y., 1981, Burial diagenesis and porosity evolution, Upper Jurassic Smackover, Arkansas and Louisiana: Am. Assoc. Pet. Geol. Bull., v. 65, p. 597-628.

Morrow, N.R., 1970, Irreducible wetting phase saturations in porous media: Chem. Engr. Sci., v. 25, p. 1799-1815.

Morrow, N.C., 1971, Small-scale packing heterogeneities in porous sedimentary rocks,: Am. Assoc. Pet. Geol. Bull., v. 55, p. 514-522.

Morrow, N.R., and Heller, J.P., 1985, Fundamentals of enhanced recovery, p. 47-74, In Enhanced Oil Recovery 1-Fundamentals and Analysis, Donaldson, E.C., Chillingarian, G.V., and Yen, T.F., (Ed.),

Elsevier Publ. Comp., New York, 357 pp.

Munn, M.J., 1909, The anticlinal and hydraulic theories of oil and gas accumulation: Economic Geology, v. 4, p. 509-529.

Murray, R.C., 1960, Origin of porosity in carbonate rocks: Jour. Sed. Petrol., v. 30, p. 59-84.

Neumann, A.C., Gebelein, C.D. and Scoffin, T.P., 1970, The composition, structure and erodability of subtidal mats, Abaco, Bahamas: Jour. Sed. Pet., v. 40, p. 274-297.

Newell, N.D., Imbrie, J., and Purdy, E.G., 1960, Bahamian oolitic sand: Jour. Geol., v. 68, p. 481-497.

Newell, N.D., Rigby, J.K., Fischer, A.G., Whiteman, A.J., Hickox, J.E., and Bradley, J.S., 1953, The Permian Reef Complex of the Guadalupe Mountains region, Texas and New Mexico, W.A. Freeman and Co Publ. Comp., San Francisco, 236pp.

Nutting, P.G., 1934, Some physical and chemical properties of reservoir rocks bearing on the accumulation and discharge of oil, p. 825-832, In Problems in Petroleum Geology, Wrather, W.E., and Lahee, F.H., (Ed.), Am. Assoc. Pet. Geol., Tulsa.

Ottmann, R.D., Keyes, P.L., and Ziegler, M.A., 1973, Jay Field-A Jurassic stratigraphic trap: Gulf Coast Assoc. Geol. Soc. Trans., v. 23, p. 146-157.

Peryt, T.M., 1983, Vadoids, p. 437-449, In Coated Grains, Peryt, T.M. (Ed.), Springer-Verlag Publ. Comp., New York, 655pp.

Pickell, J.J., Swanson, B.F., Hickman, W.B., 1966, Application of air-mercury and oil-air capillary pressure data in the study of pore structure and fluid distribution: Soc. Pet. Engr. Jour., March issue, p. 55-61.

Pray, L.C., 1986, Capitan Reef Complex (Permian), Guadalupe Mountains, Southwestern United States: Reinterpretation of deposition and diagenesis of a classic sedimentologic model, (abs.): West Texas Geol. Soc. Bull., V. 26, p. 18.

Purcell, W.R., 1949, Capillary pressure-their mearurment using mercury and the calculation of permeability therefrom: Jour. Pet. Technology, v. 1, p. 39-48.

Purdy, E.G., 1963, Recent calcium carbonate facies of the Great Bahama Bank. 2. Sedimentary Facies: Jour. Geol., v. 71, p. 472-497.

Raza, S.H., Treiber, L.E., and Archer, D.L., 1968, Wettability of reservoir rocks and its evaluation: Producers Monthly, v. 33, p. 2-7.

Reitzel, G.A., Callow, G.O., 1977, Pool description and performance analysis leads to understanding Golden Spike's miscible flood, Jour. Pet. Tech., July issue, p. 867-872.

Riding, R., 1983, Cyanoliths (cyanoids): Oncoids formed by calcified cyanophytes, p. 276-283, In Coated Grains, Peryt, T. (Ed.), Springer-Verlag Publ. Comp., New York, 655pp.

Robinson, R.B., 1966, Classification of reservoir rocks by surface texture, Am. Assoc. Pet. Geol. Bull., v. 50, p. 547-559.

Rogers, D.A., 1984, Mexia and Talco fault zones, East Texas: Comparison of origins predicted by two tectonic models, p. 23-31, In The Jurassic of East Texas, Presley, M.W., (Ed.), East Texas Geological Society, 304pp.

Ruedemann, R., 1929, Coralline algae, Guadalupe Mountains: Am. Assoc. Pet. Geol. Bull., v. 13, p. 1079-1080.

Russel, W.L., 1952, Interpretation of neutron well logs: Am. Assoc. Pet. Geol. Bull., v. 36, p. 312-341.

Saraf, D.N., and McCaffery, F.G., 1985, Relative permeabilities, p. 75-118, In Enhanced Oil Recovery 1-Fundamentals and Analysis, Donaldson, E.C., Chillingarian, G.V., and Yen, T.F., (Ed.), Elsevier Publ. Comp., New York, 357pp.

Schlumberger, 1987, Log Interpretation Principles/ Applications, Houston, Texas, Schlumberger Educational Services, 198pp.

Schmidt, V., McDonald., D.A., and Platt, R.I., 1977,

Pore geomentry and reservoir aspects of secondary recovery in sandstone: Can. Pet. Geol. Bull., v. 25, p. 271-290.

Schneider, J.F., 1975, Recent tidal deposits, Abu Dhabi, UAE, Arabian Gulf, p. 209-214, In Tidal Deposits, Ginsburg, R.N. (Ed.), Springer-Verlag Publ. Comp., New York, 428pp.

Scholle, P.A., and Kinsman, D.J.J., 1974, Aragonitic and high-Mg calcite from the Persian Gulf-A modern analog for the Permian of Texas and New Mexico: Jour. Sed. Pet. v. 44, p. 904-916.

Schowalter, T.T., 1979, Mechanics of secondary hydrocarbon migration and entrapment: Am. Assoc. Pet. Geol. Bull., v. 63, p. 723-760.

Sears, S.O., and Lucia, F.J., 1980, Dolomitization of northern Michigan Niagara reefs by brine refluxation and freshwater/sea water mixing p. 216-235 In Concepts and Models of Dolomitization, Zenger, D.H., Dunham, J.B., and Ethington, R.L. (Ed.), Soc. Econ. Paleont. Mineral., Sp. Pub. #28, 320pp.

Shirer, J.A., Langston, E.P., and Strong, R.B., 1978, Application of field-wide conventional coring in the Jay/Little Escambia Creek unit: Jour. Pet. Tech., v. 30, p. 1774-1780.

Sigsby, R.S., 1976, Paleoenvironmental analysis of the Big Escambia Creek-Jay-Blackjack Creek Field area: Trans. Gulf Coast Asssoc. Geol. Soc. Trans., v. 26, p. 258-278.

Smith, D.A., 1966, Theoretical considerations of sealing and nonsealing faults: Am. Assoc. Pet. Geol. Bull., v. 50, p. 363-374.

Sneh, A. and Friedman, G.M., 1985, Hypersaline sea-marginal flats of the Gulfs of Elat and Suez, p. 103-135, In Hypersaline Ecosystems, Friedman, G.M. and Krumbein, W.E. (Ed.), Springer-Verlag, New York, 454pp.

Stout, J.L., 1964, Pore geometry as related to carbonate stratigrapic trap: Bull. Am. Assoc. Pet. Geol., v. 48, no. 3, p. 329-337.

Thomas, C.M., 1965, Origin of pisolites, (abs.): Am. Assoc. Pet. Geol. Bull., v. 49, p. 360.

Thomeer, J.H.M., 1960, Introduction of a pore geometrical factor defined by the capillary pressure curve: Jour. Pet. Tech., Note 2057, March issue, p. 73-77.

Treiber, L.E., Archer, D.L., and Owens, W.W., 1972, A laboratory evaluation of the wettability of fifty oil-producing reservoirs: Am. Inst. Met. Eng. Petroleum Trans., v. 253, p. 531-540.

Vinet, M.J., 1984, Geochemistry and origin of Smackover and Buckner dolomites (Upper Jurassic) Jay field area, Alabama-Florida, p. 365-374, In Ventress, W.P.S., Bebout, D.G., Perkins, B.F., and Moore, C.H. (Eds.), The Jurassic of the Gulf Rim, Proceedings of the Third Annual Research Conference, Gulf Coast Section, Soc. Econ. Paleont. Mineral. Foundation, 408pp.

Walper, J.L, and Rowett, C.L., 1972, Plate tectonics and the origin of the Caribbean Sea and the Gulf of Mexico: Gulf Coast Assoc. Geol. Soc. Trans., v. 22, p. 105-116.

Wardlaw, N.C, 1976, Pore geometry of carbonate rocks as revealed by pore casts and capillary pressure: Am. Assoc. Pet. Geol. Bull., v. 60, no. 2, p. 245-257.

Wardlaw, N.C., 1980, The effects of pores structure on displacement efficiency in reservoir rocks and in glass micromodel, Soc. Petr. Engr., no. 8843., p. 345-352 (Paper presented at 1st SPE/DOE symp. on Enhanced Oil Recovery, Tulsa, Okla, April 20/23 1980).

Wardlaw, N.C., and Cassan, J.P., 1978, Estimation of recovery efficiency by visual observation of pore systems in resevoir rocks: Bull. Can. Pet. Geol., v. 26, p. 572-585.

Wardlaw, N.C., and Cassan, J.P., 1979, Oil recovery efficiency and the rock-pore properties of some sandstone reservoirs: Bull. Can. Pet. Geol., v. 27, p. 117-138.

Wardlaw, N.C., and McKellar, M., 1981, Mercury porosimetry and the interpretation of pore geometry

in sedimentary rocks and artificial models: Powder Technology, v. 29, p. 127-143.

Wardlaw, N.C., McKellar, M., and Li Yu,1988, Pore and throat size distributions determined by mercury porosimetry and by direct observation: Carbonates and Evaporites, v. 3, p. 1-15.

Wardlaw, N.C., and Reinson, G.E., 1971, Carbonate and evaporite deposition and diagenesis, Middle Devonian Winnipegosis and Prairie Formations of south-central Saskatchewan: Am. Assoc. Pet. Geol. Bull., v. 55, p. 1759-1786.

Wardlaw, N.C., and Taylor, R.P., 1976, Mercury capillary pressure curves and the interpretation of pore structure and capillary behavior in reservoir rocks, Bull, Can. Pet. Geol., v. 24, p. 225-262.

Warren, J.K., 1982, The hydrological setting, occurence and significance of gypsum in late Quaternary salt lakes in South Australia: Sedimentology, v. 29, p. 609-637.

Warren, J.K., and Kendall, C.G.St.C., 1985, Comparison of sequences formed in marine sabkha (subaerial) and salina (subaqueous) settings-Modern and anchient: Am. Assoc. Pet. Geol. Bull., v. 69, p. 1013-1023.

Wayhan, D.A., McCaleb, J.A., 1969, Elk Basin Madison hetergeneity-its influence on performance: Jour. Pet. Tech., February issue, p. 153-159.

Wilson, G.V., 1975, Early differential subsidence and configuration of the northern Gulf Coast Basin in southwest Alabama and northwest Florida: Gulf Coast Assoc. Geol. Soc. Trans., v. 25, p. 196-206.